Title
LOW ENERGY ELECTRON DIFFRACTION

Authors
Somorjai, G.A.
Farrell, H. H.

Publication Date
1970-03-01

Submitted to Advances in Chemical Physics

UCRL-19195
Preprint

c. 2

LOW ENERGY ELECTRON DIFFRACTION

G. A. Somorjai and H. H. Farrell

March 1970

AEC Contract No. W-7405-eng-48

LAWRENCE RADIATION LABORATORY
UNIVERSITY of CALIFORNIA BERKELEY

UCRL-19195

DISCLAIMER

TABLE OF CONTENTS

LOW ENERGY ELECTRON DIFFRACTION*

G. A. Somorjai and H. H. Farrell**

Inorganic Materials Research Division, Lawrence Radiation Laboratory
and Department of Chemistry, University of California
Berkeley, California

*This work was done under the auspices of the U. S. Atomic Energy Commission

** Current address: Department of Applied Science
Brookhaven National Laboratory
Upton, N. Y. 11973

I. INTRODUCTION

In recent years there has been remarkable progress in our understanding of the structure of surfaces. Most of the structural investigations have been carried out using low energy electron diffraction (LEED). Just as x-ray diffraction may be used to study the bulk structure, low energy electron diffraction probes the structure of surfaces.

The lack of structural information in surface reactions has long impeded the progress of surface science. Using LEED one can determine the structure of the clean surface and monitor the structure of adsorbed gases during the different stages of chemical surface reaction. Thus, correlation between the structure and chemistry of surfaces can be established. Surface phase transformation of many kinds (order-order, order-disorder, etc), can be studied by LEED. Finally, the dynamics of surface atoms, their mean square displacements or their diffusion along the surface can be investigated.

The application of low energy electron diffraction has led to the discovery of several new surface phenomena. It was found that the arrangement of surface atoms in clean solid surfaces could be different from the arrangement of atoms in the bulk unit cell. Solid surfaces may undergo structural rearrangements or changes of chemical composition while no corresponding changes may occur in the bulk of the crystal. It was found that atoms chemisorbed on solid surfaces form ordered surface structures. The nature of the surface structure depends on the crystal orientation, the chemistry and the concentration of adsorbed gas atoms and the temperature. Low energy electron diffraction studies revealed

that the mean square displacement of surface atoms is larger than the mean square displacement of bulk atoms.

The major obstacle in the path of surface structural studies using low energy electron diffraction is the lack of a simple theory which could explain the scattered low energy electron beam intensities. The application of such a theory in model calculations where the important variables are the atomic positions should lead, just like the use of the kinematic theory in x-ray diffraction, to complete description of the surface structure. It is hoped that such a theory will become available in the very near future. Until then the assignment of atomic positions in surface structures, solely on the basis of the diffraction pattern, is not unambiguous. This explains the different interpretations which may be given to the same diffraction pattern and the concentration of LEED studies on only simple monatomic or diatomic surfaces. Frequently however the available supplementary chemical information using other experimental techniques permits one to identify the surface structure correctly and to eliminate most of the alternative models.

This review attempts to present the state of the field of low energy electron diffraction. We shall describe the theory and the experiment and then review the structural studies which were carried out using disordered surfaces, clean ordered surfaces, adsorbed gases and condensable vapors on single crystal surfaces.

In order to carry out a low energy electron diffraction experiment one needs (a) ultra high vacuum ($< 10^{-8}$ torr), (b) one face of a pure single crystal and (c) a well-focused electron beam in the energy range 1-500 eV. At the present state of our technology such an experiment can be carried out with relative ease.

II. SYMMETRY AND NOMENCLATURE OF TWO-DIMENSIONAL STRUCTURES

One of the most notable features of low energy electron diffraction from ordered single crystal surfaces is the symmetry of the diffraction pattern. This symmetry is a direct consequence of the periodic arrangement of the atoms or molecules in the surface of the crystal.

It is convenient to regard the structure of the surface to be arbitrarily constructed of a lattice and a basis. A lattice is an array of points in space such that the arrangement of atoms around any lattice point is identical to that around every other lattice point. The basis represents the arrangement of atoms around the lattice points. A basis may be as simple as a single metal atom placed on a lattice point for many metal crystals, or it may be as complex as a set of DNA molecules. A unit cell which contains lattice points only at the corners is called a primitive cell.

All lattice points are related by the translation operations

$$\vec{T} = n_a \vec{a} + n_b \vec{b} + n_c \vec{c} \qquad (1)$$

where n_a, n_b, and n_c are integers and $\vec{a}$, $\vec{b}$, and $\vec{c}$ are translation vectors whose dimensions are those of the sides of unit cell and whose directions are parallel to the sides of the unit cell. The two dimensional (2D) lattice of a surface may be characterized by two dimensional translation operations

$$\vec{T} = n_a \vec{a} + n_b \vec{b} \qquad (2)$$

Note that the translational operations are symmetry operations that leave the surface invariant. The regular arrangement of a reasonably perfect single crystal surface frequently allows for the application of other symmetry operations such as rotations and mirror reflections that will also leave the surface invariant.

It may be shown that perfect two dimensional symmetry allows for only a finite number of different types of rotations (even though each allowed rotation may be applied an infinite number of times.) Only those rotations through an angle of $2\pi/n$ where n = 1, 2, 3, 4, and 6 are allowed.[1] It is easily seen that if rotations for n = 4 are allowed, then the lattice must be square. Similarly, rotations through $2\pi/n$ for n equal 3 or 6 must be associated with hexagonal lattices. In this manner, the allowed rotations place restrictions on the types of primitive translations that may occur. Mirror operations will also restrict the types of primitive translations that are allowed. As a consequence of these mutual restrictions, there are only five two-dimensional Bravais or spare lattices that are possible. These are shown in Fig. 1.

The symmetry of the surface is only partially described by its Bravais lattice. The basis or arrangement of atoms around each lattice point will itself remain invariant under certain symmetry operations even if it is only the trivial operation of rotation through 360°. The collection of symmetry operations that leave a basis invariant is called a crystallographic point group. There are 10 two-dimensional crystallographic point groups. Five of them are characterized by the permissible rotations $2\pi/n$ for n = 1, 2, 3, 4, and 6. The other five are characterized by the permissible rotations and by mirror reflections. If one mirror plane is allowed, then the rotations will generate a set of equivalent mirror planes (except for n = 1 of course).

The total symmetry of a crystal surface is described by the combination of the Bravais lattice and the crystallographic point group of the basis. There are 17 unique and allowed combinations of the five Bravais

lattices and ten crystallographic point groups. These are called two-dimensional space groups. The reader is referred to an excellent discussion of these space groups by Wood.[2]

In the energy range usually employed in low energy electron diffraction, the de Broglie wavelength associated with the electron will be of the order of angstroms, [$\lambda(\text{Å}) = (150/\text{eV})^{1/2}$]. This length is similar to the interrow spacing of the atoms on most single crystal surfaces. As the atoms in the crystal are arranged in an orderly fashion, there will be only certain regions in space where the reflections from parallel rows of atoms will interfere constructively. When the scattering takes place from a two dimensional array, the regions in space of allowed constructive interference will be rods rather than points as in the three dimensional case. These rods, or diffraction beams, can be characterized by the equivalent parallel crystallographic planes from which the constructive interference that formed a given diffraction beam originated.

A convenient parameter for indexing a diffraction beam is the reciprocal lattice vector, $\vec{G}_{hk}$. This reciprocal lattice vector contains information about both the magnitude of the interplanar spacing under consideration and the direction of the normal to that set of crystallographic planes. For a given two dimensional Bravais lattice with primitive translational vectors, $\vec{a}$ and $\vec{b}$, the corresponding primitive reciprocal lattice vectors $\vec{G}_a$ and $\vec{G}_b$ are defined by the following relationships:

$$\vec{a} \cdot \vec{G}_a = \vec{b} \cdot \vec{G}_b = 2\pi \qquad (3a)$$

$$\vec{a} \cdot \vec{G}_b = \vec{b} \cdot \vec{G}_a = 0 \qquad (3b)$$

and

$$\vec{G}_a = 2\pi \frac{\vec{b}\times\vec{c}}{\vec{a}\cdot[\vec{b}\times\vec{c}]} \qquad \vec{G}_b = 2\pi \frac{\vec{a}\times\vec{c}}{\vec{b}\cdot[\vec{a}\times\vec{c}]} \qquad (3c)$$

where $\vec{c}$ is a unit vector perpendicular to the surface. Just as a real space translational vector, $\vec{T}$, may be constructed from an integral number of primitive real space translational vectors $n_a \vec{a} + n_b \vec{b}$; a reciprocal lattice vector $\vec{G}_{hk} = h \vec{G}_a + k \vec{G}_b$ may be constructed from the primitive reciprocal lattice vectors $\vec{G}_a$ and $\vec{G}_b$.

The reciprocal lattice vector $\vec{G}_{hk}$ has the following interesting properties. Its direction is normal to the 2D crystallographic planes with (hk) Miller indices and its length is equal to 2π times the reciprocal of the spacing of these (hk) planes.

The indexing of the various diffraction beams is a relatively simple matter. The specularly reflected beam does not involve any change in the component of the electron momentum that is parallel to the surface of the crystal. Therefore, it is associated with only the null parallel reciprocal lattice vector, $\vec{G}_{00} = 0 \cdot \vec{G}_a + 0 \cdot \vec{G}_b$ and is customarily indexed as the (00) beam. In a similar fashion, the first order diffraction beams for the square, rectangular or oblique lattices may be indexed as (01), (10), (0$\bar{1}$) or ($\bar{1}$0) as they are associated with the reciprocal lattice vectors $\vec{G}_{01} = \vec{G}_b$, $\vec{G}_{10} = \vec{G}_a$, $\vec{G}_{0\bar{1}} = -\vec{G}_b$ or $\vec{G}_{\bar{1}0} = -\vec{G}_a$ respectively. Higher order beams may be indexed in an analogous manner. The unit cell vectors of the primitive two dimensional unit cell and indexing of the three densest crystal faces in the face centered cubic and body centered cubic structures are given in Figs. 2a-j

Some caution must be exercised in the indexing of low energy electron diffraction patterns. The choice of indices is dependent upon the choice of unit cell. For example, the first order diffraction beams from the (100) face of face-centered cubic crystals may be indexed as either (10) or (11) depending upon whether the primitive two dimensional lattice (Fig. 3a) or

the full x-ray unit cell containing a centered atom is used (Fig. 3b). Both notational systems are used in the literature.

A common observation in low energy electron diffraction patterns is the occurence of "extra" or "fractional order"spots. In addition to the normal diffraction beams associated with the lattice spacing of the bulk crystal, there frequently appear other diffraction beams that often may be indexed with fractional indices. These extra diffraction beams are usually associated with structures on the surface which are characterized by larger unit cells than the projection of the bulk unit cell onto the crystal surface. For example, if molecules from the ambient were to condense out onto every other lattice site of the surface, then this new structure on the surface of the crystal would have a periodicity twice that of the "clean" substrate surface. As the reciprocal lattice vectors are inversely proportional to the interplanar spacings, then the new primitive reciprocal lattice vectors for the surface would have one-half the length of those in the original set. Therefore, in addition to the old set of reciprocal lattice vectors parallel to the surface, there would then exist a new set with fractional order indices. Associated with this new structure and these new parallel reciprocal lattice vectors, there would also be a new set of diffraction beams.

Surface structures are formed not only by the adsorption of gases onto the surface, but also by the segregation of bulk impurities onto the surface of the crystal and by the reconstruction of clean crystal surfaces. As with the simple surfaces, their Bravais lattices may be either centered or primitive. Though perhaps less common, the dimensions of the structured surface may bear a non-integral relationship to the

dimensions of the simple surface. Furthermore, the structured surface may have a unit cell that is rotated relative to that of the clean surface.

Often, a surface structure will exist that has the usual dimensions along one translation, but a large dimension along the other translation direction. These structures are frequently denoted as being (1×n) where the 1 indicates the usual bulk cell dimension along the x-direction while the n indicates n-times the bulk unit cell dimension along the y-direction. This will give rise to a diffraction pattern with the usual number of diffraction spots along one reciprocal lattice direction and n times the usual number along the other direction.(Fig. 4a-c). When the unit cell vectors of the substrate in both directions are identical on the original surface (as on the (100) face of fcc or bcc solids), then it is possible to have two types of domains, one set of the (1×n) and one set of the (n×1) kind. When this occurs, it may be observed that the diffraction pattern will have n times the normal number of spots along both directions. This type of diffraction pattern is not to be confused with that arising from a true (n×n) structure where the surface structure has n times the usual dimension along both directions on all portions of the crystal. For example, a (1×2) structure on a square surface may contain two types of domains rotated relative to one another by 90° and giving rise to (0, 1/2) and (1/2, 0), spots. A true (2×2) structure, however, will also give rise to (1/2, 1/2), spots in addition to those which appear for the domain structure (Fig. 4a-c).

Surface structures of the type (n×m) where $n \neq m$ are frequently formed. For example carbon monoxide on the palladium (100) face gives a c (4×2) structure.[3] The indices used to characterize the structure

of the surface need not be integer. If every third lattice site on a hexagonal face is distinguished from the other sites, then a $(\sqrt{3}\times\sqrt{3})$ -30° surface structure may arise. The angle given after the (n×m) notation indicates the orientation of the new unit cell relative to the original unit cell. If every other lattice site on a square face is unique, then a $(\sqrt{2}\times\sqrt{2})$-45° surface structure could be formed. To avoid the noninteger notation, this structure is usually labeled a C(2×2) where the c indicates that this is a centered (2×2) structure. Occasionally, the notation p(n×m) is used where the p indicates that a primitive unit cell has been taken. This p is frequently deleted when either it is understood that the unit cell is primitive, or when the detailed geometry of the unit cell is unknown. If a surface structure is known to be associated with some contaminant or adsorbed gas, it is customary to denote the adsorbate material in the description of the surface structure as (n×m)-S where S is the chemical symbol or formula for the adsorbate. Perhaps one of the simplest examples of this would be the oxygen surface structure on molybdenum where the oxygen atoms or molecules on the surface of the metal have the same unit mesh as the clean metal surface. This structure would be denoted as the Mo(100)-(1×1)-O structure where the chemical symbol and crystallographic face of the substrate are given first, then the unit mesh of the surface structure relative to that of the substrate and finally the chemical symbol of the impurity is denoted.

A useful and simple method for determining the real space lattice of a surface structure from its reciprocal space lattice vectors as displayed in its diffraction pattern has been developed by Park and Madden. Noting the reciprocal and the real space vectors obey the relation

$$\vec{a} \cdot \vec{G}_a = 2\pi$$

it is possible to construct two matrices, A and G, such that

$$\underset{\approx}{A} \cdot \underset{\approx}{G} = \underset{\approx}{1} \qquad (4a)$$

or

$$\underset{\approx}{A} = \underset{\approx}{G}^{-1} \qquad (4b)$$

If the components of G are taken as the indices of the partial order spots and are expressed in terms of the basis vectors of the "clean" diffraction pattern, then its inverse, $\underset{\approx}{A}$, will give the coordinates of the basis vectors of the real space lattice for the surface structure in terms of the primitive lattice vectors for the clean or unreconstructed surface. For example, a (2×2) surface structure on a rectangular or square surface will give rise to a diffraction pattern characterized by diffraction spots with the indices n/2 and m/2. In fact, the total diffraction pattern, or reciprocal lattice space net, may be regarded as being generated from the basis vectors (0 1/2) and (1/2 0) where the first order diffraction spots from the clean surface would have the indices (10) and (01). We may therefore construct a reciprocal lattice matrix $\underset{\approx}{G} = \begin{vmatrix} 0 & 1/2 \\ 1/2 & 0 \end{vmatrix}$ which has as its inverse the real space matrix $\underset{\approx}{A} = \begin{vmatrix} 0 & 2 \\ 2 & 0 \end{vmatrix}$ which may be regarded as being constructed of the real space vectors (0 2) and (20) which are simply the primitive translational vectors of the (2×2) surface structure expressed in terms of translational vectors for the clean surface. Similarly, a c(2×2) surface structure gives rise to a diffraction pattern or reciprocal lattice net which can be generated from the vectors (1/2 1/2) and (1/2 1/2). The resulting reciprocal lattice matrix $\underset{\approx}{G} = \begin{vmatrix} 1/2 & 1/2 \\ 1/2 & -1/2 \end{vmatrix}$ has as its inverse the real space matrix $\underset{\approx}{A} = \begin{vmatrix} -1 & 1 \\ 1 & 1 \end{vmatrix}$ which displays the real space translational vectors for the

c(2×2) surface structure as $(\bar{1}\ 1)$ and $(1\ 1)$. This method is very powerful for the analysis of complicated surface structures. Note, however, that any analysis of the geometry of the diffraction pattern will only give information about the two dimensional space lattice. In order to determine the arrangement of the basis around the lattice points and in a direction perpendicular to the surface, an analysis of the intensities of the diffraction features msut be performed. The problems inherent in such an analysis will be discussed in a later section.

III. THE NATURE OF LOW ENERGY ELECTRON DIFFRACTION

Many of the unique characteristics of low energy electron diffraction in the energy range 0-500 eV are due to the large scattering cross sections of the low energy electrons. Particularly at very low electron energies, 0-100 eV, these cross sections may be of the order of square angstroms. As a consequence, there will be substantial amplitudes scattered into the non-forward directions, and the probability that the electron will be found in the transmitted beam will be significantly less than unity. This results in a high probability that an electron will be incapable of penetrating very deeply into a solid under these conditions before it is scattered, either elastically or inelastically, out of the forward scattered beam. Therefore, most of the intensity that is back-scattered out of the crystal comes from either the surface or the neighborhood of the surface. This, of course, makes low energy electron diffraction an ideal tool for studying the structure of surfaces.

Unfortunately, the very aspect that makes low energy electron diffraction valuable for surface structure analysis also complicates this analysis. That is, because the scattering cross sections are large, not only will the electron be scattered predominantly from the vicinity of the surface, but it will also have a significant probability of being scattered more than once. This phenomenon is known as multiple scattering and its importance vitiates the applicability of the kinematic theory of diffraction which has been used so successfully in the x-ray case where only single scattering or kinematic events are important.

One of the interesting consequences of the fact that scattering is confined to the vicinity of the surface is that the full three dimensional periodicity of the crystal is not experienced by the electron. We therefore are dealing with a potential which has essentially perfect periodicity in the two dimensions parallel to the surface but has imperfect periodicity, perpendicular to the surface. This perfect two dimensional periodicity insures that diffraction will occur and that the electron will be scattered only into certain discrete rods or beams, destructive interferences having taken place along all other directions in space.

More concisely, as has been noted by Boudreaux and Heine,[4] the only exact quantum number in the system is that component of the wave vector, $\vec{K}_{\|}$ or $\vec{K}_{xy}$, which is parallel to the surface and this is indeterminant to the extent of adding any reciprocal lattice vector that is parallel to the surface in the usual sense of the Bloch theorem. Due to the imperfect periodicity perpendicular to the surface however, that component of the wave vector, $\vec{K}_{\perp}$ or $\vec{K}_{z}$, that is perpendicular to the surface is not constrained to take on only certain discrete values as it would be in the x-ray diffraction case.

However, when only elastic scattering is considered, this perpendicular component is defined by the parallel component and the condition that the total magnitude of the wave vector must be conserved. If the incident electrons are characterized by a total wave vector, $\vec{K}^{0}$, then the components parallel to and perpendicular to the surface may be denoted as $\vec{K}^{0}_{\|}$ and $\vec{K}^{0}_{\perp}$ respectively. In a similar manner, a diffraction beam may be characterized by K' with components $\vec{K}'_{\|}$ and $\vec{K}'_{\perp}$. Now, the constraint on the parallel component may be written as

$$\vec{K}'_{\|} = \vec{K}^{0}_{\|} + \vec{G}_{\|} \qquad (5)$$

where $\vec{G}_{\|}$ is some reciprocal lattice vector parallel to the surface. If the surface has rectangular or square symmetry, $\vec{G}_{\|} = 2\pi(\hat{x}\ h/a_x + \hat{y}\ k/a_y)$ where h and k are integers, x and y are units vectors in the x and y directions and a_x and a_y are the primitive translational vectors of the surface lattice net in the x and y directions respectively. The z direction has been taken as being perpendicular to the surface.

In free space, the energy of the electron is directly proportional to the square of the total wave vector as $E = \hbar^2 |\vec{K}|^2/2m$ where $\hbar$ is Plancks constant divided by 2π and m is the mass of the electron. Therefore, the constraint that the scattering must be elastic may be written as

$$|\vec{K}'|^2 = |\vec{K}^{\circ}|^2 \qquad (6a)$$

or

$$|\vec{K}'_{\|}|^2 + |\vec{K}'_{\perp}|^2 = |\vec{K}^{\circ}|^2 \qquad (6b)$$

Rearranging Eq. 2b, $K'_{\perp}$ may be determined as

$$\vec{K}_{\perp}^{hk} = \pm \hat{z} \sqrt{|K^{\circ}|^2 - |G_{\|}^{hk}|^2 - |K_{\|}^{\circ}|^2} \qquad (7)$$

Note that $K'_{\perp}$ may be either positive or negative, corresponding to a diffraction beam directed either into or out of the crystal. Real values of $K'_{\perp}$ correspond to travelling waves or allowed states in the crystal while complex or imaginary values correspond to damped or evanescent waves at the surface and forbidden states in the bulk of the crystal.

There are actually an infinite number of solutions to Eq. 7.[5] First, there are those within the Ewald sphere where $|\vec{K}^{\circ}|^2 > |\vec{K}_{\|}'|^2$. The Ewald sphere is that surface in reciprocal space with a radius of $|\vec{K}^{\circ}|$. When within this sphere, $\vec{K}_{\perp}'$ is real, at least when not in a band gap where it may assume complex values.[1] In the following, the states characterized by real values of $K_{\perp}'$ will be referred to as "allowed" states. Secondly, there are those solutions that lie outside of the Ewald sphere where $|\vec{K}^{\circ}|^2 < |\vec{K}_{\|}'|^2$. For these cases, $\vec{K}_{\perp}'$ is purely imaginary and the associated eigenfunctions are strongly damped. Note that $\vec{K}_{\perp}'$ may be either positive or negative, corresponding to diffraction beams directed both into and out of the crystal (Fig. 5). As most low energy electron diffraction studies are made as a function of electron energy, it is of value to inspect Eqs. 5 , 6 and 7 for their energy dependence. Equation 6 states the necessity that the diffracted beam have a wave vector of the same magnitude as the incident beam for elastic scattering whereas Eq. 5 states that the parallel component may contain some reciprocal lattice vector. It may therefore be seen that at a low enough beam voltage these two equations may not be fulfilled simultaneously with real values of $\vec{K}_{\perp}'$ except for the null parallel reciprocal lattice vector. In this region, only the transmitted and the specularly reflected beams are allowed. All other beams will be forbidden, or evanescent. Upon going to higher energies, the magnitude of the wave vector becomes large enough to accomodate the smallest reciprocal lattice vector, and the first order diffraction beams will be allowed in addition to the transmitted and specularly reflected beams. At still higher voltages, higher order diffraction beams will come into existence. When a diffraction beam first appears, the

component of its wave vector perpendicular to the surface will have zero magnitude, and the emergent beam will lie in the surface. At a slightly higher energy, $|\vec{K}_\perp|$ will have a finite value and diffraction beams directed both into and out of the surface will appear. As the energy is increased, the angle that these new beams will make with the surface increases and these beams will assymtotically approach the axis of the incident or specularly reflected beam. Viewing only the back scattered beams, upon increasing the electron energy one would first see new diffraction beams appear parallel to the surface of the crystal and then rise up out of this surface and sweep through space towards the specularly reflected beam. These considerations arise solely from the symmetry, that is, the two dimensional periodicity parallel to the surface. They are completely independent of the nature of the surface other than its symmetry and the dimensions of its unit cell parallel to the surface.

Information about dimensionalities perpendicular to the surface and about the type of scattering centers involved is, however, contained in the intensities of these diffraction beams. To appreciate the possible variations in these beam intensities, let us consider two limiting cases.

A. The Two-Dimensional Diffraction Limit

The first case is that in which there are no periodic modulations in the potential in the direction perpendicular to the surface that are experienced by the electron. This is essentially the two dimensional grating problem. Here if one monitored the intensities of the back-diffracted beams as a function of electron energy, one would fine, at best, a monotonic variation (Fig.6a). Conceptually, this situation could occur if the scattering cross sections were sufficiently large that the electrons never penetrated the first atomic layer of the surface.

B. The Three Dimensional Diffraction Limit

The second limiting case arises in the opposite limit where the cross sections for back scattering are quite small so that the electron can penetrate deeply into the crystal before being scattered. In this case, the effect of the surface can be ignored and the electron will be diffracted predominantly in an environment where it is subjected to the full three-dimensional periodicity of the crystal. Now the perpendicular component of the reciprocal lattice vector is no longer free to assume a continuum of values but is limited to certain discrete values by this periodicity in the z direction. This constraint on $\vec{K}'_\perp$ may be expressed in a manner similar to Eq.5 as

$$\vec{K}'_\perp = \vec{K}^\circ_\perp + \vec{G}_\perp \qquad (8)$$

where $\vec{G}'_\perp$ is some reciprocal lattice vector perpendicular to the surface. Note that the combination of Eqs.6 and 8 is just the Bragg equation for x-ray diffraction expressed in reciprocal space. This can be seen in the following manner. We may write $|\vec{K}'-\vec{K}^\circ| = 2K \sin(\theta/2)$, $K = 2\pi/\lambda$ and $|\vec{G}| = 2\pi\, n/d$ where θ is the angle between the initial and the final directions of travel and d is the interplanar spacing perpendicular to the scattering vector $\vec{G}$. Substituting these real space expressions into the reciprocal space expression obtained by combining Eqs.6 and 8, the classical Bragg expression

$$n\lambda = 2d \sin(\theta/2) \qquad (9)$$

is obtained.

If one were to look at the intensities of the diffracted beams in this limit, it would be observed that they were zero except at those points where Eqs.6 and 8 were met simultaneously (Fig.6b).

C. Low Energy Electron Diffraction

We now have two extreme cases, one where the intensity varies smoothly with electron energy, and the other where the intensity varies abruptly being zero except at certain discrete energies and points in space. Reality for LEED is, of course, somewhere in between. In Fig. 7 we show the intensities of the different (hk) diffraction beams, I_{hk} as a function of electron energy, eV, which is obtained for the Al(100) surface at normal incidence. There are modulations in the beam intensities, some, but not all, corresponding to maxima predicted by Eq. 8 . Furthermore, particularly at low beams voltages, there is usually finite intensity in these diffraction beams at energies that do not correspond to any diffraction condition. These observations may be explained by the fact that, even though the scattering cross sections are rather large, they are not so large that the electron does not have a finite probability of penetrating the first and even several of the top most atomic layers parallel to the surface. Consequently, the electron may experience some degree of the full three dimensional periodicity of the crystal.

However, the observation of intensity maxima at energies other than those predicted from Eq. 8 indicate that the situation is not so simple as outlined above. As mentioned before, the very fact that the scattering cross sections are reasonably large can lead to multiple scattering events. These may be envisioned in the following manner. As the amplitudes of the non-transmitted diffraction beams are substantial, and as the cross sections are large, the diffracted beams themselves may act as primary beams or electron sources. Consequently, we must

consider diffraction conditions of the form of Eq. , but between diffracted beams rather than only between the primary, or incident, beam and a diffraction beam.

We therefore have the new condition

$$\vec{K}''_{\perp} = \vec{K}'_{\perp} + \vec{G}_{\perp} \qquad (10)$$

where both $\vec{K}'_{\perp}$ and $\vec{K}''_{\perp}$ are wave vector components corresponding to diffraction beams. Note that Eq. may be considered as a special case of Eq 10. The analogous condition for the parallel components

$$\vec{K}'_{\parallel} = \vec{K}'_{\parallel} + \vec{G}_{\parallel} \qquad (11)$$

is always met. This is guaranteed by Eq. 6 .

For sufficiently large cross sections, still more phenomena can be observed. For example, when the condition expressed in Eq. 10 is met between two diffraction beams, a subsidiary maximum may be observed in a third beam, even though no appropriate diffraction condition is met. This is because all of the beams are more or less coupled for sufficiently large cross sections, and an increase in the intensity of one of them may result in an increase in the intensity of another.

The actual intensity maxima that are observed may be arbitrarily categorized into three different types on the basis of the associated diffraction conditions.

1) Kinematic or Single Diffraction: The first group is comprised of those maxima whose positions are predicted by Eq. 8. This is the kinematic or single scattering case, and peaks should appear at these positions even in the limit of negligible mutliple scattering.

2) Double Diffraction: In this case, we have those peaks whose positions are predicted by Eq.10 rather than Eq.8 . This is a simple multiple scattering situation and may be called the double diffraction case as it necessitates only two successive scattering events.

3) Tertiary and High Order Scattering: This case contains all intensity maxima not directly predicted by Eqs.8 and 10. Observation of these phenomena should be limited to those situations where multiple scattering is quite strong. One would expect when inelastic scattering was important that maxima of this type would be experimentally observed only with difficulty.

Although the division of intensity maxima into these three different categories presents a useful classiciation scheme, it is rather artificial as higher order scattering events may contribute to the intensities of maxima classified as either kinematic or double diffraction even though only one or two events need be considered to predict their positions.

How well the position (in electron energy) of the diffraction maxima is predicted just by taking single and double diffraction events into account is indicated from the work of Farrell and Somorjai.[6] They have measured the intensities of several diffraction beams [(00), (10), (11), (20) and (22)] from the (100) surface of several face centered cubic metals as a function of electron energy at normal incidence. Under these conditions the diffraction beams with the same indices and the same sign of K's are degenerate. This is one of the simplest conditions which facilitates the analysis of the data since the number of diffraction beams to be considered is much less than under conditions of non-normal

electron beam incidence. First of all they have found that when the intensity data from the different (100) fcc surfaces which were available in the literature were plotted on a "reduced" electron energy scale, $eVd^2\cos^2\theta$, the peak positions for the different materials seem to fall at the same corrected electron energies. This is shown for two different beams in Figs. 8a and 8b. By plotting the data on a "normalized" energy scale (I_{hk} vs. $eVd^2\cos^2\theta$) one can compensate for the variations of the lattice parameter among the metals. Thus, these results indicate that the same diffraction processes are operative in all of the metal surfaces with the same crystals structure and surface orientation. However, the intensities of these peaks vary considerably from material to material presumably reflecting variations in the characteristics of the atomic potentials.

Then Farrell and Somorjai[6] calculated the peak positions which could be predicted by assuming that only single and double diffraction takes place in the (100) surfaces and compared the calculated peak positions with those found by experiments for six different metals (Sl, Pd, Sg, Su, Cu and Ni).

Most of the experimental and calculated values of peak positions showed coincidence within the accuracy of the measurements. This result seems to substantiate that single and double diffraction events are the dominant scattering processes in low energy electron diffraction from fcc metal surfaces.

The double diffraction conditions, $2\vec{K}_z = \vec{G}_z$ appears to be particularly dominant in the electron energy region just above the appearance energy of the diffraction beam under consideration. There also appeared to be a general tendency for diffraction conditions with relatively small

magnitudes of $\vec{G}$ to dominate. As most atomic potentials would favor forward scattering this is physically reasonable.

IV. IMPORTANT PARAMETERS OF THE LOW ENERGY ELECTRON DIFFRACTION EXPERIMENT AND OF THE SURFACE STRUCTURE CALCULATIONS

A. The Inner Potential

A crystalline solid is composed of ordered arrays of atoms which are themselves made up of negative electrons and positive nuclei. These create a symmetrical, but complex, potential which is naturally quite different from that experienced by an incident electron in free space. Consequently, when an incident electron strikes a crystal, the change in potential which it experiences brings about a corresponding change in the De Broglie wavelength of the electron. This increase in the kinetic energy of the electron upon entering the solid is commonly described as being due to the "inner potential". The electron is accelerated as it enters the solid since at interatomic distances the nuclei are only imperfectly shielded by the core and valence electrons. The average inner potential experienced by a primary electron will be dependent upon the energy of that electron as the degree of shielding of the positive nuclei will to some extent, be dependent upon the electron-electron correlation.

If the potential of the crystal is expressed as a fourier expansion $V(\vec{r}) = \Sigma_G V_G e^{-i\vec{G}\cdot\vec{r}}$ then the inner potential is well represented by the first or static term, V_o, in the expansion. This term is essentially the matrix element of the potential taken between identical initial and final eigenstates that represent the incident electron (that is, $V_o = \langle \vec{k}^\circ | V(\vec{r}) | \vec{k}^\circ \rangle$). As the energy of the incident electron changes, its eigenstate will change causing a corresponding change in the value of the matrix element that approximates the inner potential. This

matrix element is the diagonal term of the potential in the secular determinent that describes the interaction of the electron with the crystal. When the determinent is properly diagonalized, other off-diagonal terms will appear along the diagonal and will represent contributions to the effective inner potential experienced by an incident electron. However, as higher order Fourier coefficients are usually at least an order of magnitude smaller than the zeroth order term, these contributions may be regarded as refinements on a reasonable zeroth order approximation.

Pendry has used the pseudopotential approach to calculate the average "inner potential" (i.e. the diagonal matrix element of the potential) for niobium and nickel.[7] In these calculations, the effects of screening, correlation, surface dipole, inelastic and incoherent processes have been neglected on the grounds that at higher energies their contributions will be less than about 2 eV. In Pendry's calculations, the largest contribution to the inner potential came from the Hartree term which includes the effect of the nuclear potentials and an averaged core state contribution. The Hartree contribution, is independent of the primary energy of the incident electrons and is the high energy limit of the inner potential. For nickel, Pendry calculated this term to be about 14 eV and for niobium, about 19 eV. Similar calculations gave a high energy limit of about 12 eV for the inner potential of graphite.

In the range of primary energies intermediate between the Fermi energy and that region where the inner potential approaches the high energy limit (between 50 and 100 eV), the calculated inner potentials for nickel and niobium show considerable energy dependence (Fig. 9-b). They both exhibit a minimum in absolute value that is a consequence of

the partial cancellation of an exchange term and a pseudo-potential term in Pendry's calculations. Although it is of electrostatic origin, the exchange term has no classical analogue. It expresses the difference in the coulomb interaction energy of systems where the electron spins are parallel or anti-parallel and is a consequence of the Pauli exclusion principle.[8] The pseudo-potential term expresses the deviations from a plane-wave nature due to nodes at the atom centers in the eigenfunction of the electron. Both of these terms diminish in importance at higher energies. It is tempting to extrapolate from these calculations the expectation that all materials will have an energy dependent inner potential of minimum absolute value at some energy between the fermi energy and the high energy limit. It is to be hoped that calculations will be performed in the near future for other materials. This information would greatly simplify the interpretation of low energy electron diffraction data.

A large number of experimental estimates have been made of the effective inner potential experienced by an incident electron. One of the recent publications dealing with the problems involved in an accurate experimental determination of inner potential is that by Stern and Gervais.[9] They observed for the (110) face of tungsten by how much a diffraction condition was shifted from its theoretical position calculated with zero inner potential. The difference between the calculated and the observed value was assigned to an inner potential correction. They discuss the necessity of choosing a diffraction condition for which there are no significant multiple reflections. When this condition is not met, then several diffraction conditions may be strongly coupled making the experimental extrication of an average inner potential a difficult and uncertain process.

Further, they have shown that the experimentally determined average inner potential has an effective angular dependence of $1/\sin^2\theta$ leading to large corrections at glancing angles of incidence. Careful measurements far from normal incidence for diffraction conditions that did not excite strong multiple scattering gave a value of 20 eV ± 1 eV for W(110). As all of the measurements were made above 100 eV, this may be taken as the high energy limit for the inner potential of tungsten. Note that this value is commensurate with that calculated for niobium in the high energy limit.

Seah has experimentally determined a value of 14 eV for the inner potential of Ag(11) films of mica in the high energy region.[10] This may be compared with a value of 12 eV determined by Segall[11] and a value of 10 eV at the Fermi surface obtained by adding the work function of silver to its Fermi energy. Other representative values for experimentally determined inner potential corrections are 9 eV for graphite,[12] 16 eV for nickel,[13] 22 eV for nickel,[14] and 11-12 eV for lithium fluoride.[15] Other values are 16 eV for tantalum,[16] between 8-19 eV for vanadium,[17] and 19 eV for iron.[18]

B. The Atomic Scattering Factor

One of the most important parameters which enters into all calculations of surface structure from the intensities of the diffracted low energy electron beams is the amplitude scattered by a single atom in the crystal surface. The scattered amplitude, $V_{\vec{q}}$, is called the form factor or the atomic scattering factor. The amplitude in any given diffraction beam is dependent upon the probabilities that electrons will be scattered out of the primary beam (or other diffraction beams) into that beam from various points in the crystal. These scattering probabilities are dependent upon

the atomic potential. For single scattering events, the scattering amplitude may be regarded in the first approximation as being proportional to the Fourier coefficient of the potential that is characterized by the scattering vector between the initial and the final state of the electron--that is,

$$f_{\vec{q}} \sim \langle \vec{k}' \, | V(r) | \, \vec{k}^{\circ} \rangle = V_{\vec{q}} \tag{12}$$

where $\vec{q} = \vec{k}' - \vec{k}^{\circ}$ is the scattering vector. One of the simplest model potentials used in LEED calculations is the isotropic s-wave scattering potential. With this potential, scattering in all directions has the same probability. While this is a particularly convenient potential to apply in computations, it is rather unrealistic in that most experiments indicate that atomic potentials tend to be forward scattering. That is, on the average, the probability that an electron will be scattered into a new direction that is considerably different from the original direction will be significantly less than the probability that the electron will either continue along its original direction or be deflected through only relatively small scattering angles.

A somewhat more realistic atomic potential that illustrates this forward scattering tendency is the shielded coulombic potential. Here, the positive nuclear charge is regarded as being uniformly shielded by the surrounding electrons and one may write

$$V(\vec{r}) = \frac{Ze^2}{r} \exp[-\lambda r] \tag{13}$$

where Ze^2/r is the nuclear coulombic potential and λ is the "screening length" of the core and valence electrons. Upon Fourier transformation this potential gives form factors of the form

$$V_q = \frac{4\pi e^2 Z}{\lambda^2 + q^2} \tag{14}$$

Note that when the scattering vector, $\vec{q}$, is very small and the electron has only been scattered through a small angle, that Vq will be larger than when q is large and the electron has been back-scattered away from the original direction. As the electron amplitude in any given direction is proportional to the corresponding form factor, it may be seen that forward scattering is more probable than back scattering for such a potential.

It is worth noting that the effective screening length of the electron is dependent upon the energy of the incident electron and actually decreases when the velocity of the scattered electron increases. This is because the core and valence electrons are less effective in shielding the incident electron from the coulombic nuclear charge at higher energies. It may be shown that,

$$\lambda = \frac{4\pi e^2 n}{(2/3)\epsilon_q}\left[1/2 + \frac{4k_f^2 - q^2}{8k_f q}\ln\left|\frac{2k_f + q}{2k_f - q}\right|\right] \qquad (15)$$

where n is the average electron density, e is the charge of the electron, ϵ_f is the Fermi energy k_f is the wave vector.[19] For aluminum, λ is on the order of 2Å below the Fermi surface. Note that the decrease in the screening length with the increase in electron energy increases the relative probability of forward scattering. This is reasonable as one would expect the more energetic electrons to be less easily deflected than those with relatively low velocity.

Although the shielded coulombic potential leads to form factors that are an improvement over those obtained from an isotropic potential, it is still inadequate for an accurate description of low energy electron diffraction. As the electrons in an atom are not arranged uniformly around the nucleus, real form factors will not have as simple a form as that in Eq.14 .

Further, those considerations such as exchange and correlation that contribute to the voltage dependence of the inner potential will also effect the off diagonalmatrix elements of the potential, i.e., the form factors. A detailed consideration of these effects leads to form factors that are not necessarily monotonic functions of the scattering vector or electron energy. The form factors may actually become zero and change in sign under the proper circumstances.

Few calculations have been performed that attempt to calculate the actual form factors from a detailed consideration of the electronic structure of crystals. One of the more promising approaches, is by the psuedo-potential method. Unfortunately, most available pseudo-potential form factors have been evaluated near the Fermi surface and the extension of these calculations to the energy range of interest in LEED has only recently been undertaken.

Figure 10 shows the form factor, f_q for aluminum calculated by Hine and Animalu at the Fermi surface by pseudo-potential method.[20] This may be compared with that calculated from an isotropic s-wave potential and with that calculated from a simple screened coulombic potential. Note that the pseudopotential form factor varies markedly with the magnitude of the scattering vector. However, it still has its largest absolute value in the forward scattering direction.

There is a body of experimental evidence that indicates that there is a considerable amount of structure in the form factor, or atomic scattering factor, for the scattering of low energy electrons. If an electron beam is scattered from a completely random arrangement of atoms, then, to a

first approximation, the intensity is proportional only to the number of scattering centers and to the square modulus of the atomic scattering factor. The spatial disorder of the atoms would preclude any periodic modulation of the intensity as discussed in Section VII. Therefore, if the intensity scattered by a perfectly disordered surface is measured, experimental information may be obtained about the form factors. It is however, very difficult to prepare a solid surface which shows uncorrelated disorder as atoms tend to prefer to be at some average distance from one another. Atomic arrangements that show no long range order may be obtained using liquid surfaces or by depositing amorphous layers of material on foreign substrates.

Experimental Determination of the Atomic Scattering Factor

Goodman and Somorjai have studied the background intensity from low energy electrons scattered from liquid lead, tin and bismuth surfaces.[21] They have found that there are definite non-monotonic intensity variations with both energy and scattering angle that cannot be correlated with the bulk radial distribution function due to density fluctuations in the liquids. These intensity variations are most likely due primarily to variations in the atomic scattering factor.

Lander and Morrison have studied the intensity backscattered from disordered layers deposited on ordered substrates.[22] The possibility of orienting influences and scattering by the ordered substrate materials could conceivably effect their results. Unquestionably, one of the greatest present needs in low energy electron diffraction structure calculations is information, both experimental and theoretical, on the nature of the atomic scattering factors in the energy region of interest.

C. Inelastic Scattering of Low Energy Electrons

An electron may be subjected to several different types of scattering interactions in a crystal. These scattering mechanisms may be classified as being either elastic or inelastic depending upon whether or not the energy of the electron has been changed during the interaction. The elastic mechanisms lead to the usual diffraction phenomena investigated with LEED. The inelastic mechanism are also extremely important in the interpretation of low energy electron diffraction information as inelastic processes are generally far more probable than elastic processes in the energy range where most LEED studies are performed (10 → 500 eV).

The inelastic scattering mechanisms may be further subdivided into two categories: those involving energy loss through coupling into the thermal motions of the atoms in the crystal; and those involving energy loss through electronic excitation of the core and/or the valence or conduction electrons in the crystal. The thermal effects, that is, those involving energy exchange between the electron and the phonons in the crystal, lead to thermal diffuse scattering, the Debye-Waller effect and other related phenomena.[19] These will be discussed later. The electron-electron interactions may be classified according to the types of electrons in the crystal that are excited by the incident electron.

At sufficiently low energies, the incident electrons are not energetic enough to excite the electrons in the core states of the crystal. In this region, the only electronic processes that are important are those involving the valence or the conduction electrons. Here, energy may be lost either by the excitation of a valence electron to a higher state out of the crystal, or by the excitation of plasma oscillations. For incident

electrons with energies less than the plasmon energy, (≈10 eV) inelastic processes are relatively unimportant and the scattering is mostly elastic.

Armstrong finds between 10% and 50% of the electrons back-scattered from tungsten are elastic in the range between 2 and about 16 eV incident beam energy.[24] Lander notes that the total elastic reflectivity averages about 20% for most materials in the region below 10 eV and then drops to about 1% at about 100 eV.[25] This percentage will be considerably less for the lighter elements and more for the heavier elements. At energies above 100 eV, there is, on the average, only a very slow decrease in the fraction of elastically scattered electrons. The percentage of elastically scattered electrons as a function of electron energy is plotted for the (100) face of platinum in a typical LEED experiment in Fig. 11.

The very low energy region (< 5 eV) of high elastic reflectivity is not easily accessible with the conventional commerically available apparatus. The bulk of the investigations of elastic scattering processes have been carried out above 20 eV. At these energies, surface and bulk plasmons may be excited. The energy associated with the surface plasmon mode is about $1/\sqrt{2}$ that for the bulk mode.[26] The probability that an electron will loose energy through excitation of a plasmon mode rises steeply at energies just above the excitation threshold.[27] This probability has a maxima at several times the excitation energy and then decreases slowly at higher energies.

A convenient quantity for characterizing inelastic losses through electron-electron collisions in a crystal is the "mean free path", λ. Quinn has calculated that λ is on the order of 1000Å at 1 eV and falls

rapidly to about 100Å at 3 eV for aluminum. The mean free path for plasmon emission has been calculated to be about 10Å above about twice the excitation energy of the plasmon mode.[27] Recently, Duke and Tucker have performed calculations employing values of 4 and 8Å for electron-electron mean free path lengths.[28]

Figure 12 shows the effect of damping the scattering amplitude with an arbitrary inelastic loss factor of the form $e^{-d/\lambda}$ for several values of λ. It may be seen that the penentration of electrons more than several monolayers into a crystal is severely curtailed by inelastic losses for values of λ less than about 6Å. Though the employment of an inelastic loss factor of the form $e^{-d/\lambda}$ is not mathematically rigorous, it does give some physical insight into the constraint placed on the penetration of an incident electron by inelastic collisions with conduction electrons.

Proceeding to higher energies, the primary electrons eventually become sufficiently energetic to excite the bound electrons in the core states of the atoms in the lattice into higher states. As with the plasmon modes, the probability of exciting these core states rises steeply at energies just above the excitation energy and then reaches a maxima at several times the excitation energy.[29] The probability then decreases very gradually as the primary energy is increased further. The exact value of the probability of exciting a core state will, of course, depend upon the material and the transition under consideration. Similarly, the threshold value for excitation of core states will also depends upon the same considerations, and will range from several electron volts for many elements with filled core states near the fermi surface to several hundred electron volts for elements like flourine with very low lying core states.

Recapitulating, a study of elastically scattered low energy electron from single crystal surfaces necessitiates an understanding of the inelastic scattering mechanism as well. At most electron energies of interest, it is far more probable that an electron will be inelastically scattered rather than elastically scattered. The inelastic scattering mechanism may be classified as being thermal or electronic as the incident electron exchanges energy with the lattice phonons or with the lattice electrons. The electron-electron interactions may be further classified into those processes involving excitation of plasmon modes (either surface or bulk) and those process involving the excitation of individual lattice electrons from either the core or the valence states. The inelastic processes have the effect of reducing the penetration depth of low energy electrons.

D. Temperature Dependence of the Intensity of the Low Energy Electron Diffraction Beams

1. Surface Debye-Waller Factor

Real crystal surfaces are neither perfectly ordered nor ideally flat. Real surfaces are highly irregular on an atomic scale with emerging dislocations, steps, pits, grain boundaries, vacancies and regions where atoms are disordered. The atoms in these surfaces are constantly undergoing thermal vibrations. This section is concerned with the effect of these lattice vibrations on the scattered electron beam intensities; the next section will cover the effect of surface disorder on electron beam intensities.

The main effect of lattice vibrations is to scatter a fraction of the elastically back scattered electrons out of phase. Thus the intensity of

the diffraction beams decrease while the intensity of the background (background in LEED is defined as all the back scattering excluding the diffraction beams) increases. Electrons of energies of about 100 eV, e.g., spend about $2\times10^{-17} \times \ell$ seconds scattering (where ℓ = distance in Å traversed; t = transit time = $\ell\sqrt{m_e/2eV\times}\,(\sqrt{10^{-16}}/1.6\times10^{-12})$ where m_e = mass of electron, eV = electron energy). Since characteristic vibrational frequencies are as "slow" as 10^{-12} seconds, the electron "sees" a disordered "snapshot" of the lattice. However, in the laboratory frame we monitor intensities for times of one-tenth of a second or longer and thus obtain an average of a great number of "snapshots," of the disordered lattice. We can calculate the effect of lattice vibrations on laboratory measurements of intensity. Define an arbitrary atom position at 0°K by a vector $\underset{\sim}{r}$ as shown in Fig. . At any finite temperature the atom will be displaced by an amount $\underset{\sim}{u}(t)$, a time-dependent function. In the kinematic approximation the scattered intensity from an array of such scattering centers is

$$I = |f|^2\left\{\sum_{\ell\ell'} \exp\left[i\,(\vec{k}'-\vec{k}^\circ)\cdot(\vec{r}_\ell - \vec{r}_{\ell'}) + i(\vec{k}'-\vec{k}^\circ)\cdot(\vec{u}_\ell - \vec{u}_{\ell'})\right]\right\} \qquad (16)$$

where we are summing over all pairs of scattering centers ℓ, ℓ'.[30] Only the first term in the exponential would appear for a static lattice.

Without any loss of generality we can expand the displacements in a complete set of the normal lattice mode coordinates:[31]

$$\vec{u}_\ell(t) = \sum_{qj} \underset{\sim}{\vec{u}}_{qj}\, a_{qj} \cos\left(\omega_{qj}\, T - \vec{q}\cdot\underset{\sim}{\vec{r}}_\ell - \psi_{qj}\right) \qquad 17 \qquad (17)$$

where the summation is over all the lattice modes q and polarizations, j. The u_{qj} are unit vectors in the direction of the phonon of wave vector, $\underset{\sim}{q}$ of frequency ω_{qj}, amplitude a_{qj}, and arbitrary phase angle ψ_{qj}.

Following the derivation given by James,[30] for x-ray diffraction, the effect of this "phonon" scattering on the scattering intensity can be determined. The assumptions used in this calculation are: (1) the ergodic hypothesis, i.e. that the time average over all the thermal motions (what is actually observed experimentally) is equivalent to an esemble average of the thermal motions. (2) That thermal motions are symmetric, i.e., that the net (or average) motion along any coordinate is zero. (3) That the thermal motions are small. The result of James' calculations is:

$$I = |F_{hk\ell}|^2 e^{-2W} - |\mathbb{F}|^2 e^{-2W} \sum_{\ell\ell'} 2 \cos \{\vec{q}\cdot(\vec{r}_\ell - \vec{r}_{\ell'})\} \exp i\vec{\Delta k}\cdot(\vec{r}_\ell - \vec{r}_{\ell'}) \tag{18}$$

where $|F_{hk\ell}|^2$ is the kinematic diffraction intensity for a perfectly ordered lattice, 2W is the so called Debye-Waller factor and is equal to $\Sigma q \; |\Delta \underset{\sim}{k}\cdot\underset{\sim}{u}_q|^2$ where $\Delta\underset{\sim}{k}$ is the scattering vector.

In the high temperature limit of the Debye model[1932] ($T > \theta_D$) the mean square displacement is given by

$$\langle u^2 \rangle = \frac{3N\hbar^2}{Mk} \cdot \frac{T}{\theta_D^2}, \tag{19}$$

where N = Avogadro's number, $\hbar$ = Planck's constant divided by 2π, k = Boltzmann's constant, M = atomic mass in grams, T = K°, θ_D = Debye temperature. For the specularly reflected beam, $|\Delta\underset{\sim}{k}|^2 = k^2 \cos^2\psi = 4\pi^2/\lambda^2 \cos^2\theta$, thus

$$-2W = \frac{16\pi^2 \cos^2\phi \langle u^2\rangle}{\lambda^2} = \frac{12N\hbar^2}{Mk} \cdot \frac{\cos^2\phi}{\lambda^2} \cdot \frac{T}{\theta_D^2} \tag{20}$$

or, (by substitution of $\lambda = \sqrt{150.4/eV}$ and collecting constants),

$$\exp_{10}(-2W) = \exp_{10} \frac{-KVT \cos^2\phi}{M\theta_{D,EFF}^2}, \quad K = \text{const.} = 66.6 \; \frac{g°K}{\text{mole eV}}, \tag{21}$$

where ϕ = angle of incidence, and $\theta_{D,EFF}$ = effective Debye temperature.

Equation (21) combined with (18) suggests that at a given beam voltage and angle of incidence the intensity of a diffraction feature decreases as an exponential function of temperature. From this result an effective Debye temperature for the atoms involved in the scattering can be derived. From results using LEED[32,33,34] the value of θ_D for the surface layers are smaller than for bulk layers. However, as indicated in Section VI.2., LEED samples an increasing amount of the bulk as the energy increases. Thus at different voltages, the beam penetrates a different number of layers and the measured Debye temperature which we designate as $\theta_{D,EFF}$ is some average of the surface and bulk layers. In the limit of low voltages $\theta_{D,EFF} \rightarrow \theta_D$, surface and at high voltages $\theta_{D,EFF} \rightarrow \theta_{D,BULK}$. Studies of $\theta_{D,EFF}$ as a function of beam voltage provide a means of studying the surface dynamics of crystals. However, one must be very cautious in applying Eq. 21 . First, the use of the Debye model may not be appropriate to describe the surface motions where anharmonic effects could be large. Second, the second term in Eq.18 , usually referred to as the thermal diffuse scattering, must be evaluated. For certain values of "2W" the effect of the thermal diffuse scattering on the Debye-Waller results may be significant.

Maradudin[35] has evaluated the cubic and quartic contributions to anharmonic motion and their effect on the Debye-Waller factor. He obtains the result:

$$2W = \frac{16\pi^2 \cos^2 \phi \, \alpha_o^2}{\lambda^2} \cdot \frac{T}{\theta_\infty} \cdot 1.861\times10^{-4} \left[1 + 0.0483 \frac{T}{\theta_\infty}\right] \quad (22)$$

where α_o = lattice parameter and θ_∞ is a parameter determined independently in Maradudin's model. Using lead as an example, $\alpha_o = 4.95\text{Å}$, $\theta_\infty = 143.4°K$. One may fit his value for 2W into the form of Eq. 21 if a temperature dependent θ (T) is defined as

$$\frac{1}{\theta_D^2(T)} = \frac{Mk\,\alpha_o^2}{Nh^2\,\theta_\infty}\; 0.6205\times10^{-4}\left[1 + 0.0483\;\frac{T}{\theta_\infty}\right] \qquad (23)$$

Using the values for Pb, this becomes:

$$\frac{1}{\theta_D^2(T)} = \frac{1}{154\,(143.4)}\left[1 + 0.0483\;\frac{T}{143.4}\right] \qquad (24)$$

which for $T \sim \theta_\infty$, gives $\theta_D \sim \theta_\infty$. Maradudin's model indicates that anharmoniceffects should be expected to increase linearly with temperature (being about 9% anharmonic at 0°C and about 20% at the melting point) and that to first order anharmonicity only affects the magnitude of the θ_D but not the form of the Debye -Waller factor.

Another effect which is important in LEED studies of the Debye-Waller factor is the second term in Eq. 18 called the thermal diffuse scattering. Thermal diffuse scattering arises from the independence of the phonon modes from each other. Webb et al.[36] have shown that the thermal diffuse scattering intensity, the second term in Eq. 18 is (let I_2 = second term):

$$I_2 = \frac{|fo|^2}{4}\; e^{-2W}\left[2W\; I_o\;(\vec{\Delta k} \pm \vec{q})\right] \qquad (25)$$

where $|I_o(\Delta\underset{\sim}{k})|^2 \cdot |fo|^2 = |F_{hk\,\ell}|^2$; i.e., $I_o\,(\Delta\underset{\sim}{k})$ is referred to as the interference function and is non-zero only where the argument, $\Delta\underset{\sim}{k} = \underset{\sim}{G}$, a reciprocal lattice vector. From Eq. 25 , I_2 has significant magnitude only where $\Delta\underset{\sim}{k} \pm \underset{\sim}{q} = \underset{\sim}{G}$. Webb[36] shows that the thermal diffuse intensity

falls off in a manner inversely proportional to the distance in reciprocal space from the nearest reciprocal lattice rod. Studying the ratio R of the thermal diffuse intensity to the kinematic intensity Webb finds $R = 2W/4\ (1+\Delta)$ where Δ is a small correction factor, less than unity, and of order $|\underset{\sim}{q}|^2 / |\underset{\sim}{G}^2|$ which decreases to zero for large $|\underset{\sim}{G}|$.

2. Effect of Multiple Scattering

We have, thus far, neglected multiple scattering effects, though they are definitely prominent, especially at low energies. Work in this laboratory[6] indicates that the double diffraction mechanism is the most likely. Figure 14 indicates a possible double diffraction process. An incident beam $\underset{\sim}{k}_o$ making an angle ϕ with the normal to the surface may scatter in two ways: part of the beam is specularly reflected into the beam $\underset{\sim}{k}$, another part scatters into vector $\underset{\sim}{k}_1$. The angle between $\underset{\sim}{k}_o$ and $\underset{\sim}{k}_1$ is 2ϕ. The $\underset{\sim}{k}_1$ beam may then be rescattered into $\underset{\sim}{k}_2$ beam (actually identical to $\underset{\sim}{k}$) where the angle between $\underset{\sim}{k}_1$ and $\underset{\sim}{k}_2$ is $2\phi_2$. From simple geometrical considerations: $\Delta\underset{\sim}{k} = \Delta\underset{\sim}{k}_1 + \Delta\underset{\sim}{k}_2$. Physically, the constructive interference between $\underset{\sim}{k}_2$ and $\underset{\sim}{k}$ could contribute to a diffraction maxima. The Debye-Waller factor for the double scattered case is:

$$2W = \frac{C_{VT}}{2M}\left[\frac{\cos^2\phi}{\theta_D^{\,2}} + \frac{\cos^2\phi_1}{\theta_{D_1}^{\,2}} + \frac{\cos^2\phi_2}{\theta_{D_2}^{\,2}}\right] \qquad (26)$$

where θ_{D_n} refers to the effective Debye temperature for thermal motions in the direction $\Delta\underset{\sim}{k}_n$. Comparing Eq. 21 and Eq.26 , if

$$\frac{\cos^2\phi_1}{\theta_{D_1}^2} + \frac{\cos^2\phi_2}{\theta_{D_2}^2} = \frac{\cos^2\phi}{\theta_D^2} \qquad (27)$$

then the results interpreted in terms of kinematic diffraction would be in agreeement with this dynamical result. Assuming $\theta_D = \theta_{D_1} = \theta_{D_2}$ this condition is met whenever $\phi = 0°$. However, for ϕ near $0°$ and $\theta_D \sim \theta_{D_1} \sim \theta_{D_2}$, the most usual case experimentally, the results interpreted in terms of kinematic diffraction do not significantly differ from the dynamical result. But, especially at lower energies, where the differences in surface and bulk θ_D's are most significant and at large angles of incidence, the interpretation of Debye-Waller experiments not allowing for multiple scattering effects could lead to discrepancies. The problem is tractable, however, since dynamical theory does predict the exact multiple diffraction mechanisms applicable and by a form of iterative procedure the θ_{D_n}'s could be determined.

V. COMPUTATIONAL PROCEDURES TO EVALUATE THE SCATTERED LOW ENERGY ELECTRON BEAM INTENSITIES

From the preceding considerations, we see that the geometry of the scattered beams is uniquely defined by the dimensions and two-dimensional symmetry of the crystal surface, and by the energy and angle of incidence of the primary beam. Further, we now know that intensity maxima may appear in these diffraction beams when certain diffraction conditions are met. However, the relative magnitude of these intensity maxima and their precise relationship to the chemical nature and exact positions of the scattering centers can only be determined through a more quantitative investigation of the scattering phenomena.

There are a number of different approaches currently popular in the literature, but they all involve, either explicitly or implicitly finding a solution in some degree of approximation, to the Schoedinger equation. It should be emphasized that while many of these approaches appear formalisitically different, they are all concerned with the same physical phenomena. They differ primarily in their viewpoint and in the nature of their approximations. The current literature on theoretical calculations of the intensity of LEED beams may be roughly subdivided into two parts on the basis of their starting points.

The first group begins with the differential form of the Schroedinger equation

$$(\nabla^2 + K^2)\, \psi\, (\vec{r}, \vec{K}) = u(\vec{r})\, \psi\, (\vec{r}, \vec{K}) \qquad (28)$$

where K is the magnitude of the wave vector, and $u(\vec{r})$ is $2m/\hbar^2$ times the potential. In general, both the potential and the eigenfunction are expanded in a Bloch or Fourier series and the resulting set of linear

inhomogeneous equations are then solved for the coefficients of the eigenfunctions. Frequently, these solutions are obtained for the eigenfunctions within the crystal and those in free space are determined by matching $\psi(\vec{r},\vec{K})$ and its first derivative at the surface. Variations on this approach have been employed by Hirabayaski and Takeishi,[37] Boudreaux and Heine,[4] Hoffman and Smith,[38] Jepsen and Marcus,[5] and Ohtsuki[39] among others. Historically, this method, has its roots in the works of Bethe[40] and Von Laue.[41]

The second basic approach begins with th e integral form of the Schroedinger equation

$$\psi(\vec{r},\vec{K}) = \psi^{\circ}(\vec{r},\vec{K}) - 1/4\pi \int_{r'} G(\vec{r},\vec{r}') \, u(\vec{r}') \, \psi(\vec{r},\vec{K}) \, d^3 r' \tag{29}$$

where $\psi^{\circ}(\vec{r},\vec{K})$ is the incident beam, $G(\vec{r},\vec{r}')$ is a Greens function and $u(r')$ is the potential defined above. An excellent description of the transformation of the differential form of the Schroedinger equation to its integral form is given by Merzbacher.[42] The effect of the integral operator, $\int_{\vec{r}'} d^3 r' \, G(\vec{r},\vec{r}') \, u(\vec{r}')$ on the eigenfunction $\psi(\vec{r}',\vec{K})$ may be regarded as a projection or an evolution of this eigenfunction from a point $\vec{r}'$, to another point $\vec{r}$. As the solution appears also on the right hand side of Eq.29 under the integral sign, an iterative procedure is often followed. Alternatively, the quantities involved in the integral may be expanded in some appropriate basis set, such as partial waves, the integral solved, and the resulting set of coupled linearly dependent equations resolved as in the case of the differential Schroedinger equation approach. The integral equation, or Greens' function, approach has been utilized by McRae,[43] Kambe,[44,45] and Beeby[46] among others. Historically

it is similar to the dynamical theory of x-ray diffraction developed by Darwin.[47]

Regardless of the starting point, there are several basic assumptions employed by most authors. The first is that the incident or primary beam of electrons may be represented as a plane wave. As the actual wave is presumably coherent for hundred to thousands of Angstroms,[3] this is probably not a bad approximation.

The second assumption is that the crystal has perfect periodicity parallel to the surface. The degree of perfection required perpendicular to the surface varies from paper to paper. The neglect of the existence of ledges and other surface imperfections is not important in a qualitative discussion though there is some evidence that surface damage can change the results in actual situations.[3]

It is frequently assumed that the electrons that are elastically scattered into the region exterior to the crystal are contained in a number of discrete beams whose wave vectors are defined by Eqs. 5 and 7. While this is definitely true far away from a scattering center, it is not necessarily true in the immediate vicinitty thereof. However, calculations performed by McRae[43] for the case of isotropic scatterers indicate that deviations from a plane wave nature may be negligible.

Further, the lattice is generally assumed to be static. This assumption is not valid except perhaps for those materials having a large atomic weight and a high Debye temperature.

Inelastic scattering is usually either ignored, or considered as simple a basis as possible. When considered, it is usually represented as atomic excitations and collective phenomena, such as plasma resonances,

are usually neglected. The lack of a detailed consideration of inelastic scattering is somewhat damgerous, particularly as it is frequently the dominant scattering mechanism.[25]

The last assumption is that the scattering is non-relativistic. This is a reasonably good assumption for low energies and light atoms, but further investigation into its validity under other situations is necessary. From the first assumption, we may write the incident beam as

$$\psi^{\circ}(\vec{r},\vec{K}) = e^{i\vec{K}^{\circ}\cdot r} \tag{30}$$

From the second assumption, that of perfect two dimensional periodicity parallel to the surface of the crystal, we may express the potential of the crystal as a Fourier expansion

$$u(\vec{r}) = \Sigma_{G\|} \; V_{G\|}(z) \; e^{-i\vec{G}_{\|}\cdot\vec{r}_{\|}} \tag{31}$$

where $\vec{G}_{\|}$ is a reciprocal lattive cector parallel to the surface and z is the coordinate perpendicular to the surface. There are several alternate expressions for $V_{G\|}(z)$ which will be used below. The first is in the limit of perfect three dimensional periodicity,

$$V_{G\|}(z) = \Sigma_{G\perp} \; V_G \; e^{-i\vec{G}_{\perp}\cdot\vec{z}} \tag{32}$$

where $\vec{G}_{\perp}$ is some reciprocal lattice vector perpendicular to the surface and $\vec{G} = \vec{G}_{\|} + \vec{G}_{\perp}$. This expansion will be used in the x-ray or kinematic limit, and for the matching calculations.

The second expansion of $V_{G_{\|}}(z)$ is an integral Fourier expansion

$$V_{G_{\|}}(z) = \int_{-\infty}^{+\infty} d\gamma \; V_G \; e^{-i\vec{\gamma}\cdot\vec{r}}$$

where $\vec{G} = \vec{G}_{\|} + \vec{\gamma}$ and $\vec{\gamma}$ is some continuously varying parameter in the z direction. This expression is useful near the surface where the periodicity in the z idrection is weak or non-existant. Further, when the

potential is expressed as a sum of scattering centers

$$u(\vec{r}) = \sum_s W_s (\vec{r} - \vec{R}_s) \tag{34}$$

where the summation is either over layers, or atomic sites, then

$$u(\vec{r}) = \sum_{G,s} W_{s,G} \, e^{-i\vec{G}\cdot(\vec{r}-\vec{R}_s)} \tag{35}$$

and

$$V_G = \Sigma_s \, W_{s,G} \, e^{+i\vec{G}\cdot\vec{R}_s} \tag{36}$$

where the summation over G can be taken to formally include an integration over γ. This expansion is important when there are two or more atoms per unit cell. Below, the structure factor terms, $e^{i\vec{G}\cdot\vec{R}_s}$, will usually be carried implicitly in V_G, which may also contain the Debye-Weller factor.

Another result of the second assumption is that like the potential the wave function may be expressed as a Fourier expansion

$$\psi(\vec{r},\vec{K}) = \Sigma_{G\|} \, f_{G\|}(z) \, e^{i(\vec{K}^\circ_\| + \vec{G}_\|)\cdot\vec{r}_\|} \tag{37}$$

This is a result of Bloch's theorem for two dimensional periodicity. As for $V_{G\|}(z)$, $A_{G\|}(z)$ may be expressed as a discrete or continuous Fourier expansion as the situation warrents. Again $\vec{G} = \vec{G}_\| + \vec{G}_\perp$ or $\vec{G} = \vec{G}_\| + \vec{\gamma}$ will be used, and Σ_G will be taken to contain an implicit summation over $\vec{G}_\perp$ or integration over γ as is appropriate to the circumstances. With this is mind, we may write

$$\psi(\vec{r},\vec{K}) = \Sigma_G \, f_G \, e^{i(\vec{K}^\circ+\vec{G})\cdot\vec{r}} \tag{38}$$

It is instructive to consider the calculational procedures in the limit of negligible multiple scattering. More extensive calculations must reduce to these solutions for very small cross sections and these results serve as a basic frame of reference within which multiple scattering phenomena may be discussed. In addition, general techniques can be outlined with a minimum of detail.

In the kinematic limit, when multiple scattering is insignificant, it may be assumed that the electron has a much greater probability of being found in the primary, or transmitted beam than in any other. In addition it may be assumed that the electron penetrates deeply enough into the crystal to experience its full three dimensional periodicity, and that surface effects are negligible. We therefore may use the three dimensional expansion of the potential and wave function.

Substituting Eqs. 31, 32 and 38 into the differential form of the Schroedingers equation, there results

$$(\nabla^2 + K^2) \; \Sigma_G A_G \; e^{i(\vec{K}^\circ+\vec{G})\cdot r} = \Sigma_{G''} V_{G''} e^{-\vec{G}\cdot\vec{r}} \times \Sigma_{G'} f_{G'} e^{i(\vec{K}^\circ+\vec{G})\cdot\vec{r}} \tag{39}$$

which becomes

$$\Sigma_G \{(K^2 - |\vec{K}^\circ + \vec{G}|^2) \; f_G - \Sigma_{G'} V_{G'-G'} f_{G'}\} e^{i(\vec{K}^\circ+\vec{G})\cdot\vec{r}} = 0. \tag{40}$$

As the function $e^{i(\vec{K}^\circ+\vec{G})\cdot\vec{r}}$ form a linearly independent basis set, we need only consider the set of equations

$$(K^2 - |\vec{K}^\circ+\vec{G}|^2) \; f_G - \Sigma_G V_{G'-G} f_{G'} = 0 \tag{41}$$

In this limit, it is not necessary to solve simultaneously this total set of equations in order to determine the amplitudes, $_G$, as we have made the assumption that $f_0 \gg f_G$. Therefore Eq. 41 becomes

$$(K^2 - |\vec{K}^\circ+\vec{G}|^2 - V_0) \; f_G - V_G \; f_0 = 0 \tag{42}$$

or

$$f_G = \frac{V_G}{(K^2 - |\vec{K}^\circ+\vec{G}|^2 - V_0)} \; f_0 \tag{43}$$

This is essentially the x-ray result, that the amplitude of the various diffraction beams is proportional to a Fourier coefficient in the expansion of the potential.

We obtain a similar result by using the integral equation approach. There, assuming that $f_0 \gg f_G$ is the same as making the first Born approximation. That is, we may substitute $\psi^\circ(\vec{r},\vec{K})$ for $\psi(\vec{r},\vec{K})$ under the integral sign on the right hand side of Eq. 29 . Making this approximation and substituting Eq. 31 and 32 into Eq. 29 we obtain

$$\psi(\vec{r},\vec{K}) \cong -\int_{\vec{r}'}\int_{\vec{K}'} d^3K' \frac{e^{i\vec{K}'\cdot(\vec{r}-\vec{r}')}}{|\vec{K}'|^2 - |\vec{K}^\circ|^2} \sum_G V_G e^{-i\vec{G}\cdot\vec{r}} e^{i\vec{K}^\circ\cdot\vec{r}'} d^3r' \tag{44}$$

where the spectral form of the Greens function is used (see the following section). Utilizing the following two equations

$$\int_{\vec{r}} e^{i\vec{Q}\cdot\vec{r}} d^3\vec{r} = \sigma(\vec{Q}); \quad \vec{Q} = \vec{K}^\circ - \vec{G} - \vec{K}' \tag{45}$$

and

$$\int_{\vec{K}'} d^3K' \frac{e^{i\vec{K}\cdot\vec{r}}}{|\vec{K}'|^2 - |\vec{K}^\circ|^2} \delta(\vec{K}',\vec{K}2-\vec{G}) = \frac{e^{i(\vec{K}^\circ-\vec{G})\cdot\vec{r}}}{|\vec{K}^\circ-\vec{G}|^2 - |\vec{K}^\circ|^2} \tag{46}$$

we obtain.

$$\psi(\vec{r},\vec{K}) = \Sigma_G \frac{V_G}{|\vec{K}^\circ|^2 - |\vec{K}^\circ - \vec{G}|^2} e^{-i(\vec{K}^\circ-\vec{G})\cdot\vec{r}} \tag{47}$$

where, by a comparison with Eq. 38 and 43 it may be seen that the relative amplitudes are identical with those from the differential form of the Schroedinger equation.

1. Differential Equation Approach

One of the earliest non-kinematic LEED calculations was performed by Hirabayashi and Takeishi.[37] They used the differential equation approach in an extension of Von Laue's[41] dynamical theory. An explicity accounting

of the termination of the crystal periodicity at the surface was made by utilizing the forms for the potential and wave function given in Eqs.31 and 37 . This set of coupled first order differential equations in $f_{G\|}(z)$ could conceivable be solved for the amplitudes of the various diffraction beams. However, Kirabayashi and Takeishi did not attempt a completely self consistent solution, but rather made the approximation $|f_G(z)| \gg |f_G(z)|$ i.e. that the intensity of the incident beam is much stronger than that of any of the diffracted beams. Numerical calculations were performed for the specularly reflected beam in the case of graphite and were compared with experimental results. The agreement is not bad in the region above 100eV but becomes progressively worse at lower voltages. This is not unexpected as the approximation $|f_0(z)| \gg |f_G(z)|$ becomes less valid at lower energies. This paper is of significance as it was the first to attempt a dynamical treatment of lowenergy electron diffraction. Not only did it illustrate that reasonable agreement with experimental data could be obtained at higher energies by considering only a limited number of beams, but it further underlined the fact that the amplitudes of the diffracted beams are not negligible relative to that of the transmitted beam in the very low energy region. The condition that $f_G(z) \sim f_0(z)$ is precisely that which is associated with multiple scattering, and it is this condition which necessitates a more self consistent treatment of the problems.

A related but more complete method has gained considerably popularity recently, particularly among the solid state physcis. This is the wave matching approach where the wave equation is first solved within the perfectly infinite crystal and then the eigenfunctions outside of the crystal

are determined by matching these wave functions and their normal derivatives at the surface. In this approach, the primary problem is identical with that of determining the energy band structure within the crystal, but only for that energy and that component of the wave vector, K, parallel to the surface which characterize the incident beam. This method has the advantage that it may draw upon much of the knowledge accumulated about energy band calculations. It is particularly applicable to uncontaminated and unreconstructed surfaces, and leads to a clear insight into the relationship between reflected intensities and the band structure of the solid. The wave function inside the solid may be expressed as a linear combination of the Bloch functions for the perfect bulk crystal, as in Eq. 38 . The first phase of the problem within the framework of this approach is to solve the wave equation within the crystal. Inserting equations 31 , 32 , and 38 into the differential form of the Shcroedinger equation, there results

$$(\nabla^2 + K^2) \sum_G f_G e^{i(\vec{k}+\vec{G})\cdot\vec{r}} = \sum_{G''} V_{G''} e^{-i\vec{G}''\cdot\vec{r}} \times \sum_{G'} f_{G'} e^{i(\vec{k}+\vec{G}')\cdot\vec{r}} \qquad (48)$$

which, upon performing the indicated differentitation and then rearranging becomes

$$\sum_G (K^2 - |\vec{k}-\vec{G}|^2 - V_0) f_G - \sum_{G'\neq G} f_{G'} e^{i(\vec{k}+\vec{G})\cdot\vec{r}} = 0 \qquad (49)$$

or, as the traveling wave terms, $e^{i(k+G)\cdot r}$, are linearly independent

$$(K^2 - |\vec{k}-\vec{G}|^2 - V_0) f_G - \sum_{G'\neq G} V_{G'-G} f_{G'} = 0 \qquad (50)$$

This set of linearly dependent equations in the amplitudes, f_G, has solutions if and only if the secular determinent is equal to zero, i.e.

$$\begin{vmatrix} (K^2 - |\vec{k}-\vec{G}_{11}|^2 - V_0) & - V_{G_{12}} \; - \; - \; - \\ -V_{G_{21}} & (K^2 - |k-G_{22}|^2 - V_0) \\ \vdots & \end{vmatrix} = 0 \qquad (51)$$

The relative values of the amplitudes f_G, may be determined as cofactors of the secular matrix,[48] and their absolute values then determined from the normalization condition

$$\Sigma_G \; |f_G|^2 = 1. \qquad (52)$$

Again, the above solution is essentially identical with that for an energy band problem with the exception that those solutions which attenuate or are damped, are also considered.

The second phase of the problem is to match the wave function and its first derivative with respect to the surface normal within the crystal to that wave function and its derivative that are exterior to the crystal. In this manner, the amplitude of the diffracted beams in free space may be determined. The matching equations are

$$\psi(\vec{r},\vec{K}) = \psi_B(\vec{r},\vec{K}); \quad z < z_s \qquad (53a)$$

$$\psi(\vec{r},\vec{K}) = \psi_E(\vec{r},\vec{K}); \quad z > z_s \qquad (53b)$$

$$\psi_B(\vec{r},\vec{K})|_{\vec{z}=\vec{z}_s} = \psi_E(\vec{r},\vec{K})|_{\vec{z}=\vec{z}_s} \qquad (54)$$

and

$$d\psi_B(\vec{r},\vec{K})/dz|_{\vec{z}=\vec{z}_s} = d\psi_E(\vec{r},\vec{K})/dz|_{\vec{z}=\vec{z}_s} \qquad (55)$$

$\psi_B(\vec{r},\vec{K})$ is the wave function in the bulk of the crystal, $\psi_E(\vec{r},\vec{K})$ is that exterior to the crystal, and $\vec{z}_s$ is the coordinate of the crystal surface.

The simplest case, the two beam case at normal incidence where only the transmitted and the specularly reflected beams are allowed, has been discussed in detail by Boudreaux and Heine.[4] The development is as follows. Within the crystal, the Bloch function is given by

$$\psi_B(\vec{r},\vec{K}) = f_0 e^{i\vec{K}\cdot\vec{r}} + f_{2k} e^{i(\vec{K}-\vec{G}_\perp)\cdot\vec{z}} \qquad (56)$$

where K is given by Eq.51 . When $\vec{K} = \vec{G}_\perp/2$, we are at the end of a Brillouin zone and consequently in an energy gap. For the smallest $G_\perp$ this corresponds to the first Bragg reflection. Away from the gap, the wave function within the crystal is predominantly that of a traveling wave direction into the crystal, and $f_0 > f_{2k}$. The coefficient of the back reflected wave, $f_{G_\perp}$, is given, to a first order, by Eq.43 for the kinematic case.

However, within the band gap the waves are strongly coupled and a simple perturbation approach is no longer valid. It may be shown that within the gap, f_0 and f_{2k} have the same magnitude, and differ at most only by a phase factor, 2ϕ, i.e.

$$|f_0| \; e^{+i\phi} = |f_{2k}| \; e^{-i\phi} \qquad (57)$$

where ϕ varies from 0 to + $\pi/2$ from one edge of the gap to the other.[4] The sign of ϕ depends upon the sign of $V_{G_\perp}$. Further, at energies inside of the gap, there are no corresponding real values of K. This is a direct consequence of Eq.51 and has the physical significance that there are no traveling waves allowed within the crystal at these energies. There are, however, complex values of K that are allowed that correspond to evanescent or damped waves that are localized at the surface of the crystal. It follows then that

$$\vec{k} = \vec{K}_R + i\vec{K}_M \tag{58}$$

where $\vec{K}_M$ is the imaginary part of $\vec{k}$ and $\vec{K}_R$ is the real part. $|\vec{K}_R|$ is equal to $|\vec{G}_\perp|$ within the gap and $|\vec{K}_M|$ is zero at the edges of the gap. Within the gap, the Bloch function inside of the crystal is

$$\psi_B(\vec{r},\vec{K}) = |f|\, e^{i\phi}\, e^{-K_M z}\, e^{i\vec{G}_\perp\cdot\vec{z}/2} + e^{-i\phi}\, e^{-K_M z}\, e^{i\vec{G}_\perp\cdot\vec{z}/2} \tag{59a}$$

$$\psi_B(r,K) = |f|\, e^{-K_M z} \cos\,(G_\perp\cdot z/2+\phi) \tag{59b}$$

The wave function outside of the crystal is

$$\psi_E(\vec{r},\vec{K}) = e^{i\vec{K}^\circ\cdot\vec{z}} + f'_{2k}\, e^{-i\vec{K}^\circ\cdot\vec{r}}$$

By matching ψ_B and ψ_E and their first derivatives at the surface, the value of f'_{2k}, the amplitude of the specularly reflected beam may be determined. It is found that $|f'_{2k}|$, the magnitude back reflected amplitude, is equal to unity. This is not unexpected as all of the electrons striking the crystal must be back reflected at energies within the band gap as there are no allowed travelling waves within the crystal in this region. When inelastic scattering is taken into account, $|f'_{2k}|$ of course will be less than unity. As the band gap is of width V_G, it follows that, to a first approximation this also will be the width of the Bragg peak. Similar arguements hold at higher beam voltages and for other diffraction beams. Consider the case where a higher order diffraction beam charcterized by $\vec{K}' = \vec{K}'_{\|} + \vec{K}'_\perp$ mets a diffraction condition of the form

$$2\vec{K}'_\perp = \vec{G}_\perp \tag{61}$$

The higher order diffraction beam will behave in a similar manner to the specularly reflected beam discussed above. At this point, there is a band gap, and no traveling waves with K' are allowed in the crystal.[4] Consequently, the electron must be either reflected out of the crystal or, alternatively, scattered into some beam for which there is an allowed state. Actual calculations have been perfor med using variations on this wave matching technique. Hoffman and Smith[38] have applied this approach to the problem of calculating the intensities of the (00), (01) and (11) diffraction beams from the (100) face of aluminum at normal incidence. They used a 27 term Fourier expansion of the potential with a 10 eV inner potential correction and a constant 2.5 volts imaginary part of the potential to simulate inelastic scattering. In addition to Bragg peaks predicted by kinematic theory, they found secondary peaks associated with multiple scattering phenomena. While the agreement with experimental data is imperfect, it does illustrate the validity of this approach for real problems.

Model calculations using the wave matching approach have been performed by Carpart[49] and by Marcus and Jepsen[5] for simple cubic crystals. Marcus and Jepsen effected the solution of the one-dimensional linear differential equations

matrix. They used a potential of point ions of charge Z in a sea of uniform negative charge. The calculations were performed for non-normal incidence. Their published results show both the band structure and the reflected intensities. The strong correlation between the band structure and the intensities is quite obvious. The several types of multiple scattering phenomena discussed above are well represented.

Carpart has used a pure wave matching approach. His calculations are particularly important as they were performed for a cubic ensemble of S-wave scatterers. This same model potential was used by McRae[43] in the first self consistent dynamical LEED calculations using the integral equation approach. The strong agreement between the results of these two approaches substantiates their fundamental similarities. It is of interest to note that while the S-wave scatterer potential is an easy model in the integral equation approach, it is a particularly difficult model within the differential equation approach. This is because all of the Fourier coefficients have the same magnitude and consequently, a large number of terms must be carried. Consequently, the claim is made that the achieved agreement constitutes rather important evidence that the method can be used for real situations. Carpart's work also includes a band structure calculation and, again, there is a definite relationship between the band structure and the beam intensities.

Recently, Pendry has used the pseudopotential method and the wave matching approach to calculate intensities for niobium and nickel that show a fair agreement with the experimental data.[7] This is one of the few calculations where a realistic potential has been employed and promises to be one of the more fruitful approaches.

The reader is referred to a review article by Boudreux, Perry and Stern for a more detailed discussion of the differential equation approach.[50]

2. Integral Equation Approach

While the differential form of the Schroedinger equation has been employed in a number of different approaches that are related to the determination of the band structure of solids, the integral form is conceptually more concerned with the scattering mechanisms from a number of different scattering centers. Further, the previous approach is most easily handled when the crystal has perfect three dimensional symmetry right up to the surface, while the following method initially assumed nothing about the periodicity of the system in the direction normal to the surface.

Assuming the potential to be formally expressible as a sum of individual scattering centers as in Eq.34 , the integral form of the Schroedinger equation becomes a sum of integral equations

$$\psi(\vec{r},\vec{K}) = \psi^{\circ}(\vec{r},\vec{K}) - 4\pi \sum_{s} \int_{\vec{r}'} G(\vec{r},\vec{r}')\, W_{s}(\vec{r}'-\vec{R}_{s})\psi(\vec{r}',\vec{K}')\, d^{3}r' \quad (62)$$

where, if all of the centers are identical, only one integral need be evaluated. The formal solution is now independent from the total symmetry or lack thereof, of the problem. However, as most LEED problems do have a two dimensional symmetry parallel to the surface, it is useful to introduce this as it results in some simplification of the problem. This symmetry is explicitely assumed when Eqs.35 and 38 for the potential and the wavefunction are substituted into Eq. 62 which then becomes

$$\psi(\vec{r},\vec{K}) = \psi^{\circ}(\vec{r},\vec{K}) - 4\pi \sum_{g,g'} \int_{\vec{r}'} \left[G(\vec{r},\vec{r}')\, V_{g-g'}(z')\, e^{-i(\vec{g}-\vec{g}')\cdot\vec{r}'\|} \times f_{g'}(z') e^{i(\vec{K}^{\circ}\|+\vec{g}')\cdot\vec{r}'\|}\, d^{3}r' \right] \quad (63)$$

Here, g has been used to indicate $G_{\|}$ in order to avoid confusion with the Green's function $G(r,r')$. The terms of the structure factor, $e^{i(\vec{g}-\vec{g}')\cdot\vec{R}_s}$, have been absorbed into $V_{s,g-g'}(z)$. The Greens function has several different acceptable forms among others, it may be used as an expansion of spherical harmonics or in its spectral form

$$G(\vec{r},\vec{r}') = \int_{\vec{K}'} d^3K' \frac{e^{i\vec{K}\cdot(\vec{r}-\vec{r}')}}{|\vec{K}'|^2 - |\vec{K}^\circ|^2}. \tag{64}$$

Substituting this spectral form of the Greens function into Eq. and integrating over $\vec{r}_{\|}$ these results

$$\psi(\vec{r},\vec{K}) = \psi^\circ(\vec{r},\vec{K}) - 4\pi \sum_{g,g'} \int_z dz\, V_{g-g'}(z')\, f_{g'}(z') \int_{\vec{K}'} d^3K' \frac{e^{i\vec{K}_z\cdot(\vec{z}-\vec{z}')}}{|\vec{K}'|^2 - |\vec{K}^\circ|^2} e^{i\vec{K}_{\|}\cdot\vec{r}_{\|}} \delta(\vec{K}'_{\|}, \vec{K}^\circ_{\|} + \vec{g}) \tag{65}$$

Using the properties of the delta function to first integrate over $K'_{\|}$ and then over $\vec{k}'_z$, one obtains,

$$\psi(\vec{r},\vec{K}) = \psi^\circ(\vec{r},\vec{K}) - 4\pi^2 \sum_{g,g'} \left[\frac{e^{-i(\vec{K}^\circ_{\|} + \vec{g} + \vec{k}_g)\cdot\vec{r}}}{k_g} \int_{z'} V_{g-g'}(z')\, A_{g'}(z')\, e^{ik_g z'} dz' \right] \tag{66}$$

Here, $|k_g| \equiv \sqrt{|\vec{K}^\circ|^2 - |\vec{K}^\circ_{\|}+\vec{g}|^2}$ is the component of $\vec{K}'$ perpendicular to the surface.

This formal solution illustrates several points about the integral equation approach. The use of symmetry and the expansion of the potential into a sum of individual potentials have been mentioned above. Further, the solution may usually be exprexsed as a sum of plane wave states characterized by the appropriate parallel reciprocal lattice vector. The amplitudes in these states are, of course, dependent upon the nature

of the potential and the geometry of the crystal. Moreover, they are inversely proportional to the perpendicular component, $|\vec{K}_\perp| = |\vec{k}_g|$ of the diffracted wave vector. This is a direct consequence of the imposition of perfect two dimensional symmetry on the Greens function.

Kambe[44] has shown how to derive a specific form of the Greens function that is particularly tailored to this problem as

$$G(\vec{r},\vec{r}') = \Sigma_g \frac{e^{i(\vec{K}^\circ_{\parallel} + \vec{g} + \vec{k}_g) \cdot (\vec{r}-\vec{r}')}}{2i\, k_g} \qquad (67)$$

In addition, he has given an excellent discussion of the relationship between the Greens function and the integral equation approach.

Kambe has also developed a solution to the integral form of the Schroedinger equation.[45] Key to the whole approach is the particular choice of the form of the potential. As in Eq.34 , it is assumed that the potential can be expressed as a sum of potentials centered at particular atomic positions. Further it is assumed that these potentials are of the "muffin-tin" type; specifically, that the total potential is contained in a series of spherically symmetric non-overlapping globes and that there is a constant potential between these spheres of zero value. As the wave function and its first derivative must both be continuous, it follows that at the surface of these spheres, the wave functions that are inside any given sphere must match those that are external to it. Moreover, because there is no potential between the spheres, any outgoing wave that leaves a sphere must travel unperturbed, at least until it enters another sphere. Therefore, by knowing $\psi(\vec{r},\vec{K})$ at the surface of the sphere, its value in free space may be calculated.

The first self-consistent dynamical theory of LEED to be published was that of E. G. McRae.[43a] This paper was particularly significant not only for the mathematical formalism, but also for the model calculations that it contained. These calculations qualitatively illustrated many of the important aspects of multiple scattering such as its dependence upon cross-section, angle of incidence, etc.

In many ways, McRae's derivation of a solution for the wave equation is similar to that of Kambe's. They both employ a Greens function approach a "muffin tin" potential and both expand into spherical harmonics to perform the integration. However, McRaes' approach differs in that the potential between the spheres is not constrained to have a zero value. In addition Greens theorem is not evoked and only volume integrals are used. Further $G(\vec{r},\vec{r}')$ is utilized in its real space expression rather than as an expansion of Bloch like functions.

The salient feature of McRaes' theory is the concept of the effective field $\psi^s(r,K)$. The total field is considered to be composed of the primary field, $\psi^\circ(r,K)$, and the fields emitted by all of the atoms, $\Sigma_s \psi^s(r,K)$. Within this viewpoint, the effective field incident on any given atom is the sum of the primary field and all of the fields emitted by all of the other atoms. This is the basis of this self-consistent approach. The field emitted by any atom is a function of all of the fields emitted by all of the other atoms and, for sufficiently large cross-sections, multiple scattering of all orders is a logical consequence of this interdependence.

This formalism was used to calculate the intensity of back diffracted electron beams from the (100) face of a hypthetical simple cubic crystal.

A number of different intensity maxima were observed in the calculated plots.

McRae has studied the behavior of these intensity maxima, or peaks, as a function of cross section.[43] He has found that as the cross section is reduced, those peaks which are non-kinematic in nature diminish in intensity more rapidly than do those that are allowed in the kinematic limit. This is reasonable as the non-kinematic peaks have their origin in multiple scattering in contrast to the single scattering kinetmatic peaks. The smaller that one makes the cross sections, the more improbable multiple scattering will be relative to single scattering, all things else being equal. In addition to changes in the ratios of peak heights, McRae has found that the peak positions may move when the cross sections are reduced. In the limit of small cross sections, the positions approach those predicted from the free electron model. This is to be expected as reducing the cross sections is essentially the same as reducing the interactions of the electron with the crystal. Therefore, the band gaps become more narrow and the coupling between different beams is diminished.

Both McRae[43] and Marcus and Jepsen[5] have considered the effect of non-normal incidence on the intensity vs energy curves. In general, those beams that are strongly coupled to other beams in a given energy range developed very pronounced fine structure when the degeneracy is broken by deviating from normal incidence. This is in sharp contrast to the kinematic case where maxima would be expected to move, but would not be expected to split and develop fine structure when the angle of incidence is varied. The development and variation of fine structure with changes in the angle of incidence has been observed experimentally.[51]

McRae has also studied the effect of introducing inelastic scattering by assigning a complex value to the scattering phase shift.[43] The effect was to change the shape and reduce the height of the peaks without changing their position or their base width. In addition, there is a tendancy for inelastic scattering is considered in the form of individual atomic excitations.

Ohtsuki has also considered the effect of inelastic scattering.[39] He has formally developed a theoretical approach to the LEED problem in the limit of strong absorption, that is, when the diffraction potential is small compared with the inelastic potential. His qualitative conclusions are similar to those of McRae. His formalism is sufficiently general to include bulk phenomena that are not well represented by individual atomic excitations.

Jones and Strozier[23] have also considered the effect of inelastic scattering on low energy electron diffraction. They have performed calculations that indicate that the inclusion of inelastic effects lead to low reflectivities, asymmetric peak shapes and, in contrast to McRae, broad (10-20eV) peak widths.

Duke and Tucker have derived a single electron propagator formalism that includes inelastic processes.[28] Their calculations indicate that inelastic electron-electron interactions in the solid limit the penetration of the incident elastic beam to a depth of 10Å or less for electrons between 15 and 150 eV incident energy.

When a surface structure is present, that is, when the surface layer is different from all of the underlying bulk layers, it is more convenient to use a detailed scattering approach such as the integral

equation method rather than the differential equation, or band structure approach. The formalisms of McRae[43] and Kambe[45] may be used to affect a solution to this problem. In addition, several authors have approached this problem through the use of a scattering or transfer matrix.

Beeby[46] has developed a method where the amplitude of the diffracted beam is expressed as an infinite summation. This form is particularly interesting because of the physical interpretation of his result. The first term in the summation is the single scattering term. It represents the electron being scattered only once before leaving the crystal and would be the dominent term in the kinematic limit. The second term is a double scattering term. The electron is first scattered at a point r_1 and is then scattered again at a second point r_2 before leaving the crystal. The following terms correspond to higher order multiple scattering events. This approach is of course similar to an iterative Born expansion. The step wise picture leads to a fairly direct interpretation of the physical signficance of the various terms.

McRae[52] has considered the problem in a similar manner. He has approached the problem as a generalization of Darwins theory of diffraction.[47] Here, however, unlike Darwin, he has considered all beams to be coupled and has allowed for the possibility that the surface may differ from the bulk of the crystal. McRae[53] has considered, in particular the case where only single and double diffraction are important. Like Beeby, he has expressed the amplitude of the diffracted beam as a summation

$$\underset{\sim}{b}_0 = \underset{\sim}{b}_1 + \underset{\sim}{b}_2 \qquad (68)$$

where $\underset{\approx}{b}_0$ is a column vector whose components are the amplitudes of the plane wave components of the total wave field emitted by the crystal. The term $\underset{\approx}{b}_1$ contains those contributions from single scattering events and may be regarded as a modified kinematical expression for the diffraction amplitude. The term $\underset{\approx}{b}_2$ corresponds to double diffraction events where the electron has been scattered twice before leaving the crystal.

The physical meaning of the various terms is illustrated in Fig. 15 The heavy line indicates the unique surface layer. The bulk layers that are chosen are to be considered as representative terms.

This approach has been suggested by Bauer,[54] among others, and should be useful where multiple scattering is weak, but not so weak as to place the problem in the kinematic limit. This situation could conceivably arise when inelastic scattering is strong, or when the number of diffraction beams is sufficiently large that the amplitude in any given beam is small.

When the surface layer has a periodicity that bears an integral multiple realtionship to the periodicity of the bulk, fractional order beams will be diffracted back from the crystal. The only non-vanishing contributions from b_1 to the intensity of these fractional order beams will come from the surface layer. This contribution will contribute little to the modulation of the intensity of these fractional order beams. Therefore, the contributions primarily from b_2 will determine the structure of the intensity curves. Furthermore, according to McRae[53] the peak position should resemble a superposition of intensity curves for the integral order beams. Physcially, one may regard this process in the following manner. The

diffraction beams that are formed within the crystal have large amplitudes in the back direction in the neighborhood of band gaps. As these large amplitude integral order diffraction beams leave the crystals, they impinge upon the surface layer. Part of their intensity is lost by scattering at the surface layer into the fractional order beams. Thus, the surface layer serves to mix the intensities of the various beams. From these considerations, it is to be expected that surface structures with the same periodicity, but different chemical natures, should give rise to peaks in the same positions. The intensities of these peaks should of course be dependent upon the detailed nature of the scattering centers.

McRae and Winkler[55] have considered the case where a gas is adsorbed in register on a crystal. They find that when the surface layer differs significantly from the bulk, that the secondary or fractional order Bragg peaks are damped relative to the kinematically allowed Bragg peaks. This result may be interpreted in terms of destructive interference in the double diffraction terms because of the disparity between the surface and the bulk. The step-wise diffraction picture formally developed by McRae[53] and Beeby[46] has been used earlier in a more intuitive form by Gafner.[56] He has carried out a multiple diffraction calculation for several of the diffraction beams from the Ni(111) face. The amplitudes of the waves which were formed at each diffraction event were adjusted to make their sum equal the incident amplitude multiplied by an adsorption factor to account for inelastic scattering. This is in contrast to the usual method of normalizing through intensities rather than amplitudes. The relative scattering factor was assumed to be unity for all scattering angles other than zero where it was given the value of 9. The step wise scattering pro-

cess was considered in the following manner. The normally incident beam was diffracted into the several allowed diffraction beams at the first layer. The beams scattered into the crystal were allowed to undergo oscillatory diffraction between the first and second layer until all of the beams had amplitudes less than some prescribed value. The beams that were scattered out of the crystal in this process were gathered up with those scattered back out of the incident beam. The beams that were scattered forward in this process were combined vectorially and oscillatory diffraction between layers 2 and 3 was allowed to proceed as in the preceding case. This process was continued until all beam amplitudes in the crystal had fallen below the prescribed limit. Despite the approximations and assumptions within this model (or, perhaps because of them), the agreement between the calculated and the experimentally observed intensity curves is quite encouraging.

C. Effect of Multiple Scattering on the Temperature Dependence of the Diffraction Beam Intensities

Let us finally consider, in general, the effect of multiple scattering on the temperature dependence of the diffraction beam intensities. Using an approach similar to that of Beeby[46] and McRae[53], one may express the total eigenfunction for a diffraction beam in a Born type expansion as

$$\psi_f(\vec{r},\vec{K}) = \psi_0(\vec{r},\vec{K}) + \psi_1(\vec{r},\vec{K}) + \psi_2(\vec{r},\vec{K}) + \ldots \qquad (69)$$

where

$$\psi_n(\vec{r},\vec{K}) = 1/4\pi \int G(\vec{r},\vec{r}')\, V(\vec{r}')\, \psi_{n-1}(\vec{r}\vec{K})\, d^3\vec{r}'. \qquad (70)$$

Here $\psi_0(\vec{r},\vec{K})$ is the eigenfunction of the incident beam. The term $\psi_1(\vec{r},\vec{K})$ corresponds to that portion of the total eigenfunction that has been

kinematically or singly scattered. Double scattering events would be contained in $\psi_2(r,K)$ and higher order events would be represented by the other terms in the expansion. It may be shown that

$$\psi_1(\vec{r},\vec{K}') = 4\pi K'_z \; e^{i(\vec{K}^\circ+\vec{G})\cdot\vec{r}} \; \Sigma_s \; e^{i\vec{G}\cdot\vec{r}_s} \; V_{s,G} \tag{71a}$$

or

$$\psi_1(\vec{r},\vec{K}) = 4\pi K'_z \; e^{i(\vec{K}^\circ+\vec{G})\cdot\vec{r}} \; \Sigma_s \; e^{i\cdot\vec{G}\cdot\vec{r}_s^\circ} \; e^{-W_s} \; V_{s,G} \tag{71b}$$

If one makes the assumption that all of the layers are identical, then

$$\psi_1(\vec{r},\vec{K}') = f_G \; e^{i(\vec{K}^\circ+\vec{G})\cdot\vec{r}} \tag{72}$$

where

$$f_G = 4\pi e^{-W} \; \frac{V_{s,G}}{2K'_z} \; \Sigma_s \; e^{i\vec{G}\cdot\vec{r}_s^\circ} \tag{73}$$

In a similar manner, it may be shown that the double diffraction term can be written as

$$\psi_2(\vec{r},\vec{K}) = \Sigma_{G'} \, f_{G-G'} \, f_{G'} \; e^{i(\vec{K}^\circ+\vec{G})\cdot\vec{r}} \tag{74}$$

In general,

$$\psi_n(\vec{K}',\vec{r}) = [\pi_{i=1}^{n} \; (\Sigma_{G_i} \; f_{G_i} \; e^{i\vec{G}_i\cdot\vec{r}})] \; e^{i\vec{K}^\circ\cdot\vec{r}}. \tag{75}$$

The intensities of the various beams characterized by G are given by

$$\begin{aligned} I &= \psi_T{}^*(\vec{r},\vec{K}^\circ+\vec{G}) \; \psi_T(\vec{r},\vec{K}^\circ+\vec{G}) \\ &= (\Sigma_n \; \psi_n{}^*(\vec{r},\vec{K}')) \; (\Sigma_m \; \psi_m(\vec{r},\vec{K}')) \\ &= \Sigma_{n,m} \; \psi_n{}^*(\vec{r},\vec{K}') \; \psi_m(\vec{r},\vec{K}') \end{aligned} \tag{76}$$

where the eigenfunctions have been expanded in a Born type series. On the basis of this expansion, the intensity itself may be expressed as a series as

$$I_T = \Sigma_n \; I_n, \tag{77}$$

Here, the first term

$$I_1 = |f_G|^2 \tag{78}$$

is the kinematic term and would contribute to the intensity even in the absence of multiple scattering. This term, of course, carried the kinematic temperature dependence as

$$I_1 = I^\circ_1 \, e^{-2W} \tag{79}$$

where W is a linear function of temperature in the Debye approximation. I_1 arises as the product of the amplitudes for single scattering events.

The second term, I_2 is generated as the product of the amplitudes for single scattering events with the amplitude for double scattering events and may be written as

$$I_2 = \Sigma_{G'} \, |f_G{}^* f_{G-G'} f_{G'}| . \tag{80}$$

This term will be referred to as the double diffraction contribution to the total intensity. It has the temperature dependent form

$$I_2 = I_2^\circ \; e^{-W_1} \; e^{-W_{12}} \, e^{-W_2} \tag{81}$$

where W_1 is proportional to $|\vec{G}|^2$, W_{12} to $|\vec{G}'\vec{G}|^2$ and W_2 to $|\vec{G}'|^2$ in the approximation that the crystal is isotropic and that all of the layers are identical.

There will be two contributions to the third term in the expansion of the intensity. The first will arise as a product of the single scattering amplitude and the triple scattering amplitude. The second term comes from a product of the double scattering amplitudes. Consequently, this intensity term will have the form

$$I_3 = \sum_{G_1, G_2} \left[|f_G{}^* f_{G-G_1-G_2} f_{G_1-G_2} f_{G_2}| + |f^*_{G-G_1} f_{G_1}{}^* f_{G-G_2} f_{G_2}| \right] \tag{82}$$

Its temperature dependence may be determined in a manner similar to that for I_2. Higher order scattering contributions to the intensity will have increasingly complex forms and will bring correspondingly more complicated temperature dependent terms into the total intensity. As f_G must be less than or equal to unity, these higher order terms should be generally less important. However, there do exist cases where a term may be more important than the preceding lower order terms. For example, there are observed "secondary" Bragg peaks in the specularly reflected intensity that do not correspond to kinematic diffraction conditions. When multiple scattering is reasonably strong, diffraction conditions of the form

$$K_z^{00} + K_z^{hk} = G_z \qquad (83)$$

can lead to intensity maxima in the (00) beam. Note that, even though this condition is kinematic for the (h,k) beam, it must involve at least double diffraction to produce an intensity maximum in the (00) beam. Consequently, the double diffraction contribution to the total intensity, I_2, may be expected to be larger than the kinematic contribution, I_1. Higher ordercontributions may also be significant. Therefore, it may be expected that the experimentally determined quantity, Td ℓnI/dT, will more closely resemble $W_1 + W_{12} + W_2$ rather than the kinematic 2W, assumed in the simple model. As one might expect terms like $W_1 + W_{12} + W_2$ to be larger than 2W, it would seem at first glance that multiple scattering alone could lead to the apparent determination of lower "effective" Debye temperatures or higher "effective" r m s displacements for the surface. This is however not necessarily true in all cases. For simplicity, let us retain the assumption that the crystal is isotropic and that all of the layers are identical. We may then write

$$W = 3/2 \frac{\hbar^2 T}{mk} \left[\frac{G_x^2}{\theta_x^2} + \frac{G_y^2}{\theta_y^2} + \frac{G_z^2}{\theta_z^2} \right] \tag{84}$$

as

$$W = B |\vec{G}|^2 \tag{85}$$

Within this approximation

$$2W_1 = 2B |\vec{G}_1|^2 \tag{86}$$

and

$$W_1 + W_{12} + W_2 = B(|\vec{G}_1|^2 + |\vec{G}_1 - \vec{G}_2|^2 + |\vec{G}_2|^2) \tag{87}$$

It may easily be seen that three cases arise. When

$$|\vec{G}_1|^2 - \vec{G}_1 \cdot \vec{G}_2 < |\vec{G}_1|^2, \tag{88}$$

then $W_1 + W_{12} + W_2$ will be less than $2W_1$. In this case the experimentally determined effective Debye temperature derived from the simple model would be less than the actual effective Debye temperature. Alternatively, the apparent r m s displacements would be greater than those actually contributing to the temperature dependence of the intensity.

In the second case, $|\vec{G}_2|^2 - \vec{G}_1 \cdot \vec{G}_2 < |\vec{G}_1|^2$ and $W_1 + W_{12} + W_2$ is greater than $2W_1$. Here, the experimentally determined value for the r m s displacements would be less than the real value.

In the third case $|\vec{G}_2|^2 - \vec{G}_1 \cdot \vec{G}_2 = |\vec{G}_1|^2$ and $W_1 + W_{12} + W_2$ is equal to $2W_1$. In this case, the use of the simple kinematic model to determine the effective Debye temperature and the atomic displacements would lead to the same results as the use of a more complicated multiple scattering model.

At normal incidence, double diffraction contributions to the specularly reflected beam fall in the last case. Thus, if one neglects any possible asymmetry of the surface, one would expect that the contributions from this type of mechanism would give results that were experimentally

indistinguishable from those arising from kinematic scattering. Away from normal incidence, double diffraction contributions will no longer fall into the third case, but will give rise to contributions of both the first and the second type. Whether the experimentally determined r m s displacements will be greater than or smaller than the actual displacements will depend upon the detailed nature of the scattering potential. For simple forward scattering potentials, such as the screened Coulombic potentials, one would expect those terms giving smaller apparent r m s displacements to dominate.

Higher order scattering events can also lead to apparent displacements that are either greater than or less than the real displacements. In the limit of an isotropic crystal with identical layers, the relationship between $\Sigma_i W_i$ and $2W$ may be determined in a manner similar to that for the double diffraction situation. Again, one would expect that those terms leading to smaller apparent r m s displacements would dominate when the scattering potential was of a smooth, forward scattering type. Similar arguements may be made concerning the effect of multiple scattering on the temperature dependence of the intensity of the higher order diffraction beams.

The assumption that all of the layers of the crystal are identical is unrealistic, particularly in the presence of a surface structure.

Let us then consider the case where the first layer is different from all of the other layers. For simplicity, the factors V_G / K'_z will be taken to be unity. The kinematic contribution to the eigenfunction for a given diffraction beam may then be written as

$$\psi_1(\vec{r},\vec{K}') = e^{i(\vec{K}^\circ+\vec{G})\cdot r} \sum_{S,1}^{\infty} e^{i\vec{G}\cdot\vec{r}_s^\circ} e^{-W_s} \qquad (89a)$$

or

$$\psi_1(\vec{r},\vec{K}') = e^{i\vec{K}'\cdot\vec{r}} e^{i\vec{G}\cdot\vec{r}^\circ} + e^{-W} \sum_{S=2}^{\infty} [e^{i\vec{G}\cdot\vec{r}_1}]^{S-1} \qquad (89b)$$

where W_0 is the Debye-Waller factor for the first layer, W is the Debye Waller factor for all of the other layers, $\vec{r}_1^\circ$ is the coordinate of the surface and R is the translational vector between layers. Making the definitions that $\alpha = e^{-W_0}$, $\beta = e^{-W}$, $\phi_0 = e^{i\vec{G}\cdot\vec{r}_1^\circ}$ and $\phi^{i\vec{G}\cdot\vec{R}}$, it may be shown that

$$\psi_1(\vec{r},\vec{K}') = e^{i\vec{K}'\cdot\vec{r}} [\alpha\phi_0 - \beta\phi/(1-\phi)] \qquad (90)$$

The corresponding single scattering contribution to the intensity may be written as

$$I_1 = \left|\alpha\phi_0 - \frac{\beta\phi}{1-\phi}\right|^2 \qquad (91)$$

when all of the interplanar spacings are equivalent, this reduces to

$$I_1 = \alpha^2 - \alpha\beta + \frac{\beta^2}{2(1+\cos(\vec{G}\cdot\vec{R}))} . \qquad (92)$$

This, of course, is essentially Darwin's result with the inclusion of the Debye-Waller factor previously considered by Lyon and Somorjai.[31,57]

Proceeding to higher order scattering events, the double scatterin contribution to the total eigenfunction may be written as

$$\psi_2(\vec{r},\vec{K}) = e^{i(\vec{K}^\circ+\vec{G})\cdot\vec{r}} (\Sigma_s e^{i(\vec{G}-\vec{G}_1)\cdot\vec{r}_s} e^{-W_{12}}) (\Sigma_t e^{i\vec{G}_1\cdot\vec{r}_t^\circ} e^{-W_2}) \qquad (93)$$

or

$$\psi_2(\vec{r},\vec{K}) = e^{i(\vec{K}^\circ+\vec{G})\cdot\vec{r}} \left(\alpha_1 - \frac{\beta_1\phi_1}{1-\phi_1}\right) \left(\alpha_2 - \frac{\beta_2\phi_2}{1-\phi_2}\right) \qquad (94)$$

where it has been assumed that all of the interplanar spacings are equivalent and α_i and β_i have been defined in a manner similar to that for the kinematic case. The double diffraction contribution to the total intensity

partakes of the form

$$I_2 = \left|(\alpha - \beta \frac{\phi^*}{1-\phi^*})(\alpha_1-\beta_1 \frac{\phi_1}{1-\phi_1})(\alpha_2-\beta_2 \frac{\phi_2}{1-\phi_2})\right|. \quad (95)$$

where α and β correspond to the singly scattered amplitude and the α_i and β_i correspond to the doubly scattered amplitude. This term has a particularly interesting form when applied to fractional order beam arising from the presence of a surface structure. These beams are forbidden in the bulk of the crystal. One may therefore make the simplifying assumption that scattering into these beams can only occur at the surface. When this is the case, I_2 reduces to

$$I_2 = \left|\alpha \alpha_2 \beta_1 \frac{\phi_1}{1-\phi_1}\right| \quad (96)$$

The terms α and α_2 correspond to scattering events at the surface layer where the electron is diffracted into back scattered fractional order beams. The term $(\beta_1 \phi_1/1-\phi)$ corresponds to scattering events that can occur in the bulk of the crystal between the incident and some intermediate integral order beam. It may be seen that if the surface species is loosely bonded relative to the bulk species, then the intensities of the fractional order beams should exhibit a stronger temperature dependence when double diffraction occurs than would be observed for the integral order beams. This of course, is also true for the kinematic contribution where

$$I_1 = |\alpha|^2 \quad (97)$$

It may be shown that higher order contributions to the total intensity will be of the form

$$I_n = \left|\pi_{i=1}^{n+1} (\alpha_i - \beta_i \frac{\phi_i}{1-\phi_i})\right| \quad (98)$$

VI. THE LOW ENERGY ELECTRON DIFFRACTION EXPERIMENT

In order to carry out surface studies by low energy electron diffraction one needs (a) a well defined electron beam (b) a single crystal surface and (c) ultra high vacuum in order to keep the surface under conditions desired in the experiment. We shall now discuss these three experimental parameters in some detail.

A. Electron Optics

1. Thermal Spread and Coherence Length

The electrons are obtained by thermionic emission from a hot cathode. For a barium oxide cathode the operating surface temperature is about 800°C. If the cathode material is a refractory metal such as tungsten which may be coated with lanthanum hexaboride, the surface temperature of the cathode is of the order of 2000°C. For cathodes made out of barium silicates in operating surface temperature of the order of 1200°C is used. The temperature of the cathode determines the initial thermal energy spread of the electron beam. Assuming a Maxwellian distribution of electron velocities, the average thermal energy of the electrons is 3/2 kT. If we consider the energy spread ΔE equal to 3/2 kT, approximately 95% of the electron beam is contained in the thermal energy spread of $2\Delta E = 3kT$. Thus, the energy spread at 800°C is of the order of .2 eV while at 2000°C it is of the order of .6 eV. These electrons are then focused electrostatically and allowed to impinge on the crystal surface which is held at ground potential. The electron beam is on the order of one millimeter in diameter. For a completely ordered surface, the coherence length of the electron to large extent, is determined by the size of the source of the

electron beam. Incoherence within the electron wave packet sets the upper limit to the number of atoms which can contribute to coherent scattering. This incoherence arises from the finite size of the electron source and the incoherence due to the spreading of the wave pockets over the distance between two scattering centers. This latter distance is usually referred to as the Fresnel zone. If r = width of Fresnel zone = $(R\lambda/2)^{1/2}$, where R = distance from scattering center to detector, and λ = wavelength of the incident wave, then using the appropriate values for LEED: $R \cong 7\times10^{8}$ Å; gives $r = 2\times10^{4}$ Å. However, because of the need for high intensities in LEED, the instrumental incoherence introduced by the use of a large electron source is much more significant. The coherence width of the electron beam at the scattering object,

$$\Delta X = \frac{\lambda}{2(1+\Delta E/2E)\beta_s} \qquad (99)$$

where β_s = half angle indeterminacy in the angle of incidence for an incident electron due to the size of the electron source, ΔE = thermal spread of electron beam, and E = energy of the electron beam. In LEED, $\beta_s \sim .001$ radians, $\lambda = 1$ Å (for E = 150 eV), $\Delta E \sim .2$ eV. These values give a coherence width of about 500Å, i.e. much smaller than the width of the Fresnel zone. Thus, in LEED, no area larger than $\sim(\Delta X)^2$ can contribute coherently to the diffraction pattern since no area larger than this receives coherent radiation.

The question of what is the minimum area necessary to give a coherent diffraction pattern has not been definitely answered experimentally. However, if one assumes that ordered arrays of 25-100 atoms are sufficient to give coherent diffraction best agreement with present results is obtained.

Thus, considering all of these factors, we can characterize coherence in LEED by the following description: minimum order necessary to give a coherent diffraction beam consists of ordered patches on about 10% of the crystal surface. As the surface is further ordered, the intensity of the diffraction spots should increase, and the sharpness of the spots improve until the surface consists almost entirely of regions of ordered arrays of about 10,000 atoms. Beyond this degree of ordering, the experimental factors prevent any improvement in the pattern; the macroscopic beam width (about 1 mm) limiting the sharpness of the spots, and the source incoherence limiting the intensity.

2. Penetration of the Low Energy Electron Beam and Energy Analysis of the Bulk-Scattered Electrons

In order to obtain experimental information about the structure of the surface we would like to have most of the low energy electrons which are elastically scattered and thus, contain diffraction information to scatter from the topmost layer of atoms at the surface without any further penetration into the bulk of the crystal. As expected, the actual penetration depth depends on the energy of the low energy electron beam. The penetration depth of the electron beam has been probed experimentally by depositing an epitaxial layer of one metal over another metal, detecting the amount deposited as a function of time and correlating the result with the gradual disappearance of the diffraction features from the underlying substrate. It was concluded that an reasonable estimate for the penetration of low energy electrons is 2 to 5 atomic layers in the energy range 5 to 100 eV. Studies of the deposition of amorphous silicon on silicon single crystal surfaces by Jona have also indicated that the intensity of the diffraction spots of the underlying substrate could be reduced by over

95% upon the deposition of two monolayers of amorphous material.[58] An empirical correlation between the penetration depth and the energy of electrons is given by Heidenreich.[58]

The equation, L,(penetration depth) = $2 + (eV/150)^2$, gives a reasonable estimate of the electron beam penetration.[60]

LEED experiments indicate that the number of elastically scattered electrons which are back reflected from crystal surfaces varies with the incident electron beam energy. About 20% of the incident electrons are back-scattered elastically at 10 eV and about 1% at 100 eV and less at higher energies.[25] Figure 11 shows the representative result obtained for scattering from a number of face centered metal (100) surfaces. Although the in elastically scattered electrons contain much valuable information about the structure and composition of surfaces which have been brought to light by recent advances in Auger spectroscopy in a diffraction experiment the elastic and inelastic components of an electron beam have to be separated as the primary diffraction information is contained only in the elastic component. Since the elastic fraction is a small part of the total scattered electron beam the energy separation of these two components is a prerequisite of a successful low energy electron diffraction experiment. This separation can be carried out in a number of different ways. Perhaps the most popular and the most prominent at the present is the so-called post acceleration technique. The scheme of the electron optics is shown in Fig. 16 the back-scattered electrons travel a field free path to the first grid which is also held at ground potential as is the crystal. Energy analysis takes place at the second grid which is held at cathode potential. This grid, in principle, repells all of the electrons

which have lost energy in the collision with the surface and allows only the elastically scattered electrons to penetrate through. The elastic component which has penetrated the grid system is then accelerated by the application of a large positive potential, 5,000-7,000 eV on to a fluorescent screen where, due to radiative recombinations after excitation by the electron beam, light is emitted where the electron hits. The light intensity is proportional to the number of electrons hitting the screen. This post-acceleration technique is an excellent means of instantaneously displaying the diffraction pattern. In order to improve the energy selection of the repelling grid often two grids instead of one are used for rejecting the inelastically scattered electrons. The cut-off characteristics of a three grid system are shown in Fig. 17 . If the single crystal surface is placed at the center of curvature of the three grids and the fluorescent screen, one should obtain an undistorted low energy electron diffraction patterns. The solid angle subtended by the fluorescent screen is ~95°. There are other detection techniques which are often used in low energy electron diffraction studies. A Faraday cup which can be rotated 180° is frequently used to monitor the low energy electron beam intensity. While the fluorescent screen intensities allow one to measure relative intensities the, Faraday cup detection allows absolute intensity measurements which are necessary in some experiments. An other experimental geometry for low energy electron diffraction studies which has been developed uses a magnetically deflected low energy electron beam An advantage of this geometry is that the (00) or specular beam is not shadowed by the electron gun under conditions of normal electron

beam incidence as it is with the "post acceleration" technique or the Faraday cup detection technique.

B. Crystal Preparation

The preparation of well-ordered, clean single crystal surfaces is a very important phase of the low energy electron diffraction experiment.[60] The crystals are oriented by the Laue x-ray diffraction technique using a precision goniometer, to within a $\pm 1^{\circ}$ of the desired crystal face. The crystals are then cut to a convenient shape and are polished and etched with suitable chemical or electrical-chemical techniques. For soft single crystals such as lead or bismuth, spark cutting rather than mechanical cutting should be used to prepare the sample. Furthermore for these crystals, mechanical polishing should be minimized because of the extensive damage such a mechanical treatment might introduce in the surface order. For harder metals such as silver, gold, nickel and platinum, spark cutting can also be used for preparation followed by mechanical polishing with diamond or carbides powder of successively finer mesh. Mechanical polishing can easily correct the small deviations from the desired crystal orientation which are due to erroneous orientation of the original single crystal sample. The chemical etching or electrochemical polishing treatment serves to remove the damage introduced by the mechanical polishing treatment of the crystal surface which can often be as deep as 1 micron. The chemical etching which are used vary from crystal to crystal. The etchants used for several metal and semiconductor surfaces are published in the literature. Then the samples are mounted on holder assembly and placed into the diffraction chamber. The chamber is closed, pumped down, and baked at a temperature of roughly

250°C in order to obtain ultra high vacuum conditions. Further, cleaning of the crystal surfaces is then carried out by in situ ion bombardment and heating cycles until reproducibly clean, ordered, single crystal surfaces are obtained. An ion bombardment gun is an essential part of an low energy electron diffraction apparatus. Suitable ambient conditions for ion bombardment are $1\text{-}4\times10^{-5}$ torr gas (argon and xenon are used work frequently), ion accelerating potential in the range 140 to 350 volts and ion currents in the range of 1 to 2 microamps per square cm. Such an ion bombardment treatment removes traces of contamination introduced by the etching procedure and by exposure to the ambient during the mounting of the crystal. After ion bombardment the single crystal is heated to anneal out the surface disorder introduced by the ion bombardment treatment and the crystal face may then exhibit an excellent diffraction pattern. If not, the bombardment - annealing cycle is repeated until a diffraction pattern of the desired quality is obtained.

Since the coherence length of the electron is of the order of 500Å a sharp diffraction pattern could be formed from microscopically rough surfaces. The diffraction pattern would be due to ordered domains which were approximately 500Å or larger in diameter and the intensity of the diffraction spots would depend upon the number of these domains which all contribute independently to the total scattered elastic amplitude. In several experiments where the vaporization of surfaces have been studied by low energy electron diffraction, extremely rough surfaces have given excellent diffraction patterns. One question which may continually be asked in low energy electron diffraction studies is that what fraction of the surface has to be ordered to obtain a diffraction pattern. A partial

answer to this question was provided by the experiment in which amorphous silicon was deposited on a silicon single crystal surface. It was found that as the deposition of the amorphous material continued, the intensity is reduced to about 50% of the initial intensity with the deposition of one-half of a monolayer. The reduced heights of selected specular intensity maximum as a function of the deposited amorphous silicon is shown in Fig. 18. Thus, we find that even though the surface may be covered by 5 to 10% of amorphous material or disordered atoms the diffraction patterns would not be very sensitive to the presence of this surface concentration.

Another difficulty in low energy electron diffraction experiments is to ascertain the cleanliness of the surface. Although the low energy electron diffraction patterns may change or the intensity of the diffraction spots may reflect the presence of ordered impurities by the appearance of new diffraction features, the presence of amorphous impurities even in concentrations as high as 10% of the total number of surface atoms (that is of the order of 10 to 14 atoms per square centimeter) may not be easily detectible by low energy electron diffraction. For example, the decomposition of hydrocarbons can lead to the deposition of amorphous carbon on the surface which may go undetected. In certain experiments, the deposition of amorphous impurities can be ascertained. In these situations, it is usually necessary to resort to auxiliary experimental techniques which in combination with low energy electron diffraction can be used to give detailed information about the concentration of impurities and the nature of impurities on the surface. Recent advances in Auger spectroscopy which analysis the energy distribution of inelastically

scattered electrons frequently allow one to detect impurity concentrations on the surface of less than 5% of the total number of surface atoms. The detection and identification of impurities remains one of the continual problems in low energy electron diffraction studies.

C. Ultra High Vacuum

The low energy electron diffraction experiment in principle could be carried out up to pressures of 10^{-3} torr in the diffraction chamber. At this pressure the mean free path of the electrons is still large enough on the order of the dimension of the apparatus for detection after scattering from the surface. The limiting factor, however, is not the mean free path of the electrons in the diffraction chamber but the adsorption of impurities on the surface which render the detection and the analysis of the surface structure impossible. Adsorbed gases may form ordered surface structures of their own or may be adsorbed amorphously. In any case, the diffraction features of the substrate may become undetectable upon adsorption of several monolayer or more of gas. Therefore, low energy electron diffraction experiment have to be carried out in ultra high vacuum (i.e. at pressures below 10^{-8} torr at which the rate of incidence of ambient gas atoms onto the single crystal surface still allow adequate experimental time to detect the diffraction features of the clean surface. Assuming a sticking probability of unity a surface becomes covered with a monolayer of adsorbed gas in one second at an ambient pressure of 10^{-6} torr. Thus, at 10^{-9} torr experimental times of the order of 1,000 seconds are available to carry out low energy electron experiments on a clean surface. Continuous pumping of the vacuum chamber and the maintenance

of 10^{-9} torr vacuum, permits one to study the properties of a clean surface with minimal interference from undesired gases during the experiment.

When it is necessary to open the diffraction chamber, the apparatus should be brought up to atmospheric pressure with dry nitrogen or some other relatively inert gas rather than air in order to avoid the adsorption of unwanted gases with large surface binding energies such as oxygen or water on the walls of the chamber. In order to maintain oil free conditions, mechanical pumps are not generally used to evacuate the system. Generally, the pressure is reduced to 10^{-3} torr with the use of adsorption pumps that employ a large surface area zeolite cooled to liquid nitrogen temperature. The further reduction of the pressure to about 10^{-7} - 10^{-8} torr is accomplished by the use of a vacuum ionization pump and/or an ion sublimation pump. At that point the chamber is baked at 250°C to obtain ultra high vacuum conditions. Baking is necessary since it facilitates and accelerates the desorption of gases from the surfaces of of the stainless steel diffraction chamber. After this baking process, a vacuum of the order of 10^{-9} torr and below can easily be obtained in a leak-free vacuum system. Modern vacuum technology makes the attainment and maintenance of ultra high vacuum very easy during a low energy electron diffraction experiment.

VII. LOW ENERGY ELECTRON DIFFRACTION STUDIES OF DISORDERED SURFACES

A. Effect of Surface Disorder on the Diffracted Beam Intensities

The surfaces of a crystal are for from being perfectly ordered and clear. A real surface is heterogeneous; there are atoms in different crystal positions which are distinguishable by their different numbers of nearest neighbors and thus by variations of their binding energies. There are surface atoms in (1) steps or at ledges. There are also (2) vacancies and impurity rates, (3) dislocations, (4) mosaic structures, low angle grain boundaries, (5) liquid-like regions or disorder due to surface preparation, melting, vaporization, or adsorption of foreign substances. The effect of these defects on the scattered intensity is discussed in this section.

If N_T is defined as the total number of scattering centers in an array using the simplest kinematical model the intensity is given by,

$$I = |f_q|^2 \left[N_T + \sum_{n \neq m}^{N_T} \sum^{N_T} \cos \{(\vec{k}' - \vec{k}^\circ) \cdot \vec{r}_{nm}\} \right] \qquad (100)$$

If the array of atoms form a perfect three dimensional arrangement, then the summations collapse to the particularly simple form of $N(N-1)$ for $(\vec{k}' - \vec{k}^\circ) \cdot r_{nm}$ equal to some integral multiple of 2π. Under these circumstances, $I = |f_q|^2 N^2$ and the intensity is proportional to the square of the number of scattering centers.

If, on the other hand, there is a random relationship between $\vec{r}_n$ and $\vec{r}_m$, the array of atoms is completely disordered, then the terms in the summations tend to be out of phase and cancel so that $I = |f_q|^2 N$ that is, the intensity varies linearly with the number of scattering centers. Therefore, to a first approximation, the intensity for electrons

scattered from a completely disordered surface is proportional to the number of scattering atoms and gives rise to a relatively featureless diffuse background while the intensity from a perfectly ordered surface is proportional to N^2 and is characterized by sharp and discrete diffraction spots where the condition $(\vec{k}'-\vec{k}^{\circ})\cdot\underset{\sim}{r}_{nm} = n2\pi$ is met. / In LEED on real surfaces (assuming the utility of the kinematic models) we are mostly concerned with situations between the two extreme cases of complete order and complete loss of periodicity (disorder). An interesting study of the influence of disorder on LEED instensities is provided by the results of Jona[58] plotted in Fig.18. The dotted line in Fig. 18 corresponds to the expectation if 90% of the coherent intensity was from the top three layers and Eq.100 was accurate. While the fit is not perfect, the results indicate that qualitatively the effect of disorder on LEED diffraction intensities (in the figure the circles, squares, and triangles refer to intensities at diffraction maxima at the indicated beam voltages) can be described by a simple kinematic (single scattering) model.

An interesting effect frequently noted in LEED studies is that random surface irregularities on a macroscopic scale (10^4 Å or larger) do not, in any apparent way, affect the intensity or the size of the diffraction spots.

Goodman[60] has shown that sharp high intensity diffraction features may be obtained from surfaces having a great concentration of pits, ledges, grain boundaries, etc. of about 1 to 10μ in size. These results support the basic consideration discussed earlier concerning coherence. That is, if the surface is ordered in patches of perhaps 1000 atoms, then the intensity is unaffected as long as all the patches are oriented with respect to one another. Macroscopic steps, pits, ledges, dislocations, grain boundaries, etc. have virtually no effect on either spot size or intensity in LEED as long as the spacing of the defects is of the order of the coherence length

of the electron beam or larger. However, surface imperfections closer to each other than the coherence length will contribute to an intensity decrease in the diffraction features.

Ion bombardment of single crystal surfaces using high energy noble gas ions broadens the diffraction spots and simultaneously reduces the spot intensities. Such ion bombardment damage is detectable in all single crystal surfaces where surface diffusion rates are negligible at the temperature at which the ion bombardment is carried out. Annealing the crystal by heating the surface to higher temperature increases the diffraction spot intensity and reduces the spot size.. Clearly, ion bombardment has reduced the size of the ordered domains to below the coherence length of the low energy electrons. Annealing increases the order and increases the sizes of these domains above that of the limiting size given by the coherence length. The main result of experiments on disordered surfaces is that the presence of disorder in concentrations of up to 10% of the available surface atoms have only limited or no detectable effect on the diffraction pattern. On the other hand, if impurities, vacancies or other crystal imperfections are arranged in ordered or periodic array on the crystal surface, the LEED patterns are greatly effected, new diffraction features appear immediately. Linear disorder occurs whenever atomic spacings along one crystalographic direction are disturbed while order is maintained in the others. A good example is provided by the work of Ellis on uranium dioxide[61] in which deliberately cutting a crystal face off axes at a small angle introduces very high step densities in the surface and streaking in the diffraction pattern. Such streaking is very frequently observed in low energy electron diffraction patterns during the formation of ordered surface structures of adsorbed gases or during surface phase transformation from one ordered surface structure to another ordered

surface structure. Linear disorder often reveals that the process by which a new periodicity characteristic of the new surface structure appears is surface diffusion. Monitoring intensity changes during a transformation which proceeds via linear disorder should be useful in obtaining information about kinetics of surface phase transformations which are surface diffusion controlled. Impurities often give rise to surface structures which are characterized by rotational disorder. Rotational disorder can be defined as disorder in which within one domain the surface atoms are ordered but where there is no preferred orientation of the domains with respect to each other. The result is that the diffraction pattern shows circular symmetry about the specular reflection. Carbon appears to give such a diffraction pattern on several metal surfaces. When amorphous carbon on the surfaces of gold, platinum, silver and other metals is heated to higher temperature, diffraction rings appear first in segmented form and then finally as a complete circle,[62, 63,64] (Fig. 19a,b). These ring like diffraction features indicate the reordering of amorphous carbon on the surface in a graphitic form which is characterized by rotational disorder. Nevertheless it is ordered parallel to the crystal face. A diffraction pattern of such rings characteristic of carbon on platinum surfaces on shown in Fig. 19 . Finally we should consider the complete lose of long range order, this is referred to as amorphous or liquid-like disorder. Guinier separates disordered structures into two classes: (1) Correlated disorder which refers to disorder in which the atoms are displaced from equilibrium sites a small amount relative to equilibrium intermolecular separations and the average positions of all atoms is equivalent to that in the perfect lattice.[65] The most obvious

example of this is the disorder introduced by thermal motions. On the other hand (2) uncorrelated disorder exist when displacements from equilibrium positions may be large and the microscopic atomic density may differ from that of the ordered lattice. A good example is a volume containing a monatomic gas at low pressure. However, most arrangements of atoms in condensed phases do tend to have some of the characteristics of correlated disorder under all conditions of the low energy electron diffraction experiments.

B. Low Energy Electron Scattering from Liquid Surfaces

Liquids posses unique characteristics, like all condensed phases they possess some elements of correlated disorder. The distribution of atoms in liquids can be best described by a radial distribution function, $\rho(r)$. Figure 20 shows a typical radial distribution function which was taken from Kaplows x-ray data on liquid lead.[66] The curve labeled ρ_o represents the average value from the density of the liquid. The main points to observe are $(\rho_a - \rho_o)$ goes to zero for small distances due to repulsive interactions and that it has a strong maximum near the nearest neighbor distance of the solid while at large distances $(\rho_a - \rho_o)$ approaches zero again. For diffraction from an array satisfying such a distribution function, Guinier derives the interference function[65]

$$I(s) - 1 = \int_0^\infty 4\pi r^2 [sa(v) - so] \frac{\sin(2\pi rs)}{2\pi rs} dr \qquad (101)$$

where

$$s = \frac{4\pi \sin\theta}{\lambda}$$

Figure 21 gives the x-ray intensities obtained from liquid lead at 327.4°C as a function of the scattering angle, $(\sin\theta/\lambda)$. It should be noted that the peak intensities are, at best, twice the background intensity. Similar results were obtained from liquid metals from high energy electron diffraction studies.

Elastically scattered electrons or x-rays diffracted from liquid surfaces should show a distribution which reflects two scattering mechanisms; (1) uncorrelated scattering from individual atoms in the liquid and (2) scattering which is modulated by the density fluctuations in the liquid. The former directly gives the atomic scattering factor, f. This parameter enters into calculations of surface structure from the diffraction beam intensities and its experimental determination is of great value. The latter scattering mechanism gives rise to intensity fluctuations which can be used to obtain the radial distribution function and thus the average interatomic distance and the coordination number at the surface of liquid.

In studies of low energy electron diffraction (LEED), the electrons incident on the single crystal surface are scattered predominantly by the surface layer or the first few atomic layers. Just as it is useful to determine the structure of solid surfaces, low energy electron diffraction might also be employed to obtain information about the structure of liquid surfaces. Therefore, the intensities of elastically scattered low energy electrons from liquid lead, bismuth and tin surfaces were measured as a function of scattering angle and electron energy.[21] The samples were supported in crucible materials which appeared to show no chemical reaction with the solid or the molten phases.

When the crystal was completely melted and the temperature was about 5° above the bulk melting point the experiment was commenced. Photographic and/or visual observations were made of the diffraction screen; then a telephotometer was focused on the diffraction screen. The three-grid energy analyzer system had been adjusted to minimize the

through penetration of the inelastically scattered electrons in order to reduce the inelastic contribution to the total scattered intensity detectable on the fluorescent screen. The output of the telephotometer was plotted on the ordinate of an x-y recorder while the electron energy was plotted on the abscissa. This way, the plot of screen intensity as a function of beam voltage could be obtained as the voltage was scanned. The visual and photographic evidence indicated that the intensity fluctuation had radial symmetry about the electron gun axis.

The cleanliness of the molten surface was checked by cooling the crystal below its freezing point and observing the resultant diffraction pattern of the crystal surface. The recrystalized surfaces always displayed sharp diffraction patterns and thus, the liquid surfaces were considered to be clean.

The experimental results obtained from the voltage scans at different scattering angles were normalized to constant electron emission in order to eliminate one of the experimental variables from the experimental curves. The most convenient presentation of the measured intensity at different scattering angles and beam voltages from liquid surfaces is in the form of contour maps. The ordinate is taken as the screen angle, ϕ with respect to the electron gun which is in the center of the screen (surface normal). The abscissa is the beam voltage and the contours are normalized intensities in arbitrary units. Figures 22a, 22b and 22c show results from molten lead, bismuth and tin surfaces respectively. The intensity contours connect those scattering angle and beam voltage values which are characterized by uniform intensity. To convert the screen angle, ϕ to a more usual angular variable let the scattering angle, θ, be equal

to $\theta = 180° - \phi$ where $\phi = 0$ refers to the exact back-scattering or 180° scattering. The intensity units, even though arbitrary, are directly comparable on all three contour maps (Figs.22a-c). Figure 23 is an intensity map calculated from x-ray data by Kaplow[66] on liquid lead. Similar results were obtained by Richter, et al.[67] using high energy electron diffraction. Their data was extrapolated to our region of low energies; the dotted line connects the points where the first maximum should appear. It is readily apparent that none of the experimental curves show features comparable with this calculated curve. Thus, the intensity fluctuations which we have detected cannot be used to calculate the radial distribution function from liquid surfaces.

Perhaps the most significant result of our LEED studies of liquid surfaces would be if we could associate the observed intensity distribution as being solely due to a single atom scattering mechanism. In that case the data directly gives the atomic scattering factor, f.

Let us consider additional scatterings mechanisms which could contribute to the intensities observed by scattering of low energy electrons from liquid surfaces. (a) Inelastic electrons which lost small energy (< 2 eV) may penetrate the repelling grids and contribute uniformly to the background intensity thereby diminishing the magnitude of the intensity fluctuation, (b) multiple scattering effects which are due to further interactions between the scattered electron beams and (c) thermal diffuse scattering which attenuates the intensities of the diffraction features from liquid surfaces due to increased vibrations of atoms in the disordered surface.

Inelastic contributions tothe scattered intensity would uniformly increase the background and may mask small intensity fluctuations. Thus, this term would not be expected to change the intensity distributions markedly. The effect of multiple scattering is difficult to assess. It might introduce additional intensity fluctuations which would be superposed on the single scattering distribution so that single and multiple scattering contributions could not be separated. Thermal diffuse scattering has been by Webb et al. in some detail. Since this term is proportional to the atomic scattering factor and to the Debye-Waller factor, it also should not change the intensity distribution markedly.

Therefore, it may be concluded that the intensity distribution of the low energy electrons scattered by lead, bismuth and tin liquid surfaces gives us directly the low energy electron atomic scattering factor for which single and multiple scattering contributions are inseparable.

Although it is somewhat disappointing that intensity fluctuations due to the radial distribution function in the liquid surface could not be detected by low energy electron diffraction (LEED) (in view of the easy detectability of this effect in the bulk liquid by high energy electron diffraction (HEED), x-ray and neutron diffraction) the absence of these features can easily be rationalized. All three effects, (a), (b), and (c), which were mentioned above would be instrumental in reducing the intensity changes by increasing appreciably the background intensity. It should be remembered that the peak intensities are never more than a factor of two higher than the background intensity in all of these experiments with bulk liquids near the melting point. There may be an additional reason for masking the scattering due to the liquid "surface structure" (i.e.

correlated disorder).[36] Due to the low penetration depth of the electron beam in LEED experiments the number of atoms which contribute to coherent scattering is at least two orders of magnitude smaller than in LEED experiments.

VIII. THE MEAN SQUARE DISPLACEMENT OF SURFACE ATOMS

A. The Mean Square Displacement of Surface Atoms Perpendicular to the Crystal Surface

In one of the preceding sections (N) the theory describing the thermal effects in LEED was discussed. Experimentally, the procedure for determining the surface Debye temperature is quite simple: at room temperature an intensity scan is made and a maximum in the $I_{00}(eV)$ curve is determined. The telephotometer is focused on the 00-spot at the voltage corresponding to the maximum intensity. The crystal is heated (e.g. for Pd to about 650°C) and the power is turned off. The telephotometer output signal (monitoring the spot intensity) is plotted as ordinate; the thermocouple reading as abscissa, producing a curve as shown in Fig.24 . In this way there is no interference from fields caused by the heater current. Generally it takes 1-5 minutes for a crystal to cool to below 100°C. The lower (essentially horizontal) curve in Fig.24 is obtained by rotating the 00-spot into the center of the screen and recording the intensity of the "background" at the same voltage as the previous intensity curve. To obtain the effective Debye temperatures, the intensity of the diffraction spot is read off the curve at different temperatures; the background value is substracted from this value and the $\log_{10}(I_{00}-I_{BKGRD})$ calculated. Figure 25 is a plot of $\log_{10}(I_{00}-I_{BKGRD})$ vs T (1°K) obtained from Fig.24.

The effective Debye temperatures which were obtained at the lowest electron energies were taken as values characteristic of the surface atoms, $\Theta_{D,surf}$. In some cases where extrapolation to zero electron volt could be carried out with some confidence the extrapolated value was taken as $\Theta_{D,surf}$. Then the root-mean-square displacement, of surface

atoms perpendicular to the surface plane was calculated from the equation

$$\langle u_j^2 \rangle_{surf}^{1/2} = \left[\left(\frac{3\hbar^2}{Mk} \right) \frac{T}{\theta_{D,surf}^2} \right]^{1/2} \qquad (102)$$

where M and T are the atomic weight and the temperature of the solid, respectively, N is Avogadro's number and k and h are the Boltzmann and Planck constants.

As an example, the effective Debye temperature for two crystal faces of lead and palladium are plotted in Figs 26a and 26b as a function of the electron energy. The surface Debye temperatures are about a factor of 1.8-2 times smaller than the corresponding bulk values. Conversely the root mean square displacement of surface atoms perpendicular to the surface plane $\langle u^2 \rangle_{surf}^{1/2}$, is roughly 140%-200% larger than the bulk value. In Table I we list all of the data from different crystal surfaces which have been determined so far by experiments. We list the surface and bulk Debye temperatures and/root mean square displacement ratios for comparison.

For all of the materials which have been studied so far the surface root mean square displacement perpendicular to the surface is much larger than the bulk value of the root mean square displacement. Conversely, the surface Debye temperature is much smaller than the Debey temperature characteristic of the bulk atoms. There seems to be little difference in the mean square displacements of surface atoms in different low index planes with respect to the large difference between the bulk and surface values. This is in agreement with previous experimental and theoretical predictions within the experimental accuracies. In calculating the root mean square displacements we have not corrected the electron energy for the presence of the inner potential. The attractive potential that the

electron experiences at the surface adds an energy increment to the electron energy which is of the order of 5-25 eV. Such a correction would have a little effect on the effective mean displacement which are calculated from the Debye-Waller factor determined at lower electron energies. A root mean square displacement can be corrected for the presence of the inner potential by using the formula $\langle u^2\rangle^{1/2}$(corrected)= $\langle u^2\rangle^{1/2}$(uncorrected) $(ev+ip/ev^2)$. For example at eV = 50 eV and for ip = 20 eV $\langle u^2\rangle^{1/2}$ is .86 $\langle u^2\rangle^{1/2}$uncorrected. Since the inner potential value has not been determine accurately, all of the data are given without inner potential correction. An inner potential correction will tend to decrease somewhat the calculated mean surface vibrational amplitudes.

B. Mean Square Displacement of Atoms Parallel to Crystal Surfaces

Figure 27 represents the general LEED situation useful for calculating the Debye-Waller factor for the parallel component of the mean displacement of surface atoms. 2ϕ is the angle between the electron gun which is the source of the incident electrons and the (00)-spot (specular reflection) on the fluorescent screen; $2(\theta-\phi)$ is the angle subtended by the diffraction spot, (h,k) and the electron gun. From Fig.27 we obtain that:

$$|\Delta\vec{k}'|^2 = 4|\vec{k}^\circ|^2 \cos^2(\theta-\phi) = |\Delta\vec{k}'_\perp|^2 + |\Delta k'_\parallel|^2 \qquad (103)$$

where $|\Delta\vec{k}'_\perp| = |\Delta\vec{k}'| \cos\theta$ and $|\Delta\vec{k}_\parallel| = |\Delta\vec{k}'| \sin\theta$. For any isotropic surface [i.e. (100) or (111), but not (110) for fcc crystals] we can write

$$\langle u^2\rangle_{SURF} = \langle u_\parallel^2\rangle_{SURF} + \langle u_\perp^2\rangle_{SURF} \qquad (104)$$

which can be substituted into Eq. 20 to give

$$\exp -|\Delta k'|^2 \langle u^2\rangle = \exp-\left[|\Delta\vec{k}'_\perp|^2 \langle u_\perp^2\rangle + |\Delta\vec{k}'_\parallel|^2 \langle u_\parallel^2\rangle\right] \qquad (105)$$

for the Debye-Waller factor. Substituting Eq. 103 into 105 and letting $k^o = 2\pi/\lambda$ gives

$$\exp\ [-2W'] = \exp\left[4\left(\frac{2\pi}{\lambda}\right)^2 \cos^2(\theta-\phi)\cos^2\theta\ \langle u_\perp^2\rangle + 4\left(\frac{2\pi}{\lambda}\right)^2 \cos^2(\theta-\phi)\sin^2\theta\ \langle u_\parallel^2\rangle\right] \quad (106)$$

simplifying,

$$\exp[-2W'] = \exp\left\{-\frac{16\pi^2\cos^2(\theta-\phi)}{\lambda^2}\left[\langle u_\perp^2\rangle\cos^2\theta + \langle u_\parallel^2\rangle\sin^2\theta\right]\right\} \quad (107)$$

Using Eq. 19 and changing to LEED variables as in Eq. 21, Eq. 109 becomes

$$\exp_{10}[-2\ '] = \exp_{10}\left\{-KVT\cos^2(\theta-\phi)\left[\frac{\cos^2\theta}{\theta_{D\perp}^2} + \frac{\sin^2\theta}{\theta_{D\parallel}^2}\right]\right\} \quad (108)$$

where C is the same constant as in as in Eq. 21 and $\theta_{D\perp}$ is the effective Debye temperature describing thermal motions normal to the surface; $\theta_{D\parallel}$ is the effective Debye temperature for thermal motions in the plane of the surface. $\theta_{D\perp}$ is the quantity determined from the previously described measurements on the specular reflection. The extension to non-isotropic surfaces would require the definition of an aximuthal angle and the splitting of $\langle u_\parallel\rangle$ into components along the main surface coordinates. This will not be discussed here as the extension of the above method to this situation is obvious.

The most obcious characteristic to observe about Eq. 108 is that $\theta_{D\parallel}$ can only be determined by the difference in two experimental determinations of $\log_{10}(I_{hk})$ vs T. Further, since in conventional back-reflection LEED systems, ϕ cannot exceed 24° or θ exceed 48°, the two experimental slopes ($\Delta\log I_{hk}$-$I_B/\Delta T$) will be of comparable magnitude. In practice

it has been found that an uncertainty in either experimental determination of slope propagates in determining a value for $\theta_{D\|}$ about ten-fold, so that an uncertainty in $\theta_{D\perp}$ of 5% produces a 50% uncertainty in $\theta_{D\|}$ making extrapolations of $\theta_{D\|}$ (eV) curves difficult. Experiments using grazing angle incidence low energy electron beams are therefore necessary to determine the parallel components of the mean square displacement with any degree of certainty. Surface Debye-Waller factor measurements under these conditions have been carried out for the Ni(110) face by MacRae.[34]

IX. THE STRUCTURE AND PHASE TRANSFORMATIONS OF CLEAN ORDERED SURFACES

A. Sources of Surface Impurities

We have discussed in some detail how the low energy electron diffraction pattern is sensitive to the appearance of ordered structures or ordered impurities in very small concentrations. On the other hand it is insensitive in the presence of disordered impurities in concentrations as high as 5-10% of the total number of surface atoms. Therefore, one needs additional experiment techniques which might be used in combination with low energy electron diffraction to ascertain the cleanliness of the surface. Appropriate techniques are Auger Spectroscopy, flash desorption experiments using mass spectrometry, and ellisopmetry. Although no definitive experimental criteria for cleanliness for each material is possible, if these additional experimental techniques and the low energy electron diffraction results do not suggest the presence of surface impurities and the surface structures which have been detected are reproducible in several laboratories it could then be assumed that the observed surface structure is characteristic of a clean surface. The presence of impurities below the detection limit of any of these presently available techniques cannot be excluded. These impurities may still act catalytically favoring or inhibiting certain structural transformations though the impurities themselves do not participate necessarily in forming the new surface structure.

The impurity concentration at surfaces could change during an experiment and in many ways may influence the experimental results. Therefore it is essential that we consider the different sources of surface impurities during a low energy electron diffraction experiment. One of the most probable

source of surface impurities is the adsorption of reactive gases on the surface. In ultra high vacuum systems which are used presently carbon monoxide and water vapor are those reactive molecules which are present in large concentrations. These molecules could react with the studied crystal surfaces. Adsorption of these molecules could start chemical surface reactions which can alter the nature of the solid surface. In any given experiment after extended periods of experimentation they may induce irreversible chemical or crystallographic changes in the surface. Their interaction with the electron beam can result in the deposition of unwanted surface species such as carbon on the surface. The crystal bulk is another source of impurities. Bulk impurities may migrate to the surface and segregate out while the crystal is being heated to elevated temperatures. Although this is an excellent method to free the crystal bulk from impurities which are removed to the surface, surface contamination may be unavoidable especially in the beginning of the experiment. Once these impurities reach the surface they may be removed by ion bombardment or some chemical reaction such as oxidation. One of the frequently detectable bulk impurities of this type is sulfur which has commonly been observed to diffuse to the surface of different metals.[69] Carbon is another contaminant which has been found to move from the bulk to the surface and segregate out. Nevertheless, these could be removed from the crystal surface after careful chemical treatments, repeated ion bombardment and annealing of the single crystal samples. Perhaps the most tenacious impurities are those which are in the bulk of the single crystal samples and have diffusion rates similar to the self-diffusion rate of the host lattice itself. These impurities will not diffuse to the surface and will not segregate out easily and therefore they are permanently embedded in the single

crystal samples. Such impurity is for example tantalum in niobium where the tantalum has similar diffusion rates to that of the self-diffusion rate of niobium single crystals.[71] In these cases several single crystal samples should be used in the hope that the level of impurities are different in the different samples. Inherent irreproducibility of surface structural features could be a sign of impurity controlled surface properties. The third source of unwanted impurities at the surface could be due to the interaction of the electron beam with adsorbed gases or the host lattice itself. It was found that ionic crystals, mostly alkali halides, interact chemically with the electron beam which leads to the decomposition of the surface.[72] Halogen evolution and the precipitation of alkali metal in an amorphous form at the crystal surface is commonly observed in studies of different alkali halides by low energy electron diffraction. In order to avoid excessive decomposition which would effect the diffraction spot intensities and other surface parameters,one may heat the crystal to a temperature at which the damage introduced by low energy electron beam could be removed by the annihilation of defects at the surface. Finally, it is found that certain adsorbed molecules, such as carbon monoxide, may desorb from metal surfaces due to electron impact by low energy electrons. Although the exact mechanism of the electron beam excitation of the adsorbed species has not been investigated it is particularly interesting that carbon monoxide interacts strongly with the electron beam while other gases with weaker surface binding energies such as xenon or the olefins do not seem desorb from metal surfaces at a detectable rate.

B. Order-Order Surface Phase Transformations

Most of the surfaces which have been studied by low energy electron diffraction so far were high density, low index crystal faces of monatomic or diatomic solids. Without exception, all of these faces exhibited ordered structures on an atomic scale. These ordered surfaces may be divided in two classes; (1) Those which have unit cells which are identical to the projection of the bulk unit cell to the surface and (2) those which are characterized by unit cells which are larger than the unit cell dimensions in the bulk, The solids which belong to the first class have diffraction patterns which are characteristic of a (1×1) surface structure. The different crystal faces of tungsten [(110),(100), (221)] nickel and aluminum [(111) and (100)] for example, seem to belong to this class. Most semiconductors and some of the metal surfaces which have been studied so far, belong to the second class. These surfaces exhibit diffraction patterns with extra diffraction features which are superimposed on the diffraction pattern of the substrate unit mesh (predicted by the bulk unit cell). In Tables 2 and 3 we list some of the solid surfaces which exhibit these surface rearrangements.

The surface structures on semiconductor surfaces appear to have well-defined temperature ranges of stability. At temperatures above and below this range the surface undergoes a transformation into another ordered surface structure. For example, the (111) face of silicon has a (7×7) surface structure [Si(111)-(7×7)] which forms upon heating the crystal to about 700°C.[82,83] The diffraction pattern corresponding to this structure is shown in Fig. 28 . Above 800°C this surface structure transforms into

into a (2×2) structure which below 700°C the (1×1) surface net predominates. The (111) surfaces of semiconductors with the diamond structure seem to form (2×2) surface structures.

What is the mechanism of surface rearrangements? There are several possible mechanisms which are still under investigation.

1. Relaxation of Surface Atoms

The surface structure is formed by a periodic displacement of surface atoms out of the surface plane. The surface thus, exhibits a periodic "buckling" which gives rise to new, characteristic diffraction features. This mechanism may best be illustrated by considering what happends with atoms in a solid in the neighborhood of a vacancy, i.e. vacant lattice position. If we remove an atom from its equilibrium position in the bulk to the gas phase, the atoms surrounding the now vacant site "relax", i.e. will be displaced slightly toward the vacancy. They are no longer restrained from larger displacement in the direction of the empty site by the strong, repulsive atomic potential. Therefore, the free energy of removing an atom from its bulk, equilibrium position to the gas phase is partially offset by the energy of lattice "relaxation" about the vacancy. The free energy of vacancy formation from a rigid lattice which is not allowed to relax can be approximated by the cohesive energy, the energy necessary to break a solid into single atoms infinitely separated from each other. We find that the free energy of forming vacancies is always appreciably smaller than the cohesive energy for most solids where these quantities have been measured. For example, for silicon, the cohesive energy is 81.0 kcal/mole, while the free energy of vacancy formation is 32.2 kcal/mole.[84] This leaves over 48 kcal/mole, a very large relaxation energy.

Surface atoms are in an anisotropic environment as though they were surrounded by atoms on one side and by vacancies on the other. The atoms can "relax" out of plane, perpendicular to the surface which is not allowed for the bulk atoms. Depending on the bonding properties of the solid, atoms may be displaced out of plane in a periodic manner. This way there is an increased overlap of localized electronic orbitals. Calculations indicate[85,86] that the formation of some of these buckled surfaces can be energetically favored over the formation of flat surfaces in temperature ranges below the melting point of the solid. The appearance of any new surface periodicity will be reflected in the characteristic of the LEED diffraction pattern. It is likely that surface structural rearrangements in germanium, silicon and other semiconductor surfaces are by this mechanism.

It should be noted that the periodic out-of-plane surface relaxation should be very sensitive to the presence of impurities or to certain types of lattice defects emerging at the surface (dislocations, vacancies). These could cause the collapse of surface structures by changing the chemical environment about the surface atoms or, in some cases, could also catalyze their formation.

2. Surface Phase Transformation

Some of the metal surfaces were also found to undergo atomic rearrangements (see TableII). For example, the (100) surfaces of gold[76,87] and platinum[88] exhibit a diffraction pattern which is shown in Fig.29 . The presence of the n/5-order diffraction spots indicate the appearance of a new periodicity which is five times as large along one principal axis and the

same as that in the bulk unit cell along the other. The pattern is a result of the superposition of domains of two structures of this type rotated 90° to one another. These surface structures may be designated as Au(100)-(5×1), and Pt(100)×(5×1). The diffraction patterns can be interpreted as indicating the presence of a hexagonal arrangement of scattering centers superimposed on the underlying square (100) substrate. The interatomic spacing in the hexagonal surface layer is 5/6 that of the substrate along one principal axis and the same along the other. Thus, the atoms in the hexagonal surface are coincident with every 5th substrate atoms and this could generate the observed five-fold surface periodicity. A small compression (~5%) in the hexagonal layer would allow six rows of the surface layer to fit onto the five rows of the square substrate.[87,88]

The chemical properties of this surface structure [its sensitivity to chemisorbed gases [$(5\times1) \xrightarrow[\text{adsorption}]{\text{gas}} (1\times1)$] make it likely that the surface structure is again the result of periodic "buckling" of the surface plane. In this case, however, the surface relaxation resulted in the formation of a hexagonal surface structure, i.e. there is a change of rotational multiplicity (from 4-fold to 6-fold). For semiconductors the surface structure maintained the rotational symmetry of the bulk unit cell even though the surface net became enlarged. Furthermore, the (5×1) surface structure and surface structures on other metal surfaces[75,76] are stable from 300°K up to almost the melting point of the solid. It appears that these surfaces have undergone a phase transformation from a face centered cubic to a hexagonal close packed surface structure while no corresponding transformation has occurred in the bulk of the solid.

The crystal structure which a solid will take up has been shown to depend primarily on the number of unpaired s and p valence electrons per atom which are available for binding.[89] For example, atoms which have one unpaired s or p electrons have body centered cubic crystal structure when condensed to solid (like Na, W). Atoms with two unpaired s and/or p electrons will crystallize in the close-packed hexagonal structure (Zn, Os); three unpaired valence electrons will give face centered cubic (Pt,Ag), and four unpaired valence electrons give diamond crystal structures (Ge,C). A theory based on this concept, when extended to include the contribution of unpaired d electrons to the binding can explain and predict the structure and stability range of most alloys.[90,91]

Surface atoms, in addition to being in an asymetric environment, have fewer neighbors than atoms in the bulk of the solid. Therefore, their electron density distribution should be different from that in the bulk, they may have more or less valence electrons available for binding than the bulk atoms. Thus, they may undergo phase transformations in the surface plane with respect to their crystal structure in the bulk. It appears that on the (100) face of gold and platinum a face centered cubic close packed hexagonal surface phase transformation has occurred.

It should be noted again, just like in the case of surface relaxation, impurity atoms with different numbers of unpaired valence electrons per atom may cause or accelerate surface phase transformation of this type or transition metal surfaces, or conversely may inhibit it. For example, carbon (4 unpaired valence electrons per atom) stabilizes the (1x1) surface structure on the platinum and gold (100) surfaces.[92] On the other hand there appears to be evidence that alkali metal atoms (Na,K) on these

noble metal surfaces, which have less valence electrons per atom than the platinum and/or gold surface atoms can stabilize the hexagonal surface structure (5×1).[62]

This mechanism would also predict the formation of surface alloys with a variety of structures and other intersecting physical chemical properties. These may be prepared by the deposition of other suitable metal atoms with different number of unpaired valence electrons. There is evidence that tungsten surfaces undergo structural rearrangements during carbon diffusion which indicates a 6 cc → hcp surface phase transition long before hexagonal W_2C precipitates out at the surface. For example the W(100) surface develops a (5×1) structure first which is followed by the formation of the carbide structure.

3. Faceting

Some of the more open, lower atomic density surface planes appear to be unstable upon heat treatments. At temperatures where surface atoms have enough mobility to diffuse the surface undergoes rearrangement. New, high density crystal planes form with the simultaneous disintegration of the more open crystal face. This process is frequently called faceting. LEED studies on the (110) faces of silver for example, have indicated that faceting begins at low temperatures (< 140°C).[68]

4. Structural Changes Due to Variation of Surface Chemical Composition

As noted above, the structure of metal surfaces appear to be very sensitive to the electron density at the surface. Furthermore, the presence of impurities have been shown to be very important in initiating or stabilizing surface transformations. There is, therefore, strong evidence that the structure of a surface should be very sensitive to slight variations in chemical composition. These considerations should be particularly important in studies of diatomic and polyatomic crystals where non-stoichiometry may easily be induced in the surface by heating in vacuum. As yet, this area has received relatively little attention.

The following study may be taken as an example of the importance of these considerations.

The structure of alumina surfaces is different from that which is expected by projection of the bulk unit cell to the various crystal surfaces.[92, 93, 95, 96] The (0001) crystal face exhibits its (1x1) bulk-like structure up to ~1250°C in vacuum. It rearranges above this temperature to give a weak $(\sqrt{3}x\sqrt{3})$ - (rotated 30°) surface structure, and upon further heating to the final rotated $(\sqrt{31}x\sqrt{31})$ surface structure which is stable to the highest studied temperature of 1700°C. The diffraction patterns are shown in Fig. 30a-b.

It is customary to designate the complex surface structures by the coefficients of its transformation matrix which generate the structures with the unit cell vectors of the bulk-like substrate.[97] This is given, for the rotated ($\sqrt{31}\times\sqrt{31}$) pattern by

$$A = \begin{matrix} 11/2 & \sqrt{3}/2 \\ -\sqrt{3}/2 & 11/2 \end{matrix} \qquad B = \begin{matrix} 11/2 & -\sqrt{3}/2 \\ \sqrt{3}/2 & 11/2 \end{matrix}$$

These matrices generate the two domains which must be present on the surface simulatenously in order to generate the observed diffraction pattern. These domains are formed from the original unit mesh by expanding the unit vectors by a factor of $\sqrt{31}$ and by rotating them either $+9^\circ$ or -9°. We shall show evidence that the alumina surface which exhibits the rotated ($\sqrt{31}\times\sqrt{31}$) surface structure is oxygen deficient.

The other two crystal faces, the (1012) and (1123) orientations which have been studied, give (2×1) and (4×5) surface structures, respectively at high temperatures ($> 900^\circ C$).[96]

Heating, by radiation, the freshly etched (0001) alumina surface which exhibits the (1×1) surface structure in vacuum, above $1250^\circ C$, readily produces the rotated ($\sqrt{31}\times\sqrt{31}$) surfaces structure (Fig.). During its formation oxygen evolution is detectable by mass spectrometer.

In order to establish that the stable high temperature rotated ($\sqrt{31}\times\sqrt{31}$) surface structure has a chemical composition which is different

from that of the low temperature (1×1) surface structure and to establish its stoichiometry the (0001) face was heated in excess oxygen and aluminum vapor.

When the rotated ($\sqrt{31}\times\sqrt{31}$) surface structure is heated in oxygen at pressures $> 10^{-4}$ torr (these pressures considered to be high in ultra high vacuum LEED studies) at 1200°C the (1×1) surface structure was obtained. Removal of the oxygen and heating to slightly higher temperature (1250°C or higher) in vacuum caused the reappearance of the rotated ($\sqrt{31}\times\sqrt{31}$) surface structure. This reversible phase transformation could be induced at will upon introduction or removal of oxygen.

When aluminum metal was condensed on the (0001) alumina surface which exhibits the (1×1) surface structure, the rotated ($\sqrt{31}\times\sqrt{31}$) surface structure is formed with heating to 800°C. In the absence of excess aluminum on the surface, the (1×1) surface structure would have been stable. Thus, the structural changes which occur in vacuum (mass spectrometric detection of oxygen while the rotated ($\sqrt{31}\times\sqrt{31}$) structure forms), in oxygen (the (1×1) surface structure is regenerated in a temperature range, ~1200°C, where the rotated ($\sqrt{31}\times\sqrt{31}$) structure is stable), and with aluminum (the rotated ($\sqrt{31}\times\sqrt{31}$) structure is formed in a temperature range, ~800°C where the (1×1) surface structure is stable) indicate that the (0001) face of alumina undergoes a surface phase transformation from a (1×1) surface structure to an oxygen-deficient, rotated ($\sqrt{31}\times\sqrt{31}$) surface structure which is stable at high temperatures.

It is difficult to explain the appearance of large surface unit cells which are also rotated with respect to the bulk unit cell without invoking significant chemical rearrangements in the surface layer. The

rotated ($\sqrt{31}\times\sqrt{31}$) unit mesh signifies marked mismatch between the newly formed surface structure and the underlying hexagonal substrate.

It appears that if the high temperature oxygen deficient rotated ($\sqrt{31}\times\sqrt{31}$) surface structure has a composition which corresponds to Al_2O (or AlO) it would be likely to form a cubic overlayer in which the cation is appreciably larger than in the underlying hexagonal (0001) substrate. Strong mismatch due to the differences in structure and ion sizes in the two layers should be expected.

One can generate the rotated ($\sqrt{31}\times\sqrt{31}$) surface structure by placing a cubic overlayer inwhich the interatomic distance was increased to adjust for the increased cation radius on top of the (0001) substrate. There are several cubic structures which can generate the rotated ($\sqrt{31}\times\sqrt{31}$) unit mesh by coincidence with (0001) substrate. One of these surface structures are given in Fig.

If the reduced oxides of aluminum, Al_2O or AlO, are stable in the α-alumina surface at elevated temperatures, it is likely that the other group III oxides of the M_2O type might also be stable in the surface environment. Investigation of the surface structures of Ga_2O_3 and In_2O_3 would be of interest. It is also likely that oxides of other metals (MgO, BaO for example) may have unusual oxidation states which are stabilized in the surface environment. It should be noted that vanadium pentoxide, V_2O_5 has been reported recently[98] to undergo a change of surface composition (accompanied by loss of oxygen) upon heating in vacuum with a corresponding order-order transformation of its surface structure.

C. The Structure of Vaporizing Surfaces

Experiments in which the evaporation rate of metals into vacuum was measured as a function of temperature indicated that the vacuum vaporization rates are equal to the ideal maximum rates of vaporization, and independent of crystalographic orientation. It is apparent from these results that every atom on the surface has equal probability of vaporizing. This is surprising since the surface is heterogeneous. There are several surface sites in which atoms have different numbers of recent neighbors and which are distinguishable by their different binding energies. It is therefore not to be expected that all of these surface sites can equally participate in the vaporization process. In order to explain such a high vacuum vaporization rate it was proposed that the vaporizing surface may be liquid like. The concentration of disordered atoms was proposed to be equal to the total number of surface atoms and these atoms, having high surface mobility, can wander around on the surface and vaporize when sufficient energy is imparted to them so that they can leave the surface. In order to study the structure of the vaporizing surfaces the diffraction pattern of several metal surfaces (silver, chromium and nickel), have been monitored, while these surfaces vaporize into the vacuum.[60] These metals were heated to a temperature at which the vapor flux away from the surfaces was appreciable, of the order of 100-1000Å per second. It was found that during vaporization the surface remains ordered and it was characterized by sharp diffraction features. Electron microscopic pictures of similar vaporizing surfaces indicate a large degree of heterogeneity and extreme roughness on a scale of about 10,000Å to 200,000Å. Nevertheless, on an atomic scale the surface

appeared to be ordered during vaporization. However, the low energy electron diffraction pattern is not particularly sensitive to the presence of disordered surface atoms up to concentrations to 8% of the total number of surface atoms. Therefore it is possible that such a concentration of disordered atoms might be present on the surface during vaporization. Nevertheless most of the surface atoms appear to be in their ordered, equilibrium position at the vaporizing surface during the vaporization process.

D. Low Energy Electron Diffraction Studies of Surface Melting of Lead, Bismuth and Tin Surfaces

Studies of the mean square displacement of surface atoms by measuring the temperature dependence of the low energy electron diffraction beam intensity (the surface Debye Waller factor) have shown that for several monatomic face centered cubic metals the mean square displacement of atoms in the surface is appreciably larger than the mean square displacement of atoms in the bulk. There is at least one model of melting which indicates that the mean square displacement plays an important role in determining the melting temperature.[99,100] Therefore the results would indicate that the surface may disorder, that is loses its long range order at temperatures below the bulk melting point. In order to explore the importance of surfaces in the melting process and to investigate whether the surfaces premelt (that is melt at a temperature below the bulk melting point), low energy electron diffraction studies have been carried out to monitor the surface structure up to the melting point and the order-disorder phenomona on the surface at the melting point.[21] The surface structures of the (111) (110) and (100) crystal faces of lead, the (0001) and (01$\bar{1}$2) faces of bismuth, and the (110)

faces of tin single crystal were monitored up to the melting temperature and during melting. These metals are particularly suitable for low energy electron diffraction studies, which have to be carried out in ultra high vacuum, since they have very low vapor pressure - less than 10^{-8} torr at their respective melting points. There are, however, important differences in many physical-chemical properties of these materials. They have different crystal structures. Lead and tin, like most solids, expand upon melting. Bismuth however, undergoes a negative volume change on melting it contracts. Thus we can study the effect it any of these properties on the melting and freezing kinetics. The diffraction spot intensities decrease monatomically according to the temperature dependence predicted by the Debye Waller factor but were always detectable until the bulk melting point was reached. In Fig. 31 the observed diffraction patterns below and above the bulk melting point are given. In every experiment the diffraction pattern remained intact until at the bulk melting point the molten interface reaches that region of the surface where the electron beam was focused and the diffraction spots disappear. In one experiment using a large lead disc, the temperature gradient was introduced along the surface such that melting commenced near one edge of the disc and the melting front proceeded across the surface very slowly. By suitable manipulation of the winning magnets, the electron beam was focused near the hottest part of the crystal and as the pattern from this area disappeared due to melting the beam was moved to an adjacent still solid portion a diffraction pattern was again obtained until that region melted and so on. In some experiments with bismuth, heating was performed from the bottom. Since the solid is less dense than the liquid the surface

solid remained intact and floated on the molten bismuth beneath. As the crystal melted completely the last solid portion would float around on the liquid and the diffraction spot would move correspondingly. The melting of the lead (110) surface was studied with particular care since it is the lowest density and the highest surface free energy surface of the three lead crystal surfaces studied. In fact, once melted the (110) orientation never appeared on the recrystallized lead samples. Nevertheless, the (110) surface proved to be ordered and stable to the bulk melting point of lead just as observed with the (111) and (100) crystal faces. The surface melting experiment with the tin (110) surfaces were more difficult to perform. In every case a surface structure had formed on this face. This structure agrees with the (3×1) surface structure reported by Jackson and Hooker for slow epitaxical deposition of tin on niobium (110) surfaces.[101] Surface contamination problems were certainly serious in the melting studies with the (110) surfaces of tin.

In summary, three crystals faces of lead (111) (100) and (110), and two different crystal faces of bismuth (0001) and $(01\bar{1}2)$ were studied and showed no premelting, they remained stable to the bulk melting point and they melted spontaneously at that point. Contamination of lead and bismuth surfaces could be completely avoided. Formation of a surface structure and contamination problems make the melting studies with tin (110) surfaces difficult to perform. The experiment criterion used to ascertain melting was the loss of the diffraction features (i.e. the disappearance of the diffraction spots which are due to long range order in the crystal surfaces (Fig. 31a-b). If the surface remains ordered, the diffraction spots should be visible up to the temperature at which the

loss of long range order occurs. It should be noted however again, that the concentration of disordered surface shows could be as high as 5-10% of the total surfaces concentration before there is an experimentally detectable decrease in the LEED spot intensities.

Low energy electron diffraction studies of the melting of low index lead, bismuth and tin single crystal surfaces in which the disappearance of the diffraction pattern characteristic of long range order was taken as a sign of melting indicated no surface premelting. The different surfaces seem to disorder at their respective bulk melting temperature. Although bismuth undergoes negative volume change upon melting and has a crystal structure different from that of lead the melting behavior of its surfaces are similar to that of lead surfaces. The low energy electron diffraction pattern is insensitive to the presence of disordered atoms on the surfaces as long as their concentration is only a few percent of the total surface concentration. Thus the presence of a LEED pattern from the different surfaces which suggests a dominance of long range order on the surface up to the bulk melting point does not rule out the presence of disordered atoms in a few atoms percent surface concentration.

There are several additional experimental observations accumulated in recent years which gives us indications of the mechanism of melting. Turnbull, et al. showed that bulk quartz and P_2O_5 crystals could be superheated by 300°C and 50°C respectively due to the slow propagation of the viscous molten interface into the solids.[102] Melting was found to nucleate always heterogeneously at emerging dislocations or imperfections and then move into the bulk. In order to avoid nucleating of the melt at the surface, Cass and Magun[103] heated the inside of a ice single crystal while

keeping the surface below the bulk melting point. This way they were successful in observing superheating. Similar results were obtained by other investigators using gallium crystals.[104] Several experiments shows that in the presence of small temperature gradients the melting rate varies along different crystallographic orientations. These observations indicate that melting has to be nucleated and that the crystal surfaces appear to provide nucleation centers most efficiently. Thus when melting occurs in the presence of a surface, a condition almost always melt in melting experiments, superheating cannot be observed due to the large concentration of surface nucleation sites. Although most of the surface remains ordered up to the bulk melting point, it is likely that the nucleation sites are already present before melting commences. As soon as the liquid phase becomes thermodynamically stable the solid-melt interface may propagate along the surface or into the bulk from these nucleation centers equally well. A melting theory to be successful should have to explain the kinetic, thermodynamic and statistical properties of the melting phase transformation. These are a)low index surfaces of single monatomic solids remain chiefly ordered up to the bulk melting point. b) Superheating of solids occurs only in the absence of nucleation sites or because of the slow propagation of the melt inteface. c) Nucleation of melting occurs most easily at the surface and the melt propagates into the bulk from these selected surface nucleation sites. d) X-ray, neutron, and high energy election diffraction experiments indicate that melting occurs with the loss of long range order; And, e) melting is a first order phase transition with well defined thermodynamic parameters. So far none of the melting models which have been proposed have been able to account for all

of these properties. It is to be hoped that in the near future a judicious syntheses of the favorable features of some of these proposed models, which will be briefly numerated below, will produce a melting model which allows quantitative prediction of the melting characteristics of different solids.

There are several melting models which explain the kinetic properties of melting uncovered by recent experiments. Turnbull has proposed a melting model which allows the computation of the propagation velocity of the molten interface in the temperature gradient which is provided by superheating.[105] Agreement between that theory and experiments could be reached only if it was assumed that melting occurs only at some fraction of the surface sites at the solid melt interface. What is the nature of those surface sites where melting may be nucleated? None of the experimental melting studies so far have been able to identify these centers. They may be vacancies and vacancy aggregates or disordered regions around dislocations which emerge at the surface. Stark[106] has proposed that the vacancy concentration of the surface builds up faster than in the bulk. When a critical concentration of vacancies is reached melting is nucleated at the surface. Stranski has viewed melting as the dissolution of a solid in its own melt.[107] He has observed that certain crystal surfaces (high index) are wetted by their own melt while other faces (low-index) remain stable and are not wetted by their own melt even at temperatures very near the melting point. Thus, Stranski postulates that melting is initiated on high index surfaces. The low index crystal faces being stable at all temperatures up to the melting point. These melting models recognize the importance of surfaces in nucleating melting.

There are several other melting models which describe either the thermodynamic or the statistical properties of melting without consideration of the importance of the crystal surface in nucleating and initiating melting. Perhaps the most noteable and successful is that proposed by Lennard-Jones and Devonshire.[108] They adopted the Bragg-Williams model of one-dimensional order-disorder transition in which the first order transition is generated with the help of a disorder parameter. Born[109] has considered the major difference between the solid and liquid phase is the lack of resistance of liquids to low frequency shearing stresses. Using the elastic continuum model he predicts that as melting commences and the shear modulus of the crystal, C_{44}, vanishes. Sound velocity measurements in different crystals however did not bear out this prediction and the model was later retracted.[110] Kuhlman-Wilsdorf has proposed a model in which a free energy of formation of a dislocation is taken as positive in solids and is negative for liquids. The melting temperature is postulated to be the temperature at which the free energy is zero. The liquids are thus treated as infinitely dislocated solids.

E. Studies of the Freezing of Molten Lead and Bismuth by LEED

These investigations were carried out to discover the experimental parameters which influenced the surface structure of recrystalized metals and their kinetics of freezing and growth.[21,60] Studies of the surface structure of metal crystals during solidification should provide a great deal of information on the mechanism of crystal growth from the melt. The molten lead and bismuth samples were cooled using cooling rates in the range of 2°C per sec to .02°C per sec. It was found that during freezing more than one crystalite formed. These crystalites were nucleated at the

holder walls, as expected. Although the size of these crystalites varied, most of them were large enough to show sharp diffraction features allowing us to monitor their orientation and surface structure. Their orientation was checked by locating the specular (00) spot for each prominent crystallite. In discussing the effect of cooling rates on surface orientation one may take the cooling rate of .5 C per second as the dividing line between rapid and slow freezing rates. Rapid freezing rates (larger than .5C per sec) favored the growth of the (100) surfaces of lead while slow cooling rates (less than .5C per sec) favored the formation of the lead (111) surfaces. For bismuth surfaces the opposite results were obtained, rapid cooling rates favored the appearance of crystallites oriented with the (0001) or hexagonal axis perpendicular to the crystal surface and slow freezing rates favored crystallites with the [0112] axis (which is a psuedo-cubic [100]axis) oriented perpendicular to the crystal surfaces. Undercooling of liquid lead of the order of 8° were frequently observed during studies of the recrystallization of lead. However, bismuth did not show undercooling in any of the crystal growth experiments.

It was found slow freezing rates yield a dominantly (111) surface orientation for lead and the $(01\bar{1}2)$ orientation which is the pseudo-cubic (100) for bismuth crystallites. Conversely, rapid cooling rates produce the (100) orientation for lead and the (0001) or pseudo-cubic (111) surface for bismuth. We might argue that near equilibrium lead which has to contract upon freezing should prefer to build its lattice from surfaces which show the densest backing of atoms [(111) face]. Bismuth, which expands upon freezing should prefer a more open surface which still has low surface free energy. The result that growth conditions far from

equilibrium (fast cooling rates) produce opposite surface orientations of the two solids should have to be taken into account in future theoretical studies of crystal growth kinetics.

F. Low Energy Electron Diffraction Studies of Magnetic Surface Structures

In several magnetic transitions the magnetic structures which form are characterized by a unit cell which is not the same as the atomic unit cell. For example, nickel oxide is anti-ferromagnetic; it has a transition temperature of 525°C. Along the (100) surface is should have a (2x1) magnetic unit cell. It was found that upon heating the surface near the Neel temperature, new diffraction spots appeared which correspond to the appearance of a new surfaces periodicity.[111] This could be associated with magnetic ordering in the crystal. Thus it appears that magnetic ordering, in addition to neutron diffraction, can also be studied by low energy electron diffraction. Some of these studies have been carried out in addition to nickel oxide surfaces, on chromium surfaces as well.[112] One of the difficulties in these experiments is that the surface Debye-Waller factor being large it decreases the intensity of the diffraction spots due to magnetic ordering near the magnetic transition temperature and one has to use low electron beam energies and well ordered surfaces to be able to detect the onset of magnetic ordering. Nevertheless low energy electron diffraction studies promise to be an important tool in the studies of magnetic structure and magnetic phase transitions at surfaces.

X. LEED STUDIES OF THE ADSORPTION OF GASES ON SINGLE CRYSTAL SURFACES

Adsorption studies may be divided arbitrarily into two classes physical adsorption and chemisorption. Physical adsorption involves gases which have heats of adsorption less than about 10 kcal per mole. Chemisorption however inidicates strong, mostly electrostatic interactions between the adsorbed gas and the solid surface with heats of adsorption in excess of 15 kcal per mole.

A. Physical Adsorption

Due to the low heats of adsorption of these gases, physical adsorption studies have to be carried out at low temperatures (below room temperature). Only a few systems have been studied so far. Low energy electron diffraction studies of the physical adsorption of xenon and bromine on graphite single crystal surfaces showed that well-defined surface structures may form at low temperatures.[113a,b] These studies seem to provide the first evidence that physical adsorption takes place via the formation of ordered surface structures even for noble gas adsorbates for which the bonding between adsorbed atoms is weak. The two-dimensional condensation of adsorbed bromine to the liquid state could also be monitored by low energy electron diffraction. Physical adsorption studies of several gases on silver single crystal surfaces however, indicates that the adsorption takes place without the formation of ordered surface structures.[114] These studies have been varried out in combination with ellipsometry measurements. The adsorption isotherms of several gases have been measured and the heats of adsorption as a function of surface coverage have been computed. It was found that the adsorbate-adsorbate interaction was just as strong

at low coverages as the interaction between the adsorbate and the metal surface. Consequently, most of the adsorbed atoms are situated in patches on the silver surface. At present there are only few experimental results which make it somewhat difficult to assess the role of ordering in physical adsorption processes. It appears that larger heats of adsorption are necessary to localize the adsorbed atoms on the surface. Otherwise, surface diffusion(which might require only low activation energies)will tend to disorder the adsorbed surface layer. The formation of ordered surface structures should be preferred with decreasing temperature and with the adsorption of gases with increasing heats of adsorption.

B. Chemisorption

Chemisorption has been studied extensively in several laboratories in the past few years primarily on monatomic and diatomic solids of different crystal structure. In Table IV we have summarized the experimental informations which are available by listing the solid surfaces which were studied, the adsorbed gas and the surface structures which were found under a variety of experimental conditions of surface density of adsorbed atoms, and surface temperature. It is apparent from the available experimental data that ordering of adsorbed atoms into surface structures of different kind is an essential part of the chemisorption process. Although in some cases disordered adsorbed structures have been detected, in most experimental situations ordering is preferred over disordered adsorption. It is possible to classify the different chemisorbed structures into a few well-defined types which are already apparent from the experimental data.

1. Chemisorption on Top

Gases may chemisorb on the surface and arrange themsleves in different surface structures. The arrangement of atoms depends on the crystallographic orientation of the substrate, the atomic density of the adsorbate and the particular temperature at which the experiment is taking place. By adsorption "on top" we mean that the reactants which adsorbs on the surface or, if they dissociate, the products of dissociation will stay on the surface and will not subsequently diffuse into the bulk to participate in bulk chemical processes. The structure which forms is a two-dimensional arrangement in which the participating atoms are those of the adsorbed gas and does not include substrate atoms to any large extent. The adsorption of olefins on platinum surfaces provides a good example for this type of chemisorption. Ehtylene, propylene, butenes, and butadiene can adsorb on both (100) and (111) faces of platinum single crystals. While these gases form ordered structures [(2×2) surface structures] on the (111) crystal face they appear to adsorb in a disordered manner on the (100) face of platinum (with the exception of C_2H_4 and C_2H_2). One common characteristic of adsorbed gases is clearly apparent from these studies the adsorbed atoms or molecules if available in sufficiently large concentration, seem to form structures which give rise to the highest possible surface coverages. If ordered structures form, this means that unit cell of the surface structure is as small as the closest packing of the molecules allows. Adsorbed atoms of all types may form ordered structures provided that they are far apart. In most cases however, disordered adsorption is preferred over the formation of large unit cell surface structures. The underlying symmetry and size of the

substrate unit cell to a large extent, determines the structure of the adsorbed gas layer. In the case of large polyatomic molecules on the surface there substrate structure determines weather they can order on the surface or not. There can be several side reactions which may interfere with the chemisorption. Often the adsorbed molecules in the two-dimensional surface structures may undergo chemical decomposition. In the case of olefin adsorption it was found that cracking of the molecules, upon heating the surface to temperatures in excess of 200°C, may occur. The deposition of carbon could be monitored from the appearance of new diffraction features. Careful cleaning of the surface prior to adsorption studies must always be carried out. Adsorption of olefins on graphitic surfaces which may cover platinum is different than on pure platinum surfaces. Adsorption of saturated hydrocarbons (ethane for example) have been studied successfully on nickel surfaces.[116] It was found that ordered structures form and again, the structures have the smallest possible unit cell which indicates close packing of these organic molecules on the surface. The adsorption of saturated hydrocarbons on platinum surface however could not be studied because of the competition for adsorption sites on the surfaces between carbon monoxide which is one of the major constituents of the ambient and the hydrocarbon molecules. The carbon monoxide, adsorbing preferentially, have prevented the study of the adsorption of saturated hydrocarbons at the low pressures which are used in most of the low energy electron diffraction experiments.

Most of the adsorption studies used ambient pressures between 10^{-9} and 10^{-4} torr. Above these pressures the vacuum pumps may not be able to remove the gases effectively which were introduced into the system.

Due to the low pressures which were employed in LEED experiments some of the results of low energy electron diffraction studies may not be directly correlated with studies of surface adsorption or surface reactions which were carried out at high pressures. When adsorption or reactions which were carried out at high pressures. When adsorption or reaction of diatomic molecules is accompanied by the dissociation of the molecule, the pressure-dependent dissociation might prevent certain chemical reactions or adsorption to occur while these processes are clearly detectable at high pressures. In the future, considerable effort should be made to establish a pressure region where the low and high pressure studies would overlap so one could extrapolate the results of low pressure low energy electron diffraction experiments with confidence to high pressures as well. Low energy electron diffraction studies should be extended to as high pressures as experimentally feasible.

2. Reconstruction

It has been reported from several studies that a strongly exothermic surface reaction, such as the chemisorption of oxygen on nickel or on other metal surfaces, can dislodge the substrate atoms from their equilibrium positions and cause rearrangement of the surface structure which is commonly called reconstruction.[25,117] The reconstructed surface structures is composed of both metal and chemisorbed atoms in periodic arrays. Although changes in the diffraction pattern during chemisorption can be analyzed in several different ways, complimentary experimental evidences seem to indicate that reconstruction is the most likely interpretation of the structural changes observed during the oxidation of many metal surfaces. Reconstruction of the surface may be looked upon as a precursor for

oxidation reactions or other chemical reactions which proceed into the bulk i.e. carbide formation via carbon diffusion or nitridation via nitrogen diffusion into the bulk via a diffusion contrlled mechanism. Since reconstruction displaces and rearranges metal atoms on the surface, these structures may be stable to much higher temperatures than two-dimensional surface structures which are solely due to adsorbed gases. The type of surface structure which forms depend on the structure of the substrate and on the surface density of adsorbed atoms. For example, during the initial stages of chemisorption of oxygen on the nickel (110) surface (2×1) and (3×1) surface structures are formed.[117] Heating these surface structures in vacuum casues their disappearance which indicates that diffusion of oxygen from these surface structures into the bulk has occurred. Further oxygen dosing of surfaces at high temperature re-form these surface structures which appear to be surface intermediates during the dissolution of oxygen in the bulk nickel lattice. The dissolution of oxygen via the oxygen surface structures continues until the solubility limit of oxygen in the metal crystal is reached. At that point the metal oxide may precipitate out as a second phase. The formation of a second phase is accompanied by the appearance of streaking in the surface diffraction patterns and then the gradual appearance of new diffraction features which can be attributed to the newly formed oxide. Although reconstructed surfaces may persist to higher temperatures than those due to adsorbed gases only on top of the surface, they can often be removed by well-chosen surface chemical reactions. Oxide structures or structures due to chemisorbed oxygen could be removed by heating in hydrogen. Ion bombardment or high temperature heat treatment in vacuum which causes the

vaporization of the top most atomic layers can also be used to restore the surface to its original unreconstructed state.

Surface reconstruction processes which have been discovered by LEED studies gives us a new view of the mechanism of chemisorption. Reconstructed surfaces may well be the active surface structures in many exothermic catalytic surface reactions.

3. Co-Adsorbed Structures

Low energy electron diffraction studies further showed that the surface structures are formed during the simultaneous adsorption-(co-adsorption) of two gases which would not form in the presence of only one or the other gas component. The formation of these mixed surface structures seems to be a general property of adsorbed gas layers on tungsten surfaces. It was shown that the simultaneous adsorption of nitrogen and carbon monoxide on the (100) surface of tungsten gives a series of surface structures not all of which can be formed by the individual gases.[118] Similar results were obtained by the co-adsorption of oxygen and carbon monoxide on tungsten (110) faces[119] or hydrogen and carbon monoxide on the (100) surfaces of platinum.[93] The appearance of such surface structures indicate that there is a strong interaction within the adsorbed layers between the different molecules which arrange themselves in a mixed structure where both molecules appear to participate in the primitive unit cell. These structures form most frequently when both gases which are being adsorbed have approximately equal probability of adsorption. If one gas adsorbs much more strongly than the other, (for example, during the co-adsorption of xenon and carbon monoxide) then one finds that the more tenecious species (carbon monoxide) will replace and displace the other species (xenon) adsorbed on the surface.

In this case the co-adsorbed structures are unlikely to form. The observation of such co-adsorption phenomena indicates that in many chemical reaction studies it is important how the different reactive gases are introduced into the chemical reaction. When one gas is pre-adsorbed on the surface and the other gas is allowed to react with the adsorbed species one might find different chemical reaction rates and reaction products. Then if the two gases are introduced as a mixture simultaneously onto the surface.

4. Amorphous Surface Structures

It has beenfound during studies of the adsorption of oxygen on some metal surfaces that chemisorption takes place via the formation of a disordered layer. For example, the chemisorption of oxygen on aluminum surfaces takes place in such a manner.[120,121] The adsorption of carbon monoxide on the (100) faces of tantalum is another example of this type of adsorption.[122] When the chemisorbed disordered oxygen layer is heated. Oxygen from the aluminum surface diffuses into the bulk and the surface returns to its original clean, ordered metallic state. Further dosing with oxygen at high temperatures increases the concentration of oxygen in the bulk of the metal but the surface structure remains that of clean aluminum. This is in contrast with the behavior by oxygen on nickel or on tungsten surfaces. Once the bulk of the aluminum crystal is saturated with oxygen the surface finally loses its ordered aluminum structure and forms a disordered oxide which now can no longer be removed by heat treatment. Under high temperature heat treatment, in some cases, there is a degree of ordering which may be taking place on the surface. However the oxide which appears on the surface of aluminum at room temperature is characterized by

the lack of ordering. Bedaire, Hoffman and Smith[121] have observed the partially ordered growth of Al_2O_3 when the disordered oxide on the (100) face of aluminum was heated in oxygen at about 300°C. Although the experimental information which is presently available is scanty it appears that those oxide layers which form nonporus resistant surface films form disordered surface structures. The lack of crystal impurity of the surface structures may be correlated with the degree of non porosity of the deposited oxides in future studies. In some cases, heating the adsorbed disordered structure may result in partial or complete ordering. For example, ammonia adsorbs on the (100) surface of tungsten in a disordered manner at room temperature.[124] Upon heating to elevated temperatures, a C(2×2) surface structure forms with the evolution of hydrogen indicating that this structure consists of NH_2 groups adsorbed on the tungsten surface. Upon further heating, the structure is rearranged into a (1 1)-NH_2 surface structure. Carbon monoxide seems to chemisorb at room temperature on several crystal surfaces in an disordered manner.[122,125] Heating increases the surface order and aids the formation of ordered surface structures. It seems that the formation of these surface structures requires surface diffusion to occur. Therefore, it is important that in chemisorption studies sufficient attention is given to the thermal history and the thermal treatment which is being carried out after adsorption has taken place.

5. Three-Dimensional Structures

We have already discussed that during the chemisorption of gases which may induce exothermic chemical reactions at the surfaces, reconstruction of the solid surface may occur. This reconstruction may be followed

by further chemical reactions which take place in the bulk of the solid. As the surface species diffuse into the bulk the chemical reaction is no longer two dimensional but actually involves the species which are below the surface. In the final stages ofoxidation when the second phase (for example nickel oxide) is beginning to precipitate other surface structures may appear which are characteristic of that of the bulk oxide or some mixture of the metal and the oxide structures.[117] Three-dimensional structures also form during the carburization of tungsten.[126] Methane decomposition yields a layer of carbon on tungsten surfaces which subsequently diffuses into the bulk. There are ordered structures at the surface during this process in which the surface unit cells are of some integral multiple of the bulk tungsten unit cell. That is the body centered cubic tungsten structure appears to be maintained during the carbon diffusion process. The surface structures change from one ordered structure to another during carbon diffusion. Finally a structure indicating the precipitation and formation of tungsten carbide W_2C appears at the surface. Although LEED studies gives us information about the structure of the surface or maybe structures which are a few atomic layers deep at the surface there is little doubt that these oxide or carbide structures are three-dimensional. The condensation of the second phases can conveniently be followed by low energy electron diffraction due to the streaking of the diffraction pattern by the strain introduced in the phase-transformation. Such studies provide us with new information about the formation of bulk phases or bulk phase transformation.

TaO(111) has been observed by Boggio and Farnsworth[127] to grow expitaxially on the (110) face of tantalum when the Ta(110)-(5×1) structure was exposed to oxygen at room temperature and higher temperatures. The rate of oxidation was found to increase with temperature and an activation energy for oxidation of 0.24 eV was obtained. The six fold symmetry of the oxide diffraction pattern indicated the existence of two types of domains which were rotated through 180° with respect to one another. The $[11\bar{2}]$ direction of the oxide was found to coincide with the $[\bar{1}10]$ direction of the tantalum substrate. There is about an 8% difference in the nearest neighbor spacing between the atoms present in the Ta(110) face and those in the TaO(111) orientation.

Pignocco and Pellisier[18] have studied the epitaxial growth of thin films of iron oxide on a clean Fe(110) surface. When the iron surface was exposed to oxygen at room temperature, several surface structures were formed and then the development of a discrete thin film of FeO(111) was observed. As with TaO(111) on Ta(110), the orientation of the expitaxial silm was related to that of the substrate and the hexagonal symmetry of the diffraction pattern indicated that two types of domains were present in the oxide structure.

MacRae has observed the epitaxial growth of NiO when the (100), (110) and (111) faces of nickel were oxidized in 10^{-6} torr of oxygen at around 500°C.[128] In all three cases, the (100) face of the oxide (rock salt structure) was the exposed surface. Particularly on the (110) nickel surface, there were strong indications that the oxide was nucleated at separate sites and that the crystallites then grew until the entire surface was covered. The orientations of the oxide films were related to those of the substrates.

C. Correlation of Properties of Adsorbed Gas Surface Structures

It is apparent from inspection of Table IV that chemisorption yields ordered surface structures of adsorbed gases for most systems which have been studied so far. The structure of adsorbed gases to a very large extent is determined by the symmetry, the unit cell size and the chemistry of the underlying substrate. It is not surprising that a chemisorbed gas forms the same structures on different solid surfaces which exhibit similar electronic structure, the same crystal structure and surface orientation. In fact, the structural changes which are a function of surface concentration of adsorbed atoms are also similar in many surfaces. Because of the large body of information which has been accumulated in the last several years, several tentative correlations may be established which, if used judiciously, will allow one to predict what types of surface structures might form on different solid surfaces which have not been studied so far by low energy electron diffraction. It appears that (1) ordering of adsorbed molecules on the surface requires heats of adsorption in excess of 10 RT. The lack of ordering in the few cases where physical adsorption of molecules were studied indicate that heats of adsorption of certain magnitude may be necessary to localize the atoms on the surface (2) adsorbed atoms form ordered structures which correspond to their closest packing arrangement on the surface. The chemisorption in most cases is exothermic although there might be some activation energy in the adsorption of diatomic molecules. An increase in the surface density of the surface molecules decreases the free energy of the substrate-adsorbate system.

Adsorbate-adsorbate interactions may also be attractive as well until critical packing density is attained. These factors lead to a condition where the adsorbed molecules should prefer a close packing arrangement on the surface. (3) Two dimensional ordering is more likely on surfaces of high rotational symmetry. The fact that unsaturated hydrocarbons form ordered surface structures on the (111) face of platinum while adsorbed in a disordered manner on the (100) faces of platinum is an indication that the multiplicity of the rotation axis may play an important role in ordering during chemisorption.[115] (4) On surfaces with unequal unit cell vectors (such as the (110) face for the face-centered cubic crystals) chemisorbed gases are likely to form (n×m) type ordered structures where n≠m. It should be noted that the (n×1) type domain surface structures where n = 2, 3, -- is frequently observed presumably because its formation leeds to greater packing densities.

D. The Interaction of the Electron Beam with Surfaces

The electron beam used in LEED studies has energies of the order of 5 to 500 eV. These energies are much larger than the binding energies which hold the adsorbed atoms at the surface or hold the substrate atoms together.[129] Thus it is not unlikely that the electron beam may interact with the substrate or with the adsorbed gas and induce desorption or chemical reactions. Fortunately, the efficiency of the interaction of the electron beam with the surface is very low. In most cases the electron beam desorbes surface atoms with an efficiency of $< 10^{-5}$ (that is one incident electron out of 10^5 may be effective in desorbing a surface atom). The desorption efficiencies of the electron beam for carbon monoxide,

C. Correlation of Properties of Adsorbed Gas Surface Structures

It is apparent from inspection of Table IV that chemisorption yields ordered surface structures of adsorbed gases for most systems which have been studied so far. The structure of adsorbed gases to a very large extent is determined by the symmetry, the unit cell size and the chemistry of the underlying substrate. It is not surprising that a chemisorbed gas forms the same structures on different solid surfaces which exhibit similar electronic structure, the same crystal structure and surface orientation. In fact, the structural changes which are a function of surface concentration of adsorbed atoms are also similar in many surfaces. Because of the large body of information which has been accumulated in the last several years, several tentative correlations may be established which, if used judiciously, will allow one to predict what types of surface structures might form on different solid surfaces which have not been studied so far by low energy electron diffraction. It appears that (1) ordering of adsorbed molecules on the surface requires heats of adsorption in excess of 10 RT. The lack of ordering in the few cases where physical adsorption of molecules were studied indicate that heats of adsorption of certain magnitude may be necessary to localize the atoms on the surface (2) adsorbed atoms form ordered structures which correspond to their closest packing arrangement on the surface. The chemisorption in most cases is exothermic although there might be some activation energy in the adsorption of diatomic molecules. An increase in the surface density of the surface molecules decreases the free energy of the substrate-adsorbate system.

Adsorbate-adsorbate interactions may also be attractive as well until critical packing density is attained. These factors lead to a condition where the adsorbed molecules should prefer a close packing arrangement on the surface. (3) Two dimensional ordering is more likely on surfaces of high rotational symmetry. The fact that unsaturated hydrocarbons form ordered surface structures on the (111) face of platinum while adsorbed in a disordered manner on the (100) faces of platinum is an indication that the multiplicity of the rotation axis may play an important role in ordering during chemisorption.[115] (4) On surfaces with unequal unit cell vectors (such as the (110) face for the face-centered cubic crystals) chemisorbed gases are likely to form (n×m) type ordered structures where n≠m. It should be noted that the (n×1) type domain surface structures where n = 2, 3, -- is frequently observed presumably because its formation leeds to greater packing densities.

D. The Interaction of the Electron Beam with Surfaces

The electron beam used in LEED studies has energies of the order of 5 to 500 eV. These energies are much larger than the binding energies which hold the adsorbed atoms at the surface or hold the substrate atoms together.[129] Thus it is not unlikely that the electron beam may interact with the substrate or with the adsorbed gas and induce desorption or chemical reactions. Fortunately, the efficiency of the interaction of the electron beam with the surface is very low. In most cases the electron beam desorbes surface atoms with an efficiency of $< 10^{-5}$ (that is one incident electron out of 10^5 may be effective in desorbing a surface atom). The desorption efficiencies of the electron beam for carbon monoxide,

hydrogen and oxygen on tungsten surfaces have been studied.[130] Carbon monoxide from certain binding states appears to desorb rather rapidly during electron bombardment while oxygen desorbs slowly. Carbon monoxide is rapidly desorbed by the electron beam from other metal surfaces[92,131,132] as well. Ammonia desorbs from the (100) face of tungsten by electron impact.[133] The electron beam appears to excite the adsorbed atoms and the atoms then desorb from this repulsive excited states. De-excitation processes are effective in removing the excitation energy in most cases before desorption can take place. It was found that the electron beam may cause rearrangement of the surface structure into new structures or it converts atoms adsorbed in one binding state to atoms adsorbed in a different state. These studies have been carried out using tungsten surfaces where the conversion of CO and nitrogen from one adsorption state to another was found.[134]

There is one group of materials, the alkali halides, which appear to interact chemically with the electron beam.[135] Electron bombardment seem to dissociate the alkali halides surface and leads to halogen evolution and/or the precipitation of the alkali metal atoms. Heat treatment removes the alkali metal atoms either by vaporization or by diffusion via a vacancy mechanism into the bulk of the crystals. Such an interaction makes intensity measurements on alkali halide surfaces difficult to perform since the surface structure deteriorates as a function of time in a broad temperature range during low energy electron diffraction studies. In most of the low energy electron diffraction experiments the electron beam density is low enough such that heating of the surface by the elect-

tron beam can be neglected. However, under conditions of electron bombardment heating, where high energies and high electron densities are used, chemical changes can occur.

XI. LEED STUDIES OF THE STRUCTURE OF CONDENSIBLE VAPORS (EPITAXY)

Thin films grown on a single crystal substrate are frequently crystallographically oriented relative to that substrate. This orderly growth is known as epitaxy. The sensitivity of low energy electron diffraction to ordering makes it an ideal tool for studying the epitaxial development of such films. Many different systems have been studied. They may be arbitrarily categorized as metal on metal, metal on insulator, insulator on insulator, and insulator on metal, depending upon the nature of the substrate material and that of the thin film.

One of the earliest LEED studies of epitaxy was that by Farnsworth of silver on the (100) face of gold.[205] An epitaxial film of silver was grown in register with the (100) face of the gold substrate. The intensity of the diffracted beams from the film were similar to those from bulk silver indicating that the silver film on the gold had the same structure as the top layers of a pure bulk silver crystal. The mismatch in lattice parameters between gold and silver is less than one percent. More recently, Farnsworth and Haque have studied the carefully controlled growth of a nickel monolayer on copper.[206] Gradman has concluded that this nickel monolayer must be pseudomorphic with the copper substrate.[207] That is, the first nickel layer must be constrained to take on the interatomic spacing of the copper while subsequent layers will relax back to the nickel interatomic distances. The mismatch between the lattice parameters for nickel and copper is 2.5%.

Several metal-metal systems with larger mismatches have been studied. Taylor has investigated the epitaxial deposition of copper[208] onto a single

crystal (110) face of tungsten under ultra high vacuum conditions. He concluded that evaporation onto a clean tungsten surface at room temperature resulted in partial alloying and then the formation of well oriented, uniformly thin, copper (111) surface. The copper (111) plane is parallel to the W(110) with the copper [$\bar{1}\bar{1}2$] direction parallel to the [$\bar{1}10$] tungsten direction. The lattice mismatch in the W[110] direction is 1% while that in the [001] direction is 19%. Thus, the primary diffraction spots for the tungsten and the copper essentially coincide in the W[110] direction but not in the [001] direction leading to a fairly complicated diffraction pattern. Moss and Blott have also studied the epitaxial growth of copper on a W[110]face.[209] Their observations are similar to those of Taylor. However, their conclusions are slightly different. In their interpretation, alloy formation is not involved, rather they concluded thatthe first monolayer is deposited in a strained configuration and further deposition leads to the growth of a film with a periodicity characteristic of bulk Cu(111). Heating above 600°K led to the formation of large three dimensional copper islands on the surface. Further heating to above 1050°K resulted in the evaporation of these islands leaving only the first, strained, monolayer of copper.

Taylor has also studied the effect of oxygen on the epitaxial growth of copper on W[110].[208] He found that even half a monolayer of chemisorbed oxygen severly inhibited epitaxy even after the deposition of 20 layers of copper. However, if some physisorbed oxygen was present in addition to the chemisorbed, there was a marked improvement in the epitaxy even though it was still considerably worse than that on clean tungsten.

Alloying has been observed when Nb_3Sn was grown on niobium. Jackson and Hooker have evaporated tin onto clean Nb(110) under a variety of conditions.[101] Amorphous films of tim were deposited at high evaporation rates while slow deposition rates resulted in a diffraction pattern which was interpreted as being due, in part, to the presence of Sn(110). Both, the ordered and the disordered tin films on niobium produced $NbSn_3$ (110) when heated between 500°C and 950°C depending upon the history of the film. At temperatures below the formation temperature of Nb_3Sn, a hexagonal pattern was observed that was interpreted as resulting from an attempt by the tin to match the substrate. Heating to temperatures above the Nb_3Sn formation temperature, regenerated the Nb(110) diffraction pattern.

Pollard and Danforth have studied the deposition of thorium on to the (100) face of a tantalum substrate held at 950°C.[116] At coverages below a monolayer, they observed the formation of C(2×2) surface structure which reverted to a (1×1) upon further coverage. This (1×1) pattern was still observed even after 15 monolayers had been deposited. A careful investigation of the intensity of the specularly reflected beams as a function of coverage and auxilliary studies with an optical

microscope and electron micrographs lead them to conclude that the thorium clusters into islands about 500Å high and several thousand angstroms in length whose principle crystallographic directions are aligned with those of the substrate. It appears possible for thorium to form a monolayer in registry with the tantalum because of the partially ionic nature of the thorium-tantalum bond. However, further thorium cannot go into registry and therefore migrates to nucleation centers where three dimensional thorium crystals are formed. The Th-Ta(100) system may be contrasted withthe Th-W(100) system where, after the formation of the C(2×2) surface structure, a hexagonal structure that is similar to the (111) plane of bulk thorium is formed.[210]

The (110) face of tantalum has also been used as a substrate for the epitaxial growth of aluminum thin films. Jackson, Hooker, and Haas have found that Al(111) forms on the Ta(110) face in two orientations with the proper substrate temperature.[211] The observation of two or more orientations in an epitaxially grown film is quite common. Individual Al(111) and Ta(110) planes have hexagonal symmetry. However, there are two possible ways of, for example, superimposing a second Al(111) layer on the first. The resulting ensembles have trigonal symmetry. A priory, both orientations are equally probable and the development of an epitaxial growth containing two types of domains frequently results. An Al(111) C(2×2) structure and an Al(100) - C(2×2) structure have also been observed on a Ta(110) substrate. Further, all of these aluminum films have been observed to be somewhat unreactive to oxygen and carbon monoxide. This behavior may be contrasted with that of copper on tungsten where the presence of oxygeninhibited epitaxial growth.

The high degree of order found in these metal-metal systems is not always observed. Gerlach and Rhodin has studied alkali metal adsorption on several single crystal nickel surfaces.[212] They have found that at coverages less than one monolayer, the alkali metal atoms appear to repel each other with the result that these atoms are uniformly spaced over the substrate surface. The diffraction patterns indicate that there was a definite anisotropy in the adatom distribution on the (110) face but not on the (100) or the (111) faces. At higher coverages, the adatoms form incoherent hexagonal structures presumably to maximize the packing. The deposition of several monolayers lead to the disappearance of the nickel diffraction spots, implying that at least the outer layers of the film are disordered.

Weber and Peria have used LEED to study the alkali metals; sodium, potassium and cesium, on the (100) and the (111) faces of silicon and germanium.[213] The diffraction pattern observed for deposition on the (111) faces were not characterized by well ordered surface structures. However, those for the K and Cs covered (100) surfaces were characteristic of a well ordered overlayer. Supplementary measurements of the retarding field characteristics indicated that the alkali atoms were not nucleated in clusters but were uniformly distribution over the surface. As with the nickel substrate, it is possible that the repulsive adatom forces due to the partial ionization of the electropositive alkali metal atoms is more important in determining the epitaxial geometry than the adatom--substrate forces for the (111) germanium and silicon faces.

Jona has investigated the "amorphous" deposition of silicon onto the (111) face of a silicon substrate at low temperatures.[58] However, ordered epitaxial growth can occur at higher temperatures. Joyce, Neave and Watts have also studied the autoepitaxy of silicon by decomposing a molecular beam of silane on a heated silicon substrate in an ultra high vacuum system.[214] They found that a fraction of a monolayer of carbon or a carbon compound changes the growth mechanism from an apparent step movement process to one of discrete three dimensional nucleation. The amount of impurity involved was too small to effect the Si(111) - (7×7) LEED pattern, but could be detected by Auger spectroscopy.

Silicon has been a very popular substrate material for many studies of metal-insulator systems. Among others, aluminum, lead, tin, calcium barium, cesium, indium and gold have been deposited on silicon surfaces and studied with LEED. At least five aluminum phases have been observed on the (111) face of silicon at coverages between 1/3 and a full monolayer. When aluminum is evaporated onto the β-Si(111) - $\sqrt{3}$ - Al structure, a nearly perfectly oriented Al(111) epitaxial film is formed after the deposition of about 5 to 10 monolayers.[215] The mismatch in the unit mesh is about 25 per cent. As in many cases, the rotational symmetry has been preserved even when the translational symmetry between the film and the substrate has been discarded. Ultra high vacuum conditions were necessary for the development of this epitaxial film. When deposited on a Si(111) face, indium also exhibits a complicated set of surface structures that in part resemble those formed by aluminum. However, the development of an epitaxial film was not observed. Estrup and Morrison have studied the deposition of lead and tin on the (111) face of silicon.[216]

They found that epitaxial lead films could be grown, but that heating resulted in the clustering of the lead atoms into islands separated by areas of the silicon surface covered with ordered fractional monolayer lead structures. Tin could not be epitaxied, possibly due to clustering or to inhibition by contaminants. The reader is referred to an excellent review by Lander on the usages of silicon as a substrate material.[25]

Epitaxial studies where silicon has been employed as the condensate rather than the substrate have been performed by C. C. Chang.[96] Several different faces of α-Al_2O_3 were used as substrates for the deposition of silicon films. The objective of the study was to determine whether any properties of the epitaxial films could be related to the superstructures, or surface structures present on the α-Al_2O_3 faces. An interesting correlation was found for (111) silicon films grown on the α-Al_2O_3-$(\sqrt{31}\times\sqrt{31})$ surface structure. This $\sqrt{31}$ surface structure has double domains rotated by $\pm 9^\circ$ relative to the principle crystallographic directions of α-Al_2O_3. When this substrate was held in a very narrow temperature range near 850°C, the epitaxial Si(111) films also grew in double domains rotated by about $\pm 9^\circ$ indicating that the orientation of the film was determined by that of the surface structure rather than that of the substrate. The sensitivity of this process to substrate temperatures was shown by the observation that silicon films grown on an α-Al_2O_3 $(\sqrt{31}\times\sqrt{31})$ substrate at lower temperatures were indistinguishable from those grown on an α-Al_2O_3 - (1×1) substrate and were in register with the [112] silicon direction parallel to the [10$\bar{1}$0] direction of the substrate. As in other studies, these films had hexagonal symmetry indicating the existence of considerable twinning. Several

other metal-insulator systems that have been studied are silver on mica and silver and gold on potassium chloride. Seah has prepared clean substrate by cleaving micain ultra high vacuum.[10] The mica was then heated to 300°C and silver was deposited at a rate of several monolayers per minute in an overage ambient pressure of less than $1.5\ 10^{-10}$ torr. The resulting films showed a high degree of perfection and some evidence of twinning. The epitaxial growth of tellurium on the (111) face of copper had been studied by Andersson, Marklund and Martinson.[217] As observed in other systems, the growth of the epitaxial silm was preceeded by several well charaterized surface structures at partial monolayer coverages. A Cu(111) - $(2\sqrt{3}\times 2\sqrt{3})30°$-Te surface structure was observed at room temperature after about a twelfth monolayer coverage. A third monolayer coverage gave a Cu(111)- $(\sqrt{3}\times\sqrt{3})\ 130°$-Te structure when heated to about 300°C. Further deposition of tellurium then resulted in the epitaxial growth of a Te(0001) film.

Another semiconductor, CdSe has been epitaxied on the $YMnO_3$ (0001) face by Aberdam, Bouchet and Ducros.[218] The diffraction patterns indicated that the degree of orientation of the films was greatest for low deposition rates, about 3Å per second at 210°C. They observed that the CdSe[10$\bar{1}$0] direction was parallel to the [11$\bar{2}$0] direction in the $YMnO_3$. Here, the mismatch in lattice parameters is about 17%.

The preceding enumeration of epitaxial systems that have been studied by low energy electron diffraction is by no means an exhaustive compilation but is designed solely as an illustration of the unique applicability of LEED in studying such systems. The very nature of low energy electron diffraction, such as the low penetration depths involved

and the sensitivity to order and disorder, makes it an ideal tool for investigating such important questions as whether the condensed film is ordered or amorphous, what the crystallographic orientation of such a film is, and what is the relationship between the film and substrate orientation. Frequently, these questions can be answered simply by the observation of the geometry of the diffraction pattern. In more complicated cases, an analysis of the intensitiesof the diffraction features may be helpful if and when such analysis can be performed on a routine basis. Auxilliary techniques such as Auger spectroscopy, electron microscopy, conductivity and work function measurements are frequently very useful in supplying complementary information, such as that about the presence of impurities and macroscopic structuring, that is not readily extracted from low energy electron diffraction data.

From the existing studies, a number of generalizations may be made, though it should be born in mind that these may be frequently violated. It has often been observed that where more than one physically equivalent orientation is possible, the diffraction pattern may have a higher symmetry than that of the film, indicating that twinning has occurred. The orientation of many if not most ordered films bears some relation to that of the substrate and the rotational orientation is usually preserved even when the translational symmetry is violated. The pseudomorphic growht of a film may necessitate a small lattice mismatch between the film and the substrate while clustering may occur when the mismatch is large. The state of the surface, such as the presence of surface structures, the presence of contaminants, etc. may frequently effect the nature of the film growth. Substrate temperatures deposition rates and ambient pressures also have been shown to be very important in many systems.

REFERENCES

1. C. Kittel, Introduction to Solid State Physics, 2nd ed., John Wiley and Sons, Inc., New York, 1956.
2. E. A. Wood, J. Appl. Phys. 35, 1306 (1964).
3. R. L. Park and H. H. Madden, Jr., Surface Sci. 11, 188 (1968).
4. D. S. Boudreaux and V. Heine, Surface Sci. 8, 426 (1967).
5. P. M. Marcus and D. W. Jepsen, Phys. Rev. Letters 20, 925 (1968).
6. H. H. Farrell and G. A. Somorjai, Phys. Rev. 182,[3] 751 (1969).
7. J. B. Pendry, 1969, to be published.
8. H. Eyring, J. Walter and G. E. Kemble, Quantum Chemistry, John Wiley and Sons, Inc., New York, 1963.
9. R. M. Stern and A. Gervais, Surface Sci. 17, 273 (1969).
10. M. P. Seah, Surface Sci. 17, 132 (1969).
11. B. Segall, Phys. Rev. 125, 109 (1962).
12. J. J. Lander and J. Morrison, J. Appl. Phys. 35 [12] 3593 (1964).
13. L. H. Germer and A. U. MacRae, Annals of the New York Academy of Sciences, 101, 605 (1963).
14. R. L. Gerlach and T. N. Rhodin, Surface Sci. 8, 1 (1967).
15. E. G. McRae and C. W. Caldwell, Jr., Surface Sci. 2, 509 (1964).
16. J. H. Pollard and W. E. Danforth in The Structure and Chemistry of Solid Surfaces, ed. G. A. Somorjai, John Wiley and Sons, Inc. New York, 1969.
17. K. K. Vijai and P. F. Packman, J. Chem. Phys. 50 [3] 1343 (1969).
18. A. J. Pignocco and G. E. Pellisier, Surface Sci. 7, 261 (1967).
19. J. M. Ziman, Principles of the Theory of Solids, Cambridge Univ. Press, London 1964.

20. A. O. E. Animalu and V. Heine, Phil. Mag. 12, 1269 (1965).

21. R. M. Goodman and G. A. Somorjai, J. Chem. Phys. (to be published).

22. J. J. Lander and J. Morrison, J. Appl. Phys. 34, 3517 (1963).

23. R. O. Jones and J. A. Strozier, Jr., Phys. Rev. Letters, 22 [22] 1186 (1969).

24. R. A. Armstrong, Canad. J. of Phys. 44, 1753 (1966).

25. J. J. Lander in Advances in Solid State Chemistry, Vol. II, MacMillan Co., New York, 1965.

26. H. Raether, Surface Sci. 8, 233 (1967).

27. J. J. Quinn, Phys. Rev. 126, 1453 (1962).

28. C. B. Duke and C. W. Tucker, Jr., Surface Sci. 15, 231 (1969).

29. T. W. Haas, J. T. Grant and G. J. Dooley, Phys. Rev. (to be published).

30. R. W. James, The Optical Principles of the Diffraction of X-Rays, Cornell University Press, Ithaca, New York, 1965.

31. H. B. Lyon, Jr. and G. A. Somorjai, J. Chem. Phys. 46, 2539 (1967).

32. R. M. Goodman, H. H. Farrell and G. A. Somorjai, J. Chem. Phys. 48 [3], 1046 (1968).

33. E. R. Jones, J. T. McKinney and M. B. Webb, Phys. Rev. 151 [2] 476 (1966).

34. A. U. MacRae, Surface Sci. 2, 522 (1964).

35. A. A. Maradudin and P. A. Flinn, Phys. Rev. 129 [3] 523 (1967).

37. Hirabayashi and Takeishi, Surface Sci. 4, 150 (1966).

38. F. Hoffman and H. P. Smith, Phys. Rev. Letters 19, 1472 (1967).

39. Y. H. Ohtsuki, J. Phys. Soc. Japan 24, 5 (1968).

40. H. Bethe, Ann. Phys. 87, 55 (1928).

41. M. Von Laue, Phys. Rev. 37, 53 (1941).

42. E. Merzbacher, Quantum Mechanics, John Wiley and Sons, Inc., 1961.

43a. E. G. McRae, J. Chem. Phys. 45, 3258 (1968).

b. E. G. McRae, Surface Sci., 8, 14 (1967).

c. E. G. McRae, Fundamentals of Gas Surface Interactions, Academic Press, N. Y. 1967

44. K. Kambe, Z. Naturforsch., 22a, 22 (1967).

45a. K. Kambe, Z. Naturforsch, 22a, 322 (1967).

b. K. Kambe, Z. Naturforsch. 22a, 422 (1967).

c. K. Kambe, Z. Naturforsch. 23a, 1280 (1968).

46. J. L. Beeby, J. Phys. C. (Proc. Phys. Soc.) 1 [2] 82 (1968).

47. C. G. Darwin, Phil. Mag. 27, 315 (1914).

48. H. Morgenau and G. M. Murphy, The Mathematics of Physics and Chemistry, Van Nostrand Co., Inc., Princeton, N. J. (1957).

49. G. Carpart, Surface Sci. 13, 361 (1969).

50. R. M. Stern, J. J. Perry and D. S. Boudreaux, Rev. Mod. Phys. 41 [2] 275 (1969).

51. R. M. Goodman, H. H. Farrell and G. A. Somorjai, J. Chem. Phys. 49, 692 (1968).

52. E. G. McRae, Surface Sci. 11, 479 (1968).

53. E. G. McRae, Surface Sci. 11, 492 (1968).

54. E. Bauer, Colloque Intern. CNRS 1965 No. 152, p. 19.

55. E. G. McRae and L. Winkler, Surface Sci. 14, 407 (1969).

56. G. Gafner in The Structure and Chemistry of Solid Surfaces, G. A. Somorjai, ed., John Wiley and Sons, New York 1969.

57. H. B. Lyon Jr., Ph. D. Dissertaion, University of California, Berkeley, 1967.

58. F. Jona, Surface Sci. 8, 478 (1967).

59. H. D. Heidenreich, Fundamentals of Transmission Electron Microscopy, Interscience Publishers, New York, 1961.

60. R. M. Goodman, Ph. D. Disseration, University of California at Berkeley, 1969.

61. W. P. Ellis, in Fundamentals of Gas Surface Interactions, Academic Press, New York, 1967.

62. D. G. Fedak and N. A. Gjostein, Acta. Met. 15, 827 (1967).

63. A. E. Morgan and G. A. Somorjai, Surface Sci. 12, 405 (1968).

64. A. M. Mattera, R. M. Goodman and G. A. Somorjai, Surface Sci. 7, 26 (1967).

65. A. Guinier, X Ray Diffraction, W. H. Freeman and Co., San Francisco, 1963.

66. R. Kaplow, S. L. Strong and B. C. Averbach, Phys. Rev. 138A, 1336 (1965).

67. R. Leonhardt, H. Richter and W. Rossteutscher, Z. Physik 165, 121 (1961).

68. J. M. Morabito, Jr., R. F. Steiger and G. A. Somorjai, Phys. Rev. 179, 638 (1969).

69. D. G. Fedak, J. V. Florio and W. D. Robertson, in The Structure and Chemistry of Solid Surfaces, ed. G. A. Somorjai, John Wiley and Sons, Inc., New York 1969.

70. E. J. Scheibner and L. N. Tharp, Surface Sci. 8, 247 (1967).

71. Ch. A. Wert and R. M. Thompson, Physics of Solids, McGraw Hill, New York 1964.

72. T. M. French, Ph. D. Dissertation University of California, Berkeley 1970.

73. S. Hagstrom, H. B. Lyon and G. A. Somorjai, Phys. Rev. Letters 15, 491 (1965).

74. G. A. Somorjai, J. de Physique (to be published).

75. P. W. Palmberg and T. N. Rhodin, Phys. Rev. 161, 586 (1967).

76. J. T. Grant, Surface Sci. 18, 228 (1969).

77. F. Jona, Surface Sci. 8, 57 (1967).

78. J. W. May, Ind. and Eng. Chem. 57, 13 (1965).

79. A. U. MacRae and G. W. Gobeli, J. Appl. Phys. 35, 1629 (1964).

80. B. D. Campbell, G. A. Haque and H. F. Farnsworth, in The Structure and Chemistry of Solid Surfaces, ed. G. A. Somorjai, John Wiley and Sons, Inc., New York 1969, 33-2.

81. S. Andersson, I. Marklund and D. Anderson, in The Structure and Chemistry of Solid Surfaces, ed. G. A. Somorjai, John Wiley and Sons, Inc., New York 1969, 72-1.

82. R. E. Schlier and H. E. Farnsworth, J. Chem. Phys. 30, 917 (1959).

83. J. J. Lander and J. Morrison, J. Chem. Phys. 33, 729 (1962).

84. N. B. Hannay, Semicondutors, Reinhold, N. Y. 1960.

85. J. J. Burton and G. Jura, in The Structure and Chemistry of Solid Surfaces, ed. G. A. Somorjai, John Wiley and Sons, Inc., N. Y. 1969.

86. J. J. Burton and G. Jura, J. Phys. Chem. 71, 1937 (1967).

87. P. W. Palmberg, T. N. Rhodin and C. J. Todd, Appl. Phys. Letters 10, 122 (1967).

88. A. E. Morgan and G. A. Somorjai, Surface Sci. 12, 405 (1968).

89. L. Brewer in Electronic Structure and Alloy Chemistry, Ed. P. A. Beck, Interscience, N. Y. 1963.

90. L. Brewer, in High Strength Materials, ed. V. F. Zackay, John Wiley and Sons, Inc., New York, 1965.

91. S. L. Altman, C. A. Coulson, and W. Hume-Ruthery, Proc. Roy. Soc. 240A, 145 (1957).

92. A. E. Morgan and G. A. Somorjai, J. Chem. Phys. 51, 3309 (1969).

93. J. M. Charig, Appl. Phys. Letters 10, 139 (1967).

94. C. C. Chang, J. Appl. Phys. 39, 5570 (1968).

95. J. M. Charig and D. K. Skinner, in The Structure and Chemistry of Solid Surfaces, ed. G. A. Somorjai, John Wiley and Sons, Inc., New York, 1969.

96. C. C. Chang, ibid.

97. T. M. French and G. A. Somorjai, J. Phys. Chem. (to be published).

98. L. Fiermans and J. Vennik, Surface Sci. 9, 187 (1968).

99. F. A. Lindemann, Phyzik Z. 14, 609 (1910).

100. J. J. Gilvarry, Phys. Rev. 102, 308 (1956).

101. A. G. Jackson and M. P. Hooker in The Structure and Chemistry of Solid Surfaces, ed. G. A. Somorjai, John Wiley and Sons, Inc., New York, 1969.

102. R. L. Cornia, J. D. MacKenzie and D. Turnbull, J. Appl. Phys. 34, 2239 (1963).

103. M. Kass and S. Magun, Z. Kristall. 116, 354 (1961).

104. P. R. Pennington, Ph. D. Dissertation, University of California, Berkeley, 1966.

105. W. B. Hillig and D. Turnbull, J. Chem. Phys. 24, 914 (1956).

106. J. P. Stark, Acta. Met. 13, 1181 (1965).

107. J. N. Stranski, W. Gans and H. Rau, Ber. Bunsingessell. 67, 965 (1963).

108. J. E. Lennard-Jones and A. F. Devonshire, Proc. Roy. Soc. (London) A170, 464 (1939).

109. M. Born, J. Chem. Phys. 7, 591 (1939).

110. D. Kuhlmann-Wilsdorf, Phys. Rev. 140 [5A], 1599 (1965).

111. P. W. Palmberg, R. E. DeWames and L. A. Vredevoe, Phys. Rev. Letters, 21, 682 (1968).

112. R. Kaplan and G. A. Somorjai (to be published).

113a. J. J. Lander and J. Morrison, Surface Sci. 6, 1 (1967).

113b. J. J. Lander, Fundamental of Gas-Surface Interactions, Academic Press, N. Y. 1967.

114. R. F. Steiger, J. M. Morabito, Jr., G. A. Somorjai and R. H. Muller, Surface Sci., 14, 279 (1969).

115. A. E. Morgan and G. A. Somorjai, J. Chem. Phys. 51, 3309 (1969).

116. J. C. Bertolini and G. Dalmai-Imelik, Report Inst. de Rech. sur la Catalyse - Villeurbonne, 1969.

117. A. U. MacRae, Surface Sci. 1, 319 (1964).

118. P. J. Estrup and J. Anderson, J. Chem. Phys. 46, 567 (1967).

119. J. W. May, L. H. Germer and C. C. Chang, J. Chem. Phys. 45, 2383 (1966).

120. F. Jona, J. Phys. Chem. Solids 28, 2155 (1967).

121. S. M. Bedair, F. Hoffman and H. P. Smith, Jr., J. Appl. Phys. 39, 4026 (1968).

122. T. W. Haas, in The Structure and Chemistry of Solid Surfaces, ed. G. A. Somorjai, John Wiley and Sons, Inc., New York, 1969.

123. P. J. Estrup, ibid.

124. P. J. Estrup and J. Anderson, J. Chem. Phys. 49, 523 (1968).

125. T. W. May and L. H. Germer, J. Chem. Phys. 44, 2895 (1966).

126. M. Boudart and D. F. Ollis in The Structure and Chemistry of Solid Surfaces, ed. G. A. Somorjai, John Wiley and Sons, Inc., New York 1969.

127. J. E. Boggio and H. E. Farnsworth, Surface Sci. 3, 62 (1964).

128. A. U. MacRae, Science 139, 379 (1963).

129. H. H. Farrell, Ph. D. Dissertation, University of California, Berkeley, 1969.

130. D. Menzel and R. Gomer, J. Chem. Phys. 41, 3311 (1964).

131. C. W. Tucker, Jr., Surface Sci. 2, 516 (1964).

132. R. A. Armstrong, in The Structure and Chemistry of Solid Surfaces, ed. G. A. Somorjai, John Wiley and Sons, Inc., New York 1969.

133. J. Anderson and P. J. Estrup, Surface Sci. 9, 463 (1968).

134. J. T. Yates and T. E. Madey, in The Structure and Chemistry of Surfaces, ed. G. A. Somorjai, John Wiley and Sons, Inc., New York 1969.

135. P. W. Palmberg, C. J. Todd and T. N. Rhodin, J. Appl. Phys. 39, 4650 (1968).

136. L. H. Germer, E. J. Scheibner, and C. D. Hartman, Phil. Mag. 5, 222 (1960).

137. R. L. Park and H. E. Farnsworth, Appl. Phys. Letters 3, 167 (1963).

138. T. Edmonds and R. C. Pitkethly, Surface Sci. 15, 137 (1969).

139. J. W. May and L. H. Germer in The Structure and Chemistry of Surfaces, ed. G. A. Somorjai, John Wiley and Sons, Inc., New York, 1969.

140. W. P. Ellis, J. Chem. Phys. 48, 5695 (1968).

141. R. E. Schlier and H. E. Farnsworth, J. Appl. Phys. 25, 1333 (1954).

142. H. E. Farnsworth and J. Tuul, J. Phys. Chem. Solids 9, 48 (1958).

143. J. W. May and L. H. Germer, Surface Sci. 11, 443 (1968).

144. H. E. Farnsworth, Appl. Phys. Letters 2, 199 (1963).

145. R. E. Schlier and H. E. Farnsworth, Advances Catalysis 9, 434 (1957).

146. L. H. Germer and C. D. Hartman, J. Appl. Phys. 31, 2085 (1960).

147. H. E. Farnsworth and H. H. Madden, Jr., J. Appl. Phys. 32, 1933 (1961).

148. R. L. Park and H. E. Farnsworth, J. Chem. Phys. 43, 2351 (1965).

149. L. H. Germer, Advances Catalysis 13, 191 (1962).

150. L. H. Germer, R. Stern and A. A. MacRae, in"Metal Surfaces". ASM, Metals Park, Ohio (1963), p. 287.

151. M. Orchis and H. E. Farnsworth, Surface Sci. 11, 203 (1968).

152. H. E. Farnsworth, R. E. Schlier, T. H. George and R. M. Buerger, J. Appl. Phys. 29, 1150 (1958).

153. L. H. Germer and A. U. MacRae, A. Robert, Welch Foundation Research Bull. No. 11 (1961) 5.

154. R. L. Park and H. E. Farnsworth, J. Chem. Phys. 40, 2354 (1964).

155. L. H. Germer, J. W. May and R. J. Szostak, Surface Sci. 7, 430 (1967).

156. A. G. Jackson and M. P. Hooker, Surface Sci. 6, 297 (1967).

157. L. H. Germer and A. U. MacRae, Proc. Natl. Acad. Sci. U.S. 48, 997 (1962).

158. C. A. Haque and H. E. Farnsworth, Surface Sci. 1, 378 (1964).

159. C. W. Tucker, Jr., in The Structure and Chemistry of Solid Surfaces, ed. G. A. Somorjai, John Wiley and Sons, Inc., New York 1969.

160. C. W. Tucker, Jr., Appl. Phys. Letters 3, 98 (1963).

161. C. W. Tucker, Jr., J. Appl. Phys. 35, 1897 (1964).

162. J. M. Charlot and R. Deleight, Comptes Rendus 259, 2977 (1964).

163. A. E. Morgan and G. A. Somorjai, Trans. Am. Cryst. Assoc. 4, 59 (1968).

164. C. Burggraf and Sime Mosser, C. R. Acad. Sc. 268, 1167 (1969).

165. J. C. Tracy and P. W. Palmberg, J. Chem. Phys. 51, 4852 (1969).

166. G. W. Simmons, D. F. Mitchell, K. R. Lawless, Surface Sci. 8, 130 (1967).

167. L. Trepte, C. Menzel-kopp and E. Menzel, Surface Sci. 8, 223 (1967).

168. C. W. Tucker, Jr., J. Appl. Phys. 37, 3013 (1966).

169. C. W. Tucker, Jr., J. Appl. Phys. 38, 2696 (1967).

170. C. W. Tucker, Jr., J. Appl. Phys. 37, 4147 (1966).

171. L. H. Germer and A. U. MacRae, J. Chem. Phys. 36, 1555 (1962).

172. L. H. Germer, Physics Today, July 1964, p. 19.

173. L. H. Germer and J. W. May, Surface Sci. 4, 452 (1966).

174. J. W. May and L. H. Germer, J. Chem. Phys. 44, 2895 (1966).

175. N. J. Taylor, Surface Sci. 2, 544 (1964).

176. C. C. Chang and L. H. Germer, Surface Sci. 8, 115 (1967).

177. T. C. Tracy and J. M. Blakely, in The Structure and Chemistry of Solid Surfaces, ed. G. A. Somorjai, John Wiley and Sons, Inc., New York, 1969.

178. J. W. May, R. J. Szostak and L. H. Germer, Surface Sci. 15, 37 (1969).

179. C. C. Chang, J. Electrochem. Soc. 115, 354 (1968).

180. J. Anderson and P. J. Estrup, J. Chem. Phys. 46, 563 (1969).

181. P. W. Tamm and L. D. Schmidt, J. Chem. Phys. 51, 5352 (1969).

182. P. J. Estrup and J. Anderson, J. Chem. Phys. 45, 2254 (1966).

183. J. E. Boggio and H. E. Farnsworth, Surface Sci. 1, 399 (1964).

184. T. W. Haas, A. G. Jackson and M. P. Hooker, J. Chem. Phys. 46, 3025 (1967).

185. H. H. Madden and H. E. Farnsworth, J. Chem. Phys. 34, 1186 (1961).

186. T. W. Haas and A. G. Jackson, J. Chem. Phys. 44, 2921 (1966).

187. H. E. Farnsworth and K. Hayek, Suppl. Nuovo Cimento 5, 2 (1967).

188. K. Hayek, H. E. Farnsworth, Surface Sci. 10, 429 (1968).

189. G. J. Dooley and T. W. Haas, J. Chem. Phys. 52, 993 (1970).

190. H.K.A.Kann and S. Feuerstein, J. Chem. Phys. 50, 3618 (1969).

191. R. E. Schlier and H. E. Farnsworth, J. Chem. Phys. 30, 917 (1959).

192. J. J. Lander and J. Morrison, J. Appl. Phys. 33, 2089 (1962).

193. A. J. Van Bommel and F. Meyer, Surface Sci. 6, 39 (1967).

194. R. Heckingbottom, in The Structure and Chemistry of Solid Surfaces, ed. G. A. Somorjai, John Wiley and Sons, Inc., New York, 1969.

195. A. J. Van Bommel and F. Meyer, Surface Sci. 8, 381 (1967).

196. L. H. Germer and A. U. MacRae, J. Appl. Phys. 33, 2923 (1962).

197. H. E. Farnsworth, R. E. Schlier, T. H. George and R. M. Buerger, J. Appl. Phys. 29, 1150 (1958).

198. J. J. Lander and J. Morrison, J. Chem. Phys. 37, 729 (1962).

199. J. B. Marsh and H. E. Farnsworth, Surface Sci. 1, 3 (1964).

200. D. Haneman, Phys. Rev. 119, 567 (1960).

201. J. J. Lander and J. Morrison, J. Appl. Phys. 34, 1411 (1963).

202. H. E. Farnsworth and D. M. Zehner, Surface Sci. 17, 7 (1969).

203. R. O. Adams in The Structure and Chemistry of Solid Surfaces, ed. G. A. Somorjai, John Wiley and Sons, Inc., New York, 1969.

204. B. D. Campbell, C. A. Haque and H. E. Farnsworth, ibid.

205. H. E. Farnsworth, Phys. Rev. 43, 900 (1933).

206. H. E. Farnsworth and C. A. Haque, Surface Sci. 4, 195 (1966).

207. U. Gradmann, Surface Sci. 13 [2] 498 (1969).

208. N. J. Taylor, Surface Sci. 4, 161 (1966).

209. A. R. L. Moss and B. H. Blott, Surface Sci. 17, 240 (1969).

210. P. J. Estrup, J. Anderson and W. E. Danforth, Surface Sci. 4, 286 (1966).

211. A. G. Jackson, M. P. Hooker and T. W. Hass, Surface Sci. 10, 308 (1968).

212. R. L. Gerlach and T. N. Rhodin, Surface Sci. 17, 32 (1969).

213. R. E. Weber and W. T. Peria, Surface Sci. 14, 13 (1969).

214. B. A. Joyce, J. H. Neave and B. E. Watts, Surface Sci. 15, 1 (1969).

215. J. J. Lander and J. Morrison, Surface Sci. 2, 553 (1964).

216. P. J. Estrup and J. Morrison, Surface Sci. 2, 465 (1964).

217. S. Andersson, I. Marklund and J. Martinson, Surface Sci. 12, 269 (1968).

218. D. Aberdam, G. Bouchet and P. Ducros, Surface Sci. 14, 121 (1969).

219. K. Molière and F. Portele, in The Structure and Chemistry of Solid Surfaces, ed. G. A. Somorjai, John Wiley and Sons, Inc., N. Y. 1969.

TABLE CAPTIONS

Table 1. The surface and bulk root-mean-square displacement ratios and Debye temperatures for several metals.

Table 2. Surface structures found on clean semiconductor surfaces.

Table 3. Surface structures found on clean metal surfaces.

Table 4. Structures of adsorbed gases.

Table I.

	$\frac{\langle u_\perp \rangle (\text{surface})}{\langle u \rangle (\text{bulk})}$	Θ(surface) (°K)	Θ(bulk) (°K)
Pb (110), (111) [32,60]	2.43 (1.84)	37 (49)	90
Bi (0001), (01$\bar{1}$2) [60]	2.42	48	116
Pd (100), (111) [32]	1.95	142	273
Ag (100) [68], (110) [68], (111) [33,68]	2.16 (1.48)	104 (152)	225
Pt (100), (110), (111) [31]	2.12	110	234
Ni (110) [34]	1.77	220	390
Ir (100) [60]	1.63	175	285

Table II

Material	Surface Structure
Si[27,78,82,83]	(100)-(4×4), (111)-(7×7)
Ge[25,78]	(100)-(4×4), (111)-(8×8), (110)-(2×2)
GaAs[78,79]	(111)-(2×2)
GaSb[78,79]	(111)-(2×2)
InSb[78,79]	(100)-(2×2), (111)-(2×2)
CdS[80]	(0001)-(2×2)
Te[81]	(0001)-(2×1)

Table III

Surface Structures	Temperature Range of Established Stability
Pt(100)-(5×1)[31,73,90]	25° - 1300°C
Au(100)-(5×1)[62,75]	25° - 500°C
Au(110)-(2×1)[62]	---
Ir(100)-(5×1)[76]	25° - 1500°C
Pd(100)-C(2×2)[76]	550° - 850°C
Bi($1\bar{1}20$)-(2×10)[77]	25° - melting point
Sb($1\bar{1}20$)-(6×3)[77]	25° - 250°C

Table 4

Face Centered Cubic Structures

Nickel

Surface	Adsorbed Gas	Surface Structure	Reference
Ni (111)	O_2	(2 x 2) -O	117, 136, 137
		$(\sqrt{3} \times \sqrt{3})R\ 30°$-O	117, 138
	CO	(2 x 2) - CO	136
	dissociates to C + CO_2	$(16\sqrt{3} \times 16\sqrt{3})R\ 30°$-C + $(2 \times \sqrt{3})$- CO_2	138
	H_2	(1 x 1) - H	136
		disordered	139
	N_2	not adsorbed	171
	CO_2	(2 x 2) - CO_2	138
		(2 x $\sqrt{3}$) - CO_2	
	dissociates in electron beam to	$(16\sqrt{3} \times 16\sqrt{3})$-C + $(\sqrt{3} \times \sqrt{3})R30°$ - O	138
	C_2H_4	(2 x 2) - C_2H_4	116
	C_2H_6	(2 x 2) - C_2H_6	116
	C_3H_6	(2 x 1) - C_3H_6	116
		$(\sqrt{7} \times \sqrt{7})$ R 19° - C	116
Ni (100)	O_2	(2 x 2) - O	117, 141, 142, 143
		C(2 x 2) - O	144, 145, 146, 147
			117, 148, 149, 150
	CO	C(2 x 2) - CO	147, 148, 151
	H_2	disordered	139
	N_2	not adsorbed	139
	C		142, 145, 152

Nickel

Surface	Adsorbed Gas	Surface Structure	Reference
Ni (110)	O_2	(2 x 1) - O	136,117,150,153,154
		(3 x 1) - O	117,139,143,155
		(5 x 2) - O	117
		(5 x 1) - O	117
	CO	(1 x 1) - CO	117, 156
	H_2, D_2	(1 x 2) - H	139, 156, 157, 158
	H_2O	(2 x 1) - H_2O	157
	C	C(2 x 2) - C	157
Ni (210)	I_2	facet to Ni(540)	159

Platinum

Pt (111)	O_2	(2 x 2) - O	131, 160, 161, 162
	$H_2 + O_2$	$(\sqrt{3} \times \sqrt{3})R\ 30°$	137
	CO	C(4 x 2) - CO	92
	C_2H_2	(2 x 1) - C_2H_2	92
	C_2H_4	(2 x 1) - C_2H_4	92
	C_3H_6	(2 x 1) - C_3H_6	92
	(cis and trans)C_4H_8(2-butene)	(2 x 2) - C_4H_8	92
	C_4H_6(butadiene)	(2 x 2) - C_4H_6	92
	C_4H_8(isobutylene)	$(\sqrt{7} \times \sqrt{3})R\ 13.9°$	92

Platinum

Surface	Adsorbed Gas	Surface Structures	Reference
Pt(100)-(5x1)	O_2	(1 x 1)- O	160
	H_2	(2 x 2)- H	88, 163
	CO	C(4 x 2)	88, 92, 162, 164
		$(3\sqrt{2} \times \sqrt{2})R\ 45°$	
		$(\sqrt{2} \times \sqrt{5})R\ 45°$	88, 163
	C_2H_2	C(2 x 2) - C_2H_2	88, 92
	C_2H_4	C(2 x 2) - C_2H_4	88, 92
	C_3H_6	disordered	92
(cis and trans)	C_4H_8(2-butene)	disordered	92
	C_4H_8(isobutylene)	disordered	92
	C_4H_6(butediene)	disordered	92
	CO + H_2	C(2 x 2) - (CO + H_2)	88, 163
Pt (110)	O_2	(1 x 2)	161
		(2 x 4)	161

Palladium

Pd	CO	disordered	165
		C(4 x 2) - CO	165
		compressed	165

Surface	Adsorbed Gas	Surface Structure	Reference
		Copper	
Cu (111)	O_2	(11 x 5) R 5° - O	166
Cu (100)	O_2	C(2 x 2) - O	167
		(1 x 1) - O	167
		(2 x 1) - O	167
	N_2	(1 x 1) - N	141
Cu (110)	O_2	(2 x 1) - O	166, 167
		C(6 x 2) - O	166
Cu (035)	O_2	(1 x 1) - O	167
Cu (014)	O_2	(1 x 1) - O	167
		Aluminum	
Al (100)	O_2	disordered	120, 121, 129
		Rhodium	
Rh (100)	O_2	(2 - 8) - O	168
	CO	(4 x 1) - CO	168
Rh (110)	O_2	C(2 x 4) - O	169, 170
		C(2 x 6) - O	
		C(2 x 8) - O	
		(2 x 2) - O	
		(2 x 3) - O	

Uranium Dioxide

Surface	Adsorbed Gas	Surface Structure	Reference
$UO_2(111)$	O_2	(3 x 3) - O	140
		$(2\sqrt{3} \times 2\sqrt{3})$ R 30° - O	140

Body Centered Cubic Structures

Tungsten

Surface	Adsorbed Gas	Surface Structure	Reference
W(110)	O_2	(2 x 1) - O	150, 172, 173
		C(14 x 7) - O	
		C(21 x 7) - O	173
		C(48 x 16) - O	
		C(2 x 2) - O	173
		(2 x 2) -	
		(1 x 1) - O	173
	O_2+CO coadsorption	C(11 x 5) - CO + C_2	119
	CO	disordered	174
		C(9 x 5) - CO	
	CH_4	(15 x 3) - C	126
		(15 x 12) - C	
W(111)	O_2	to (211) facets	175
	CH_4	(6 x 6) - C	126
W(211)	O_2	(2 x 1)	175
		(4 x 3)	
		(1 x 2)	
		(1 x n) - O n = 1,2,3,4.	176, 177
	NH_3 thermal breakup	C(4 x 2) - NH_2	
		12 % stretch	178
	CO	C(6 x 4) - CO	179
		(2 x 1) - CO	
		C(4 x 2) - CO	

Surface	Adsorbed Gas	Surface Structure	Reference
W(100)	O_2	(4 x 1) - O	123
		(2 x 1) - O	
	CO	C(2 x 2) - CO	123, 180
	N_2	C(2 x 2) - N	118, 123
	CH_4	(5 x 1) - C	126
	NH_3	disordered	124
		C(2 x 2) - NH_2	124
		(1 x 1) - NH_2	124
	(CO + N_2)	(4 x 1) - (CO + N_2)	118
	H_2	C(2 x 2) - H	181, 182
		(2 x 5) - H	182
		(4 x 1) - H	182
		Tantalum	
Ta(110)	O_2	(3 x 1) - O	183
		(3 x 2) R 18° 16' -O	122
		oxides	
	N_2	not adsorbed	122
	H_2	(1 x 1) - H	122
	CO	disordered	122
		decomposition to $C + CO_2$	

Surface	Adsorbed Gas	Surface Structure	Reference
Ta(112)	O_2	(3 x 1) - O	122
		oxides	
	N_2	nitride form epitaxially on (113) planes	122
	H_2	(1 x 1) - H	122
	CO	disordered	122
		decomp. to C + CO	122
		Niobium	
Nb (110)	O_2	(3 x 1) - O	184
		(3 x 2) R 18°16' - O	
	H_2	(1 x 1) - H	185
		Vanadium	
V (100)	O_2	(1 x 1) - O	17
		(2 x 2) - O	
	H_2	disordered	17
V (110)	CO	disordered	184
		Chromium	
Cr (100)	O_2	(2 x 2)- O	158
	CO	(2 x 2) - CO	
	N_2	(2 x 2) - N	

Iron

Surface	Adsorbed Gas	Surface Structure	Reference
α Fe(110)	O_2	C(2 x 2) - O	18, 219
		C(3 x 1) - O	
		C(1 x 5) - O	18
		(2 x 8) - O	18
		FeO (111) (cubic)	219
		γ-Fe_2O_3 (spinel)	219

Molybdenum

Mo (110)	O_2	(2 x 2) - O	186, 187, 188
		(2 x 1) - O	
		(1 x 1) - O	187, 188
		C(2 x 2) - O	188
	CO	(1 x 1) - CO	186, 188
		C(2 x 2) - CO	156
	H_2	adsorbed (no structure given)	186
	CO_2	disordered	156
Mo (100)	H_2	C(4 x 2) - H	189
		(1 x 1) - H	
	O_2		
		disordered	190
		C(2 x 2) - O	187,188,190
		(1 x 1) - O	190
		$\sqrt{5}$(1 x 1)R ± 26°34' -O	188, 190
		(2 x 2) - O	190
	N_2	(1 x 1) - N	188
	CO	(1 x 1) - CO	188

Diamond Structures

Silicon

Surface	Adsorbed Gas	Surface Structure	Reference
Si(111)-(1 x 1)	O_2	(1 x 1)	191, 192
(7 x 7)		disordered	
	H_2S	(2 x 2) - S	193
	H_2	not adsorbed	
	H_2Se	(2 x 2) - Se	193
	I_2	(1 x 1)	
	NH_3	(8 x 8) - N	194
	PH_3	$(6\sqrt{3} \times 6\sqrt{3})$ - P	195
		(1 x 1) - P	195
		$(2\sqrt{3} \times 2\sqrt{3})$ - P	195
Si(100)	O_2	(1 x 1)	191, 192, 196, 197
		(111) facets	
	I_2	(3 x 3)	198

Diamond

C(diamond)(111)	O_2	ordered $\overset{2}{\cdot}$	199
	CO_2	$\overset{2}{\cdot}$	
C(graphite)(0001)	O_2	not adsorbed	200
	CO	not adsorbed	
	H_2O	not adsorbed	
	I_2	not adsorbed	
	Br_2	not adsorbed	
C(diamond)(100)	O_2	disordered	199
		ordered	

Germanium

Surface	Adsorbed Gas	Surface Structure	Reference
Ge(111)	O_2	(1 x 1)	191, 197
		disordered	201
	I_2	(1 x 1)	201
Ge(100)	O_2	(1 x 1)	191, 197
		disordered	
	I_2	(3 x 3)	201
Ge(110)	O_2	(1 x 1)	191, 197
		disordered	

Hexagonal Structures

Titanium

Surface	Adsorbed Gas	Surface Structure	Reference
Ti(0001)	O_2	(1 x 1)	197
	CO	(1 x 1)	197

Rhenium

Re(0001)	O_2	(2 x 2) - O (CO)	202
		(1 x 1) - O (CO)	
	CO	(2 x 2) - CO	202

Beryllium

Be(0001)	O_2	disordered	203
	CO	disordered	203
	N_2	not adsorbed	203
	H_2	not adsorbed	203

Cadmium Sulfide

CdS(0001)	O_2	disordered	204

FIGURE CAPTIONS

Fig. 1 The five two-dimensional Bravais lattices.

Fig. 2 a-j Unit cell vectors (a-g) of the primitive two-dimensional unit cell and indeces (h-j) for the three densest f.c.c. and b.c.c. crystal faces.

Fig. 3 The a) primitive two-dimensional unit cell and the b) x-ray unit cell projection. 0 - atoms in surface, ● - atoms in second layer.

Fig. 4 a-c Schematic diagram of surface structures on the (100), (110) and (111) crystal faces of a face centered cubic crystal.

Fig. 5 Wave vectors for the incident beam and two diffraction beams showing their components parallel and perpendicular to the surface.

Fig. 6a and 6b. Intensity of the (00) - beam as a function of electron energy in the pure a) two-dimensional diffraction limit and in the pure b) three dimensional diffraction limit.

Fig. 7 Intensity of the low index diffraction beams as a function of electron energy, eV, from the (100) face of aluminum.

Fig. 8a and 8b The intensities of the a) (10) and b) (11) diffraction beams as a function of normalized electron energy for the (100) faces of aluminum, copper, nickel, palladium, silver and gold at normal incidence.

Fig. 9 a-b Inner potential as a function of the energy of the incident electron beam for nickel and for niobium.

Fig. 10 Atomic scattering factor, f_q, calculated for aluminum using a pseudopotential.

Fig. 11 Fraction of elastically scattered electrons as a function of electron energy for the (100) face of platinum.

Fig. 12 Damping of the scattering amplitude by an inelastic loss factor, $e^{-d/\lambda}$ as a function of distance, d, from the surface.

Fig. 13 Definition of $\underset{\sim}{u}(t)$, $\underset{\sim}{r}$, $\underset{\sim}{k}_0$ and $\underset{\sim}{k}$ for the scattering process.

Fig. 14 Vector diagram for double diffraction mechanism.

Fig. 15 Schematic representation of several simple scattering processes involving the surface layer of atoms and/or bulk atomic layers.

Fig. 16 Scheme of the low energy electron diffraction apparatus of the post-acceleration type.

Fig. 17 Cut-off characteristics of the 3-grid system with varying repeller grid potential with respect to the cathode potential.

Fig. 18 Intensity of the (00) beam as a function of deposited amorphous silicon.

Fig. 19 a-b Diffraction rings due to graphitic carbon on the Pt(100) surface.

Fig. 20 Radial density function for liquid lead from x-ray diffraction studies.

Fig. 21 X-ray intensities obtained from liquid lead at 327.4°C as a function of $\frac{S}{4\pi} = \sin\theta/\lambda$.

Fig. 22 a-c Equi-intensity contours as a function of electron energy for scattering of low energy electrons from lead, bismuth and tin molten surfaces.

Fig. 23 Intensity contours calculated from x-ray data by Kaplow.[66]

Fig. 24 Intensity of the (00) beam as a function of temperature and the background intensity .

Fig. 25 The $\log(I_{00}-I_{background})$ vs. T°K plot for the data in Fig. 24.

Fig. 26 a-b Effective Debye temperatures as a function of electron energy for different crystal faces of lead and palladium.

Fig. 27 Determination of scattering vectors for non-specular (hk) and specular (00) diffraction beams.

Fig. 28 Diffraction patterns of the a) Si(111) - (1x1) and the b) Si(111) - (7x7) structure.

Fig. 29 Diffraction pattern of the Pt(100) - (5x1) structure.

Fig. 30 a-b Diffraction patterns of the a) Al_2O_3(0001) - (1x1) and b) Al_2O_3(0001) - $(\sqrt{31} \times \sqrt{31})R9°$ structures.

Fig. 31 a-b Diffraction patterns of the (111) face of lead below and above the melting point (327°C).

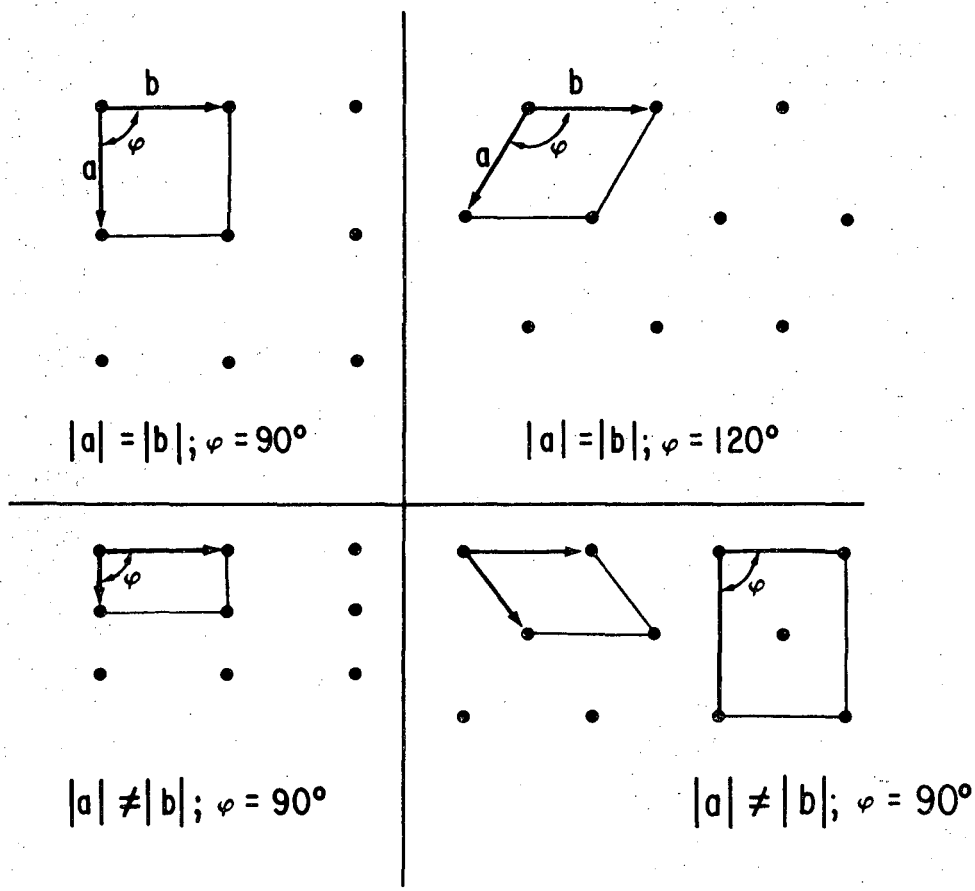

XBL 703-563

Figure 1

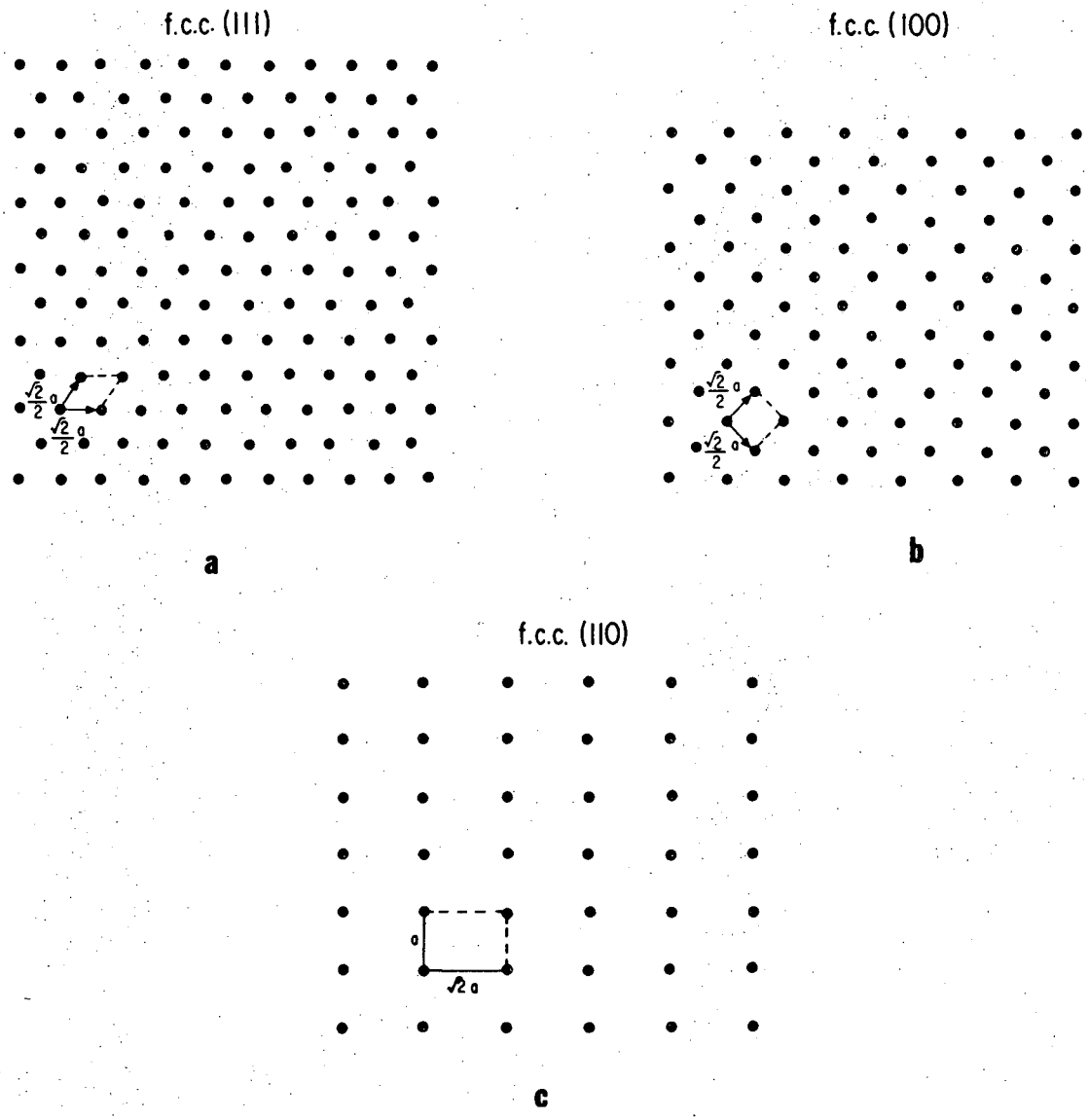

XBL 703-567

Figure 2

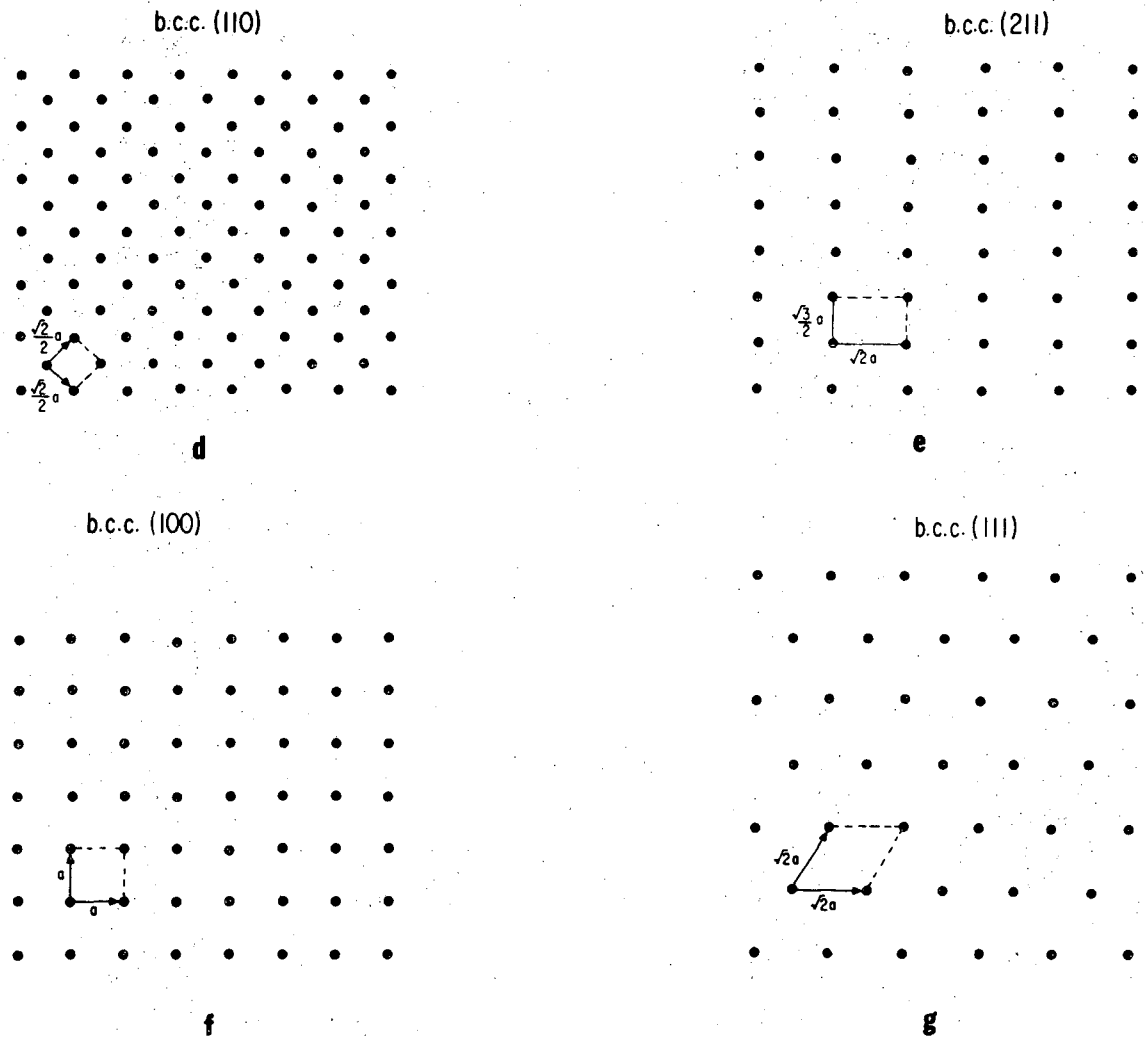

Figure 2d-g

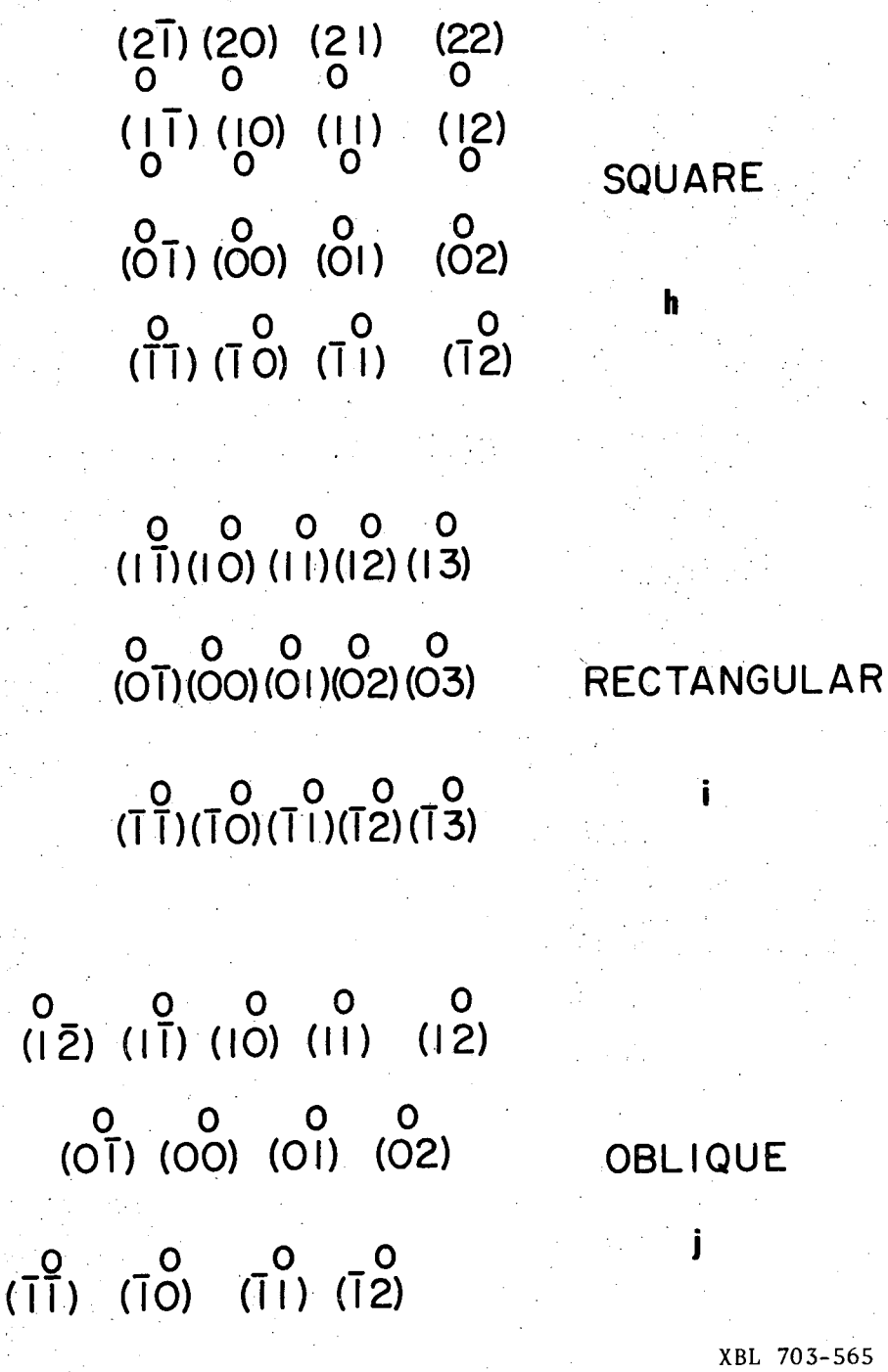

XBL 703-565

Figure 2h-j

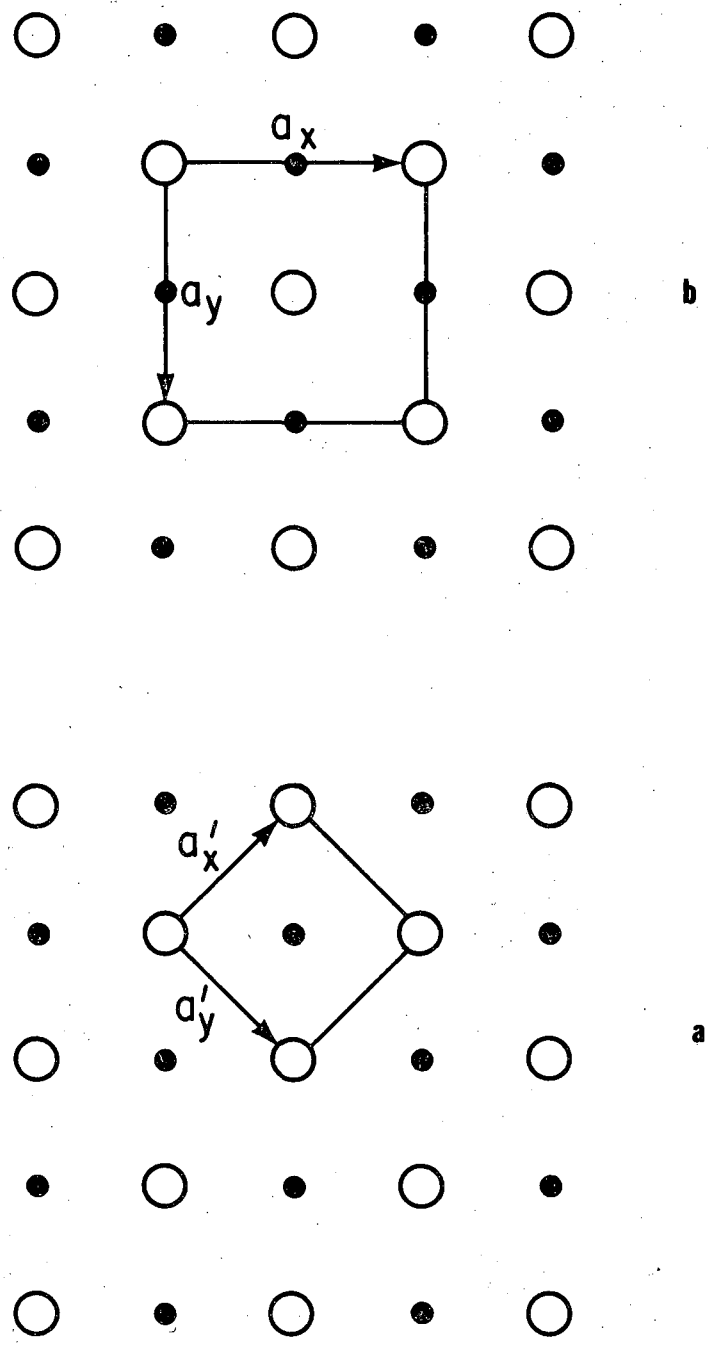

XBL 703-564

Figure 3

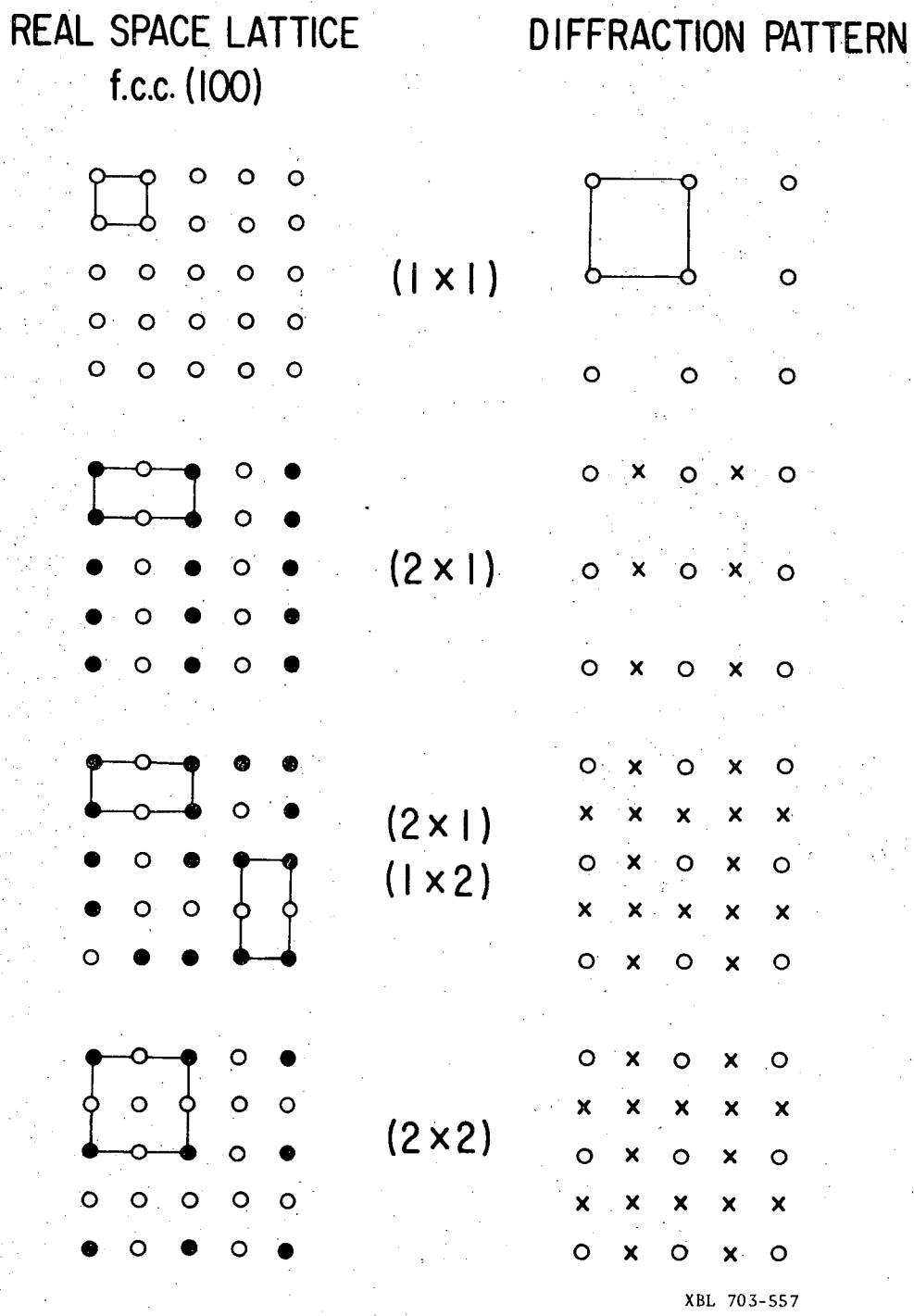
REAL SPACE LATTICE
f.c.c. (100)
DIFFRACTION PATTERN
(1 x 1)
(2 x 1)
(2 x 1)
(1 x 2)
(2 x 2)
XBL 703-557

Figure 4a

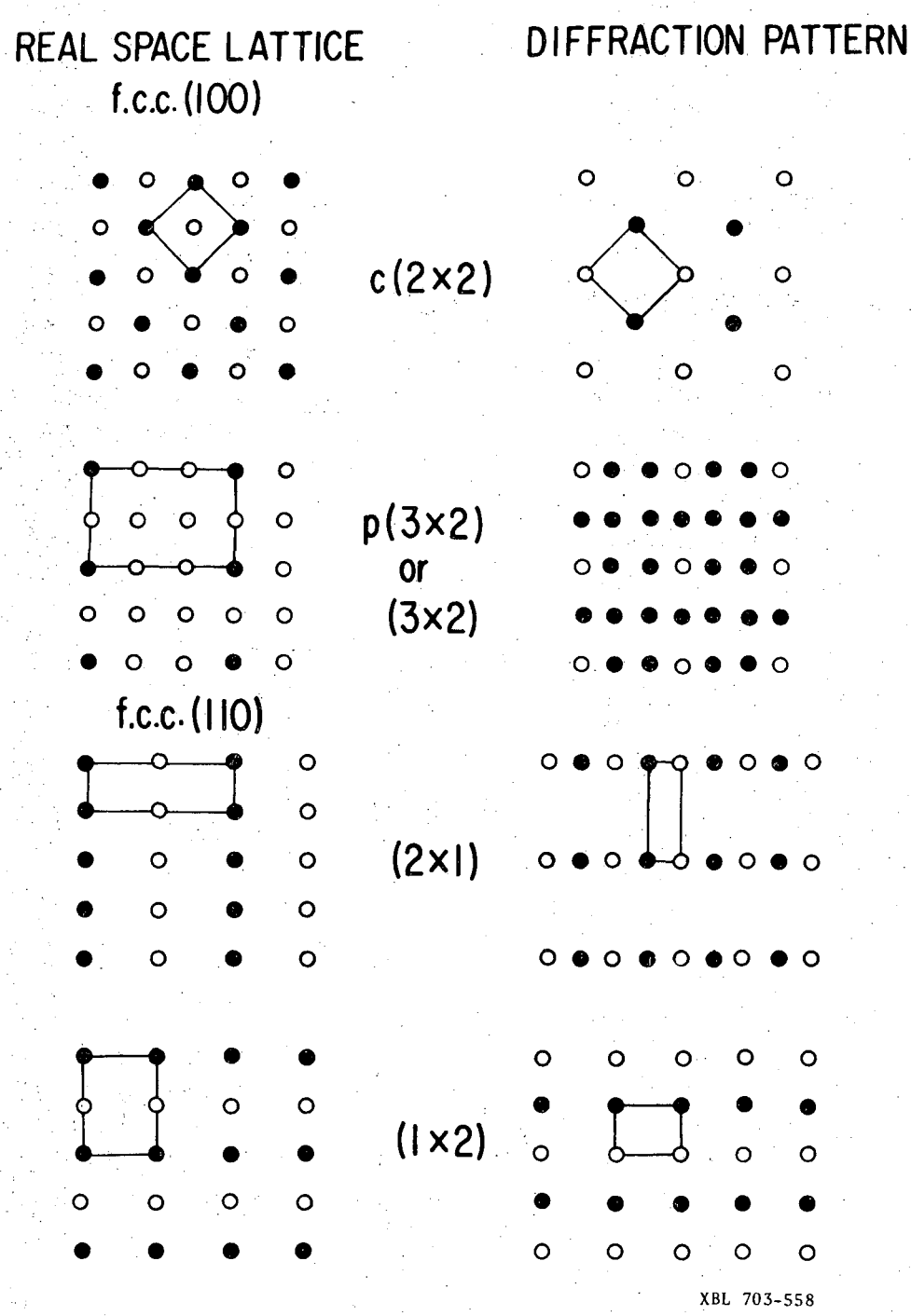
REAL SPACE LATTICE
f.c.c.(100)
DIFFRACTION PATTERN
c(2×2)
p(3×2)
or
(3×2)
f.c.c.(110)
(2×1)
(1×2)
XBL 703-558

Figure 4b

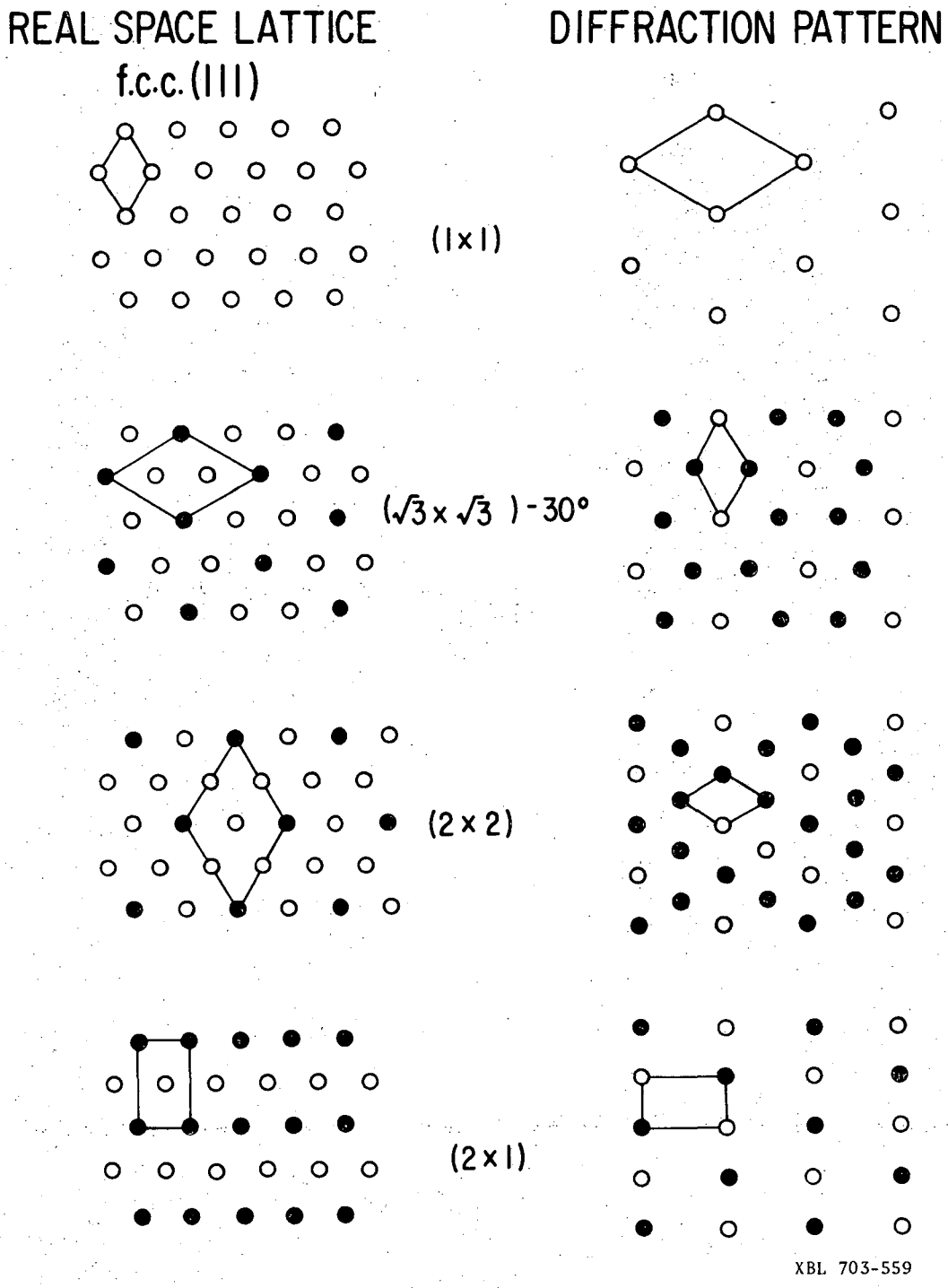
REAL SPACE LATTICE
f.c.c.(111)
DIFFRACTION PATTERN
(1×1)
(√3×√3)-30°
(2×2)
(2×1)
XBL 703-559

Figure 4c

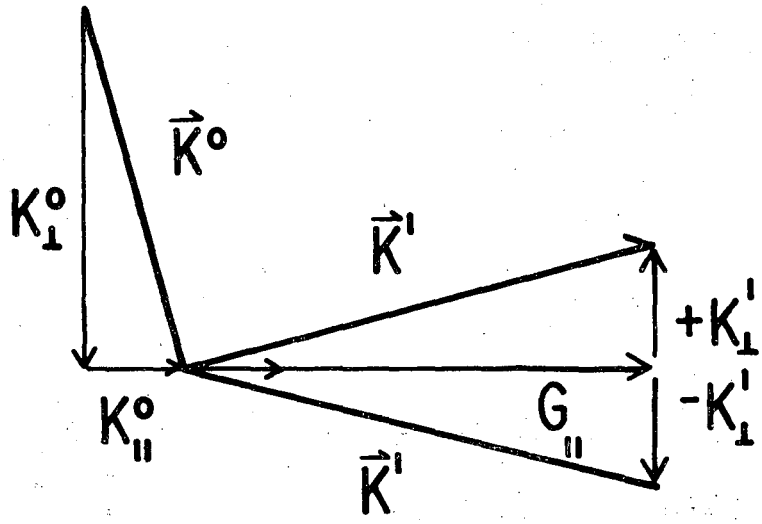

XBL 703-560

Figure 5

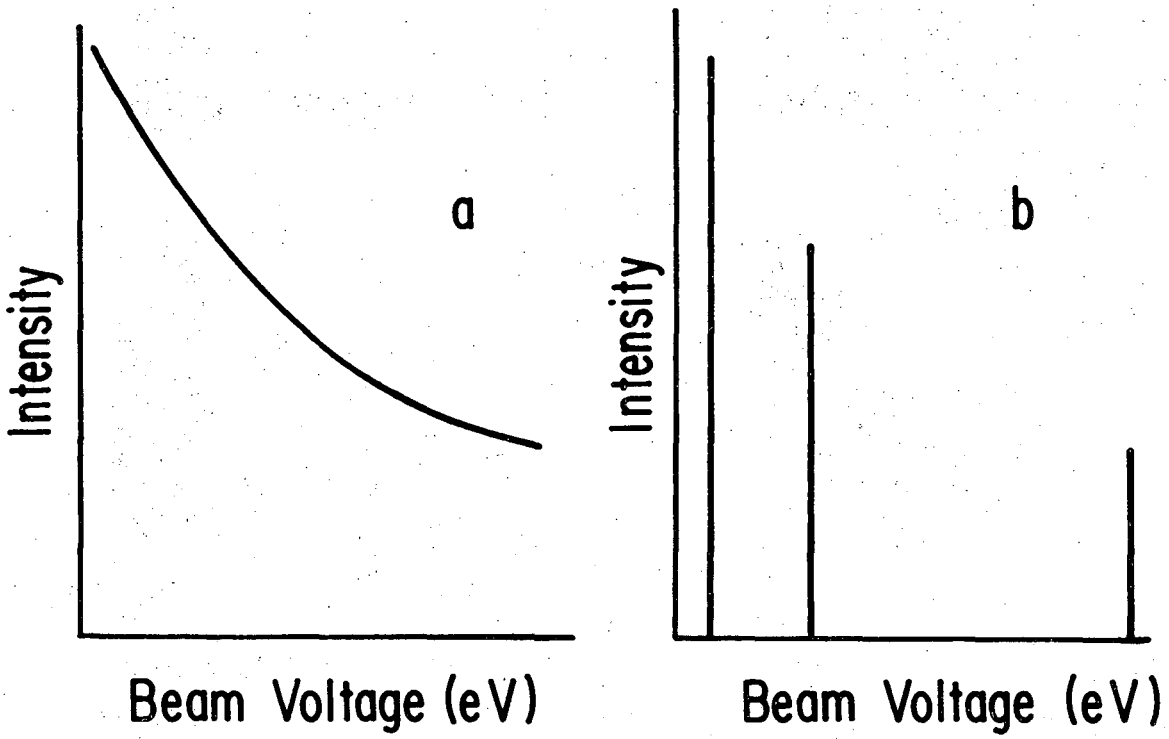

XBL 703-561

Figure 6

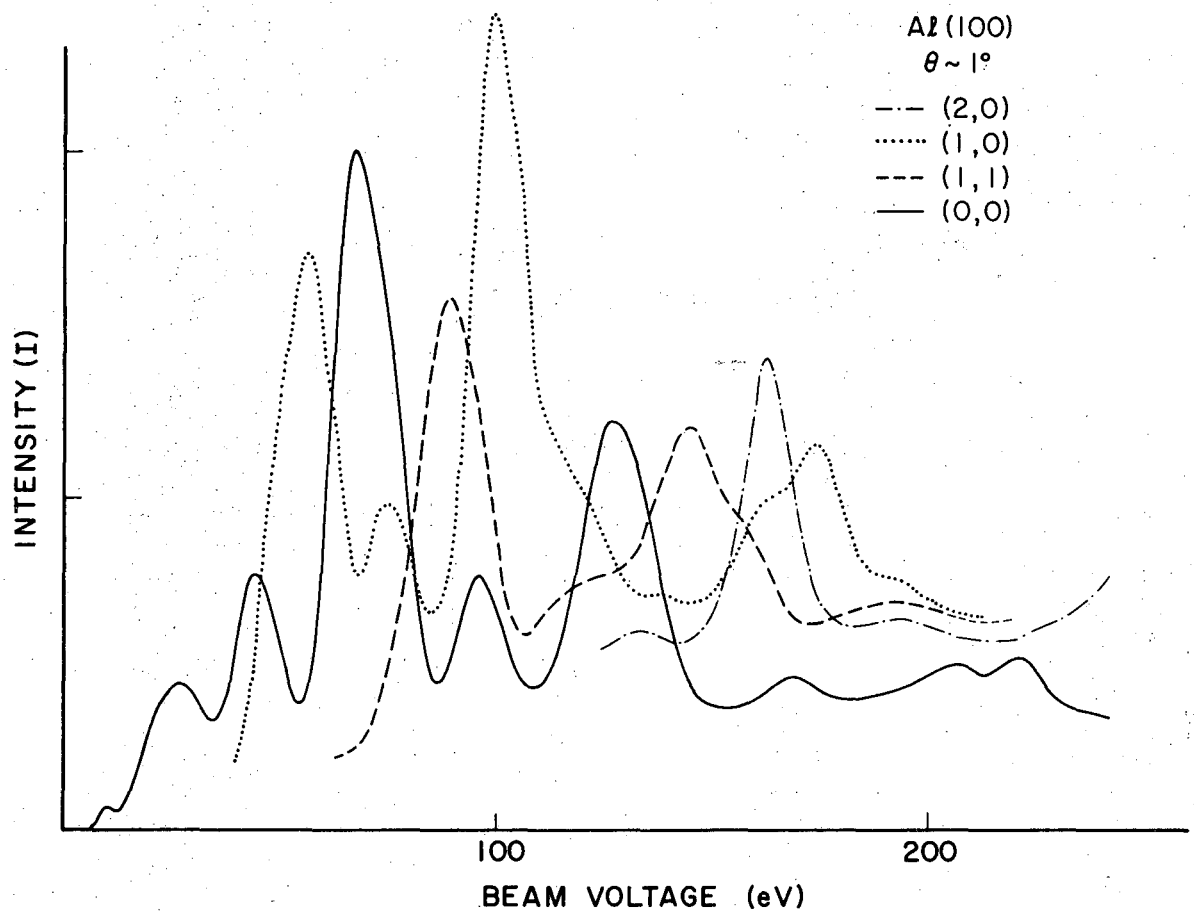

XBL 687-1451

Figure 7

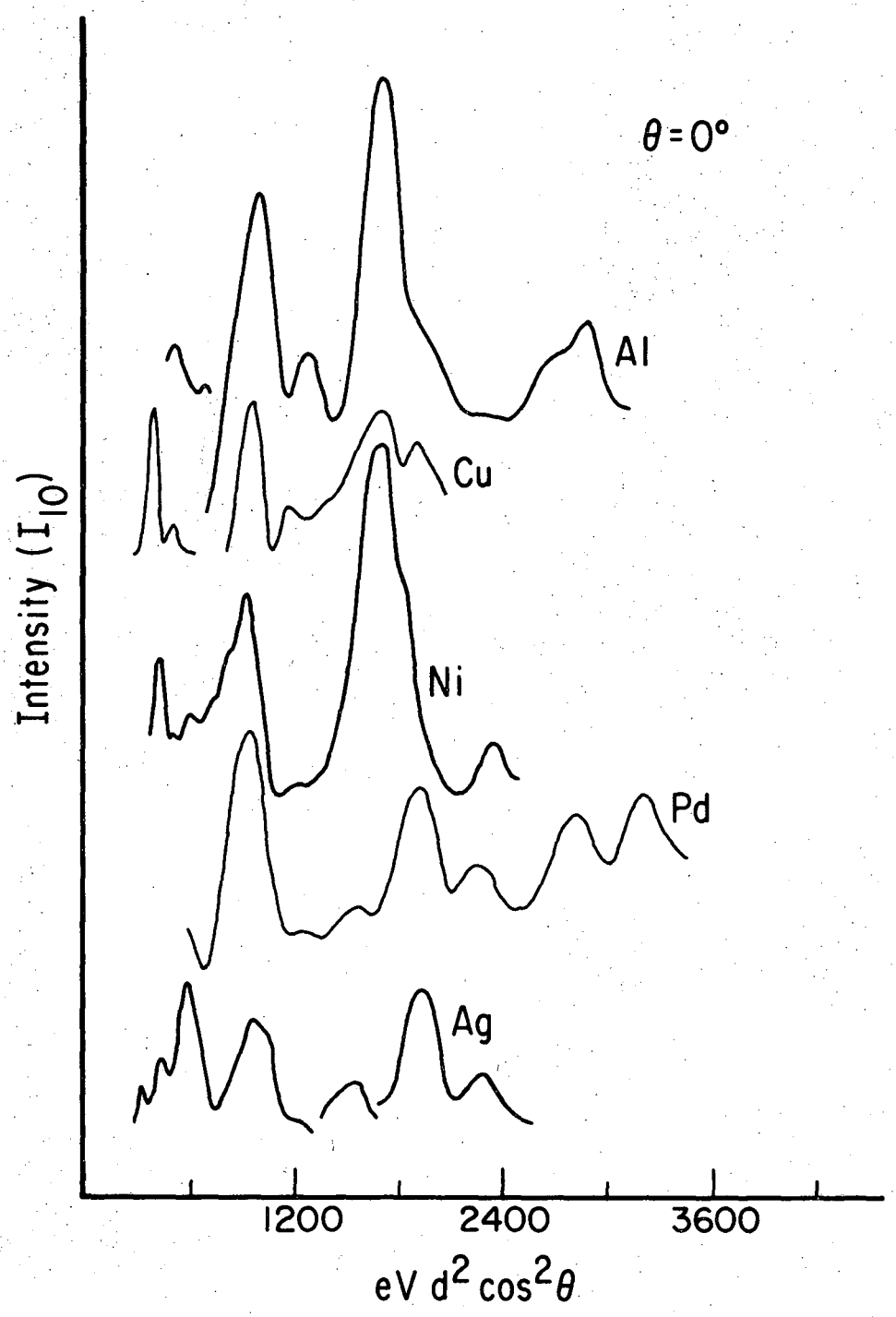

XBL 703-552

Figure 8a

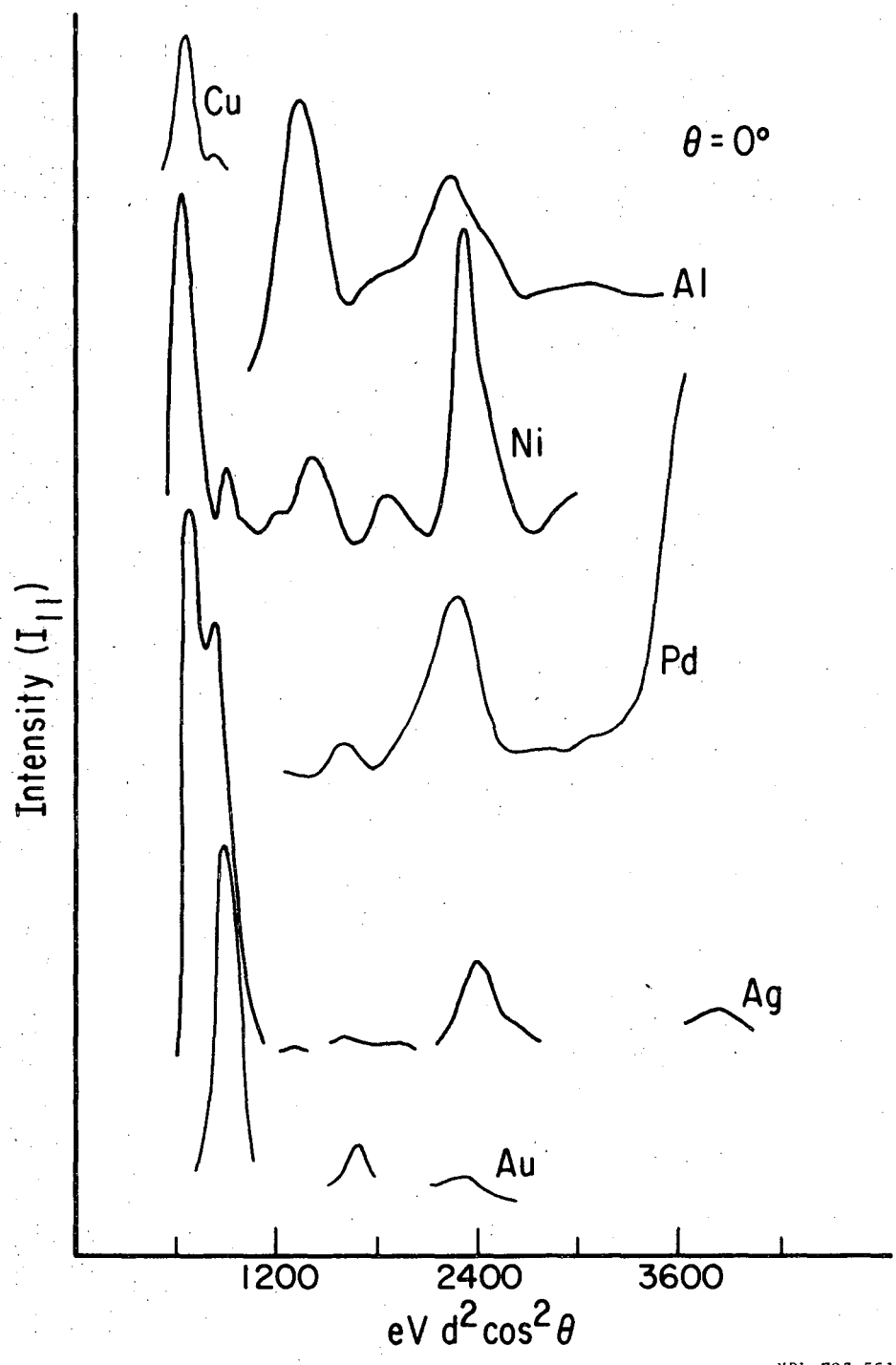
Cu
θ = 0°
Al
Ni
Pd
Ag
Au
Intensity (I_{11})
1200
2400
3600
eV $d^2 \cos^2\theta$
XBL 703-551

Figure 8b

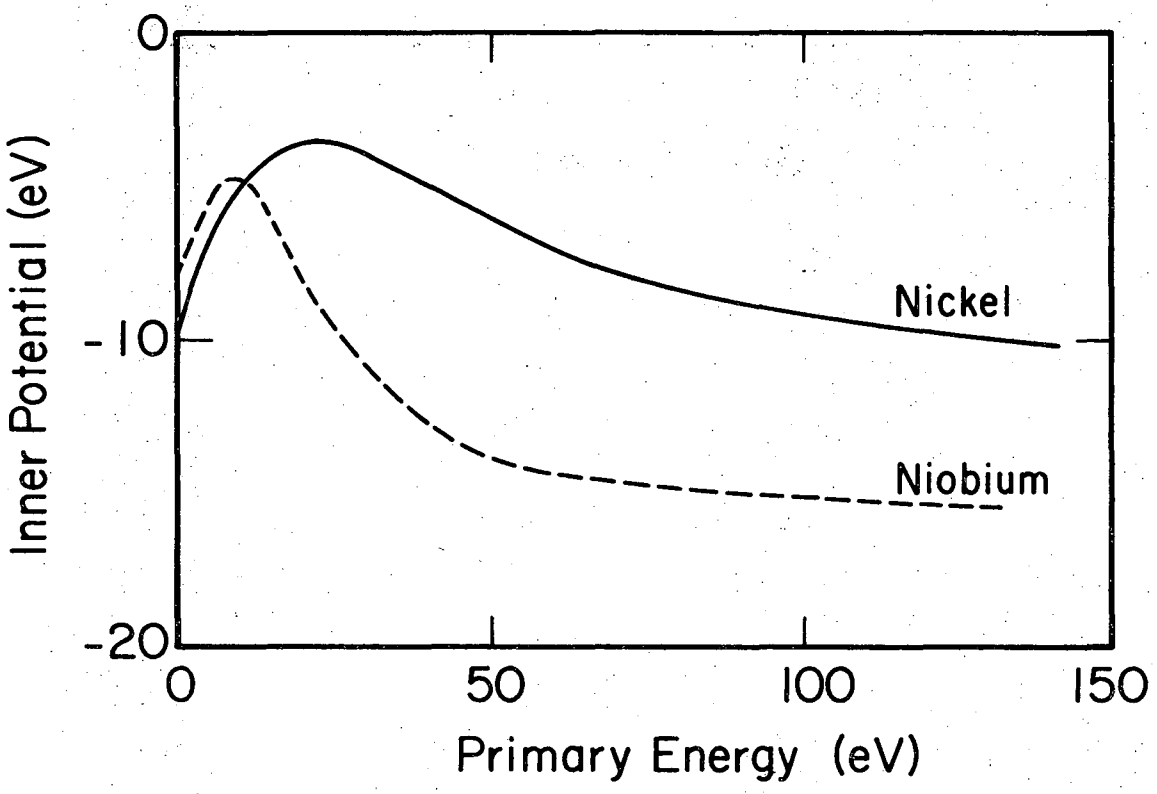

XBL 703-550

Figure 9a-b

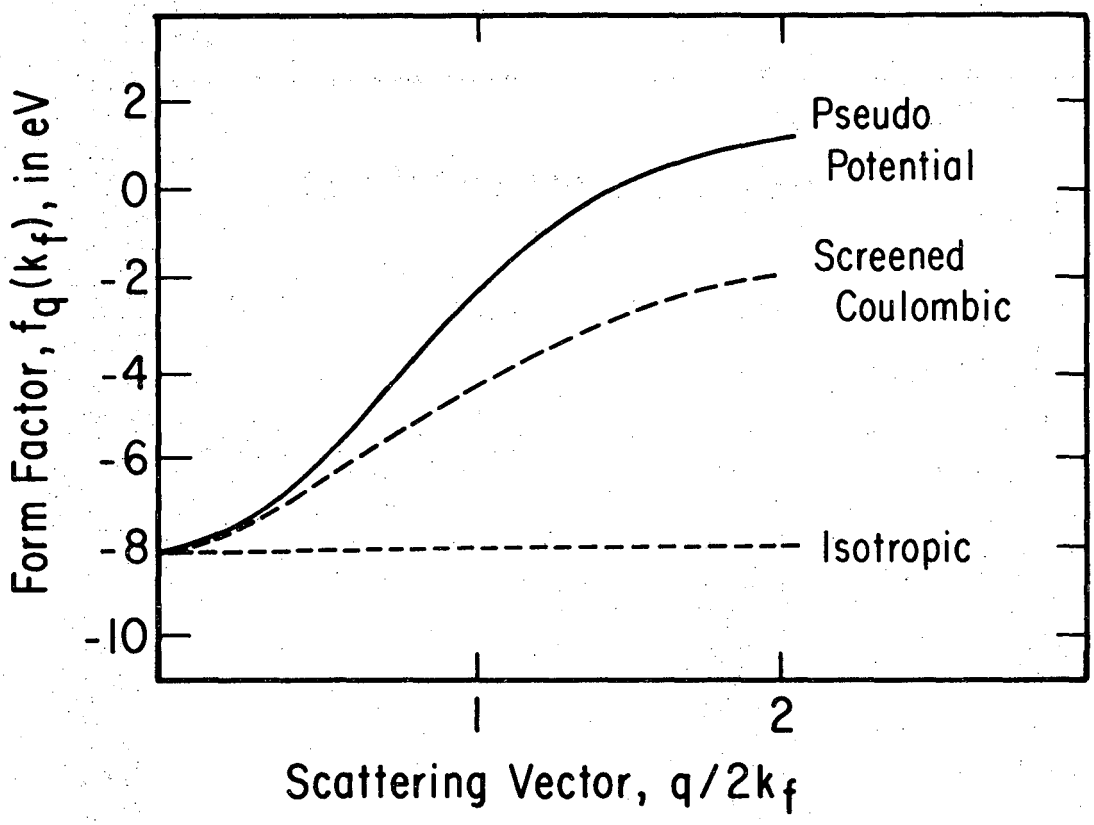

XBL 703-549

Figure 10

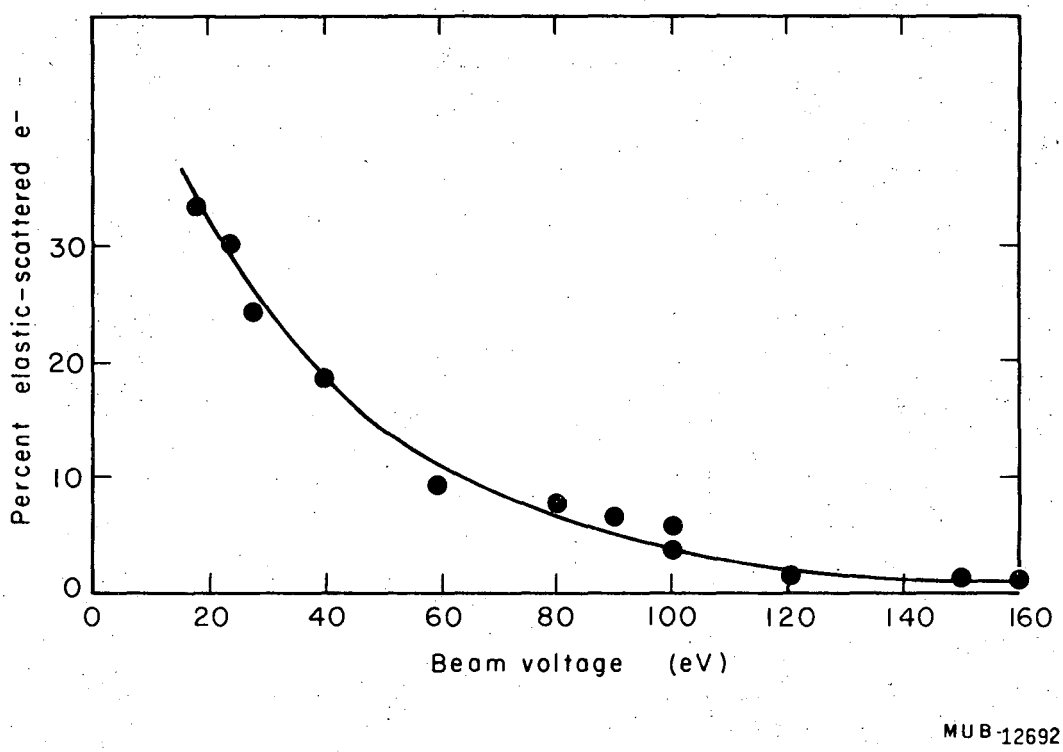
Percent elastic-scattered e⁻
0
10
20
30
0
20
40
60
80
100
120
140
160
Beam voltage (eV)
MUB-12692

Figure 11

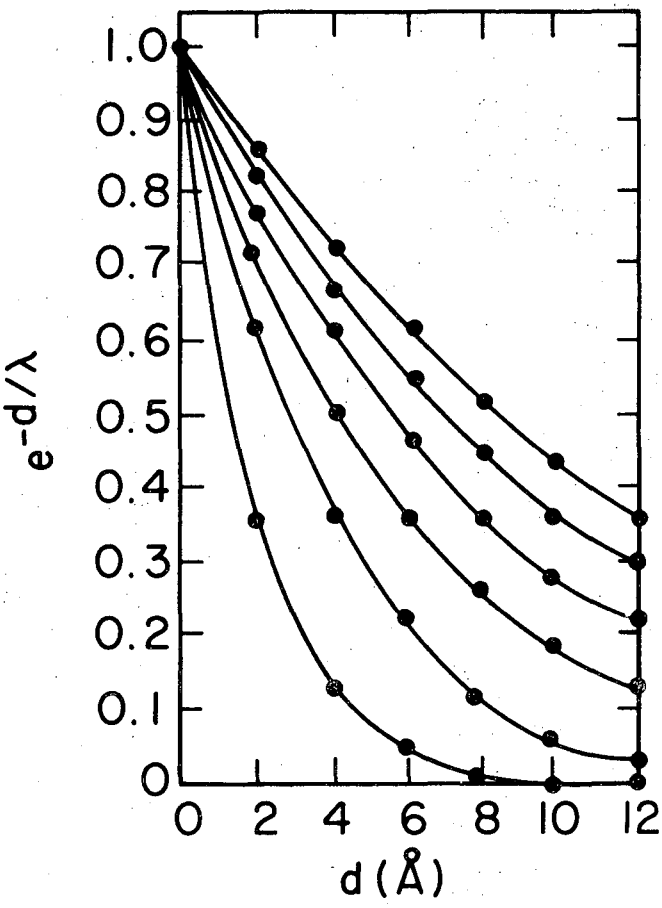

XBL 703-553

Figure 12

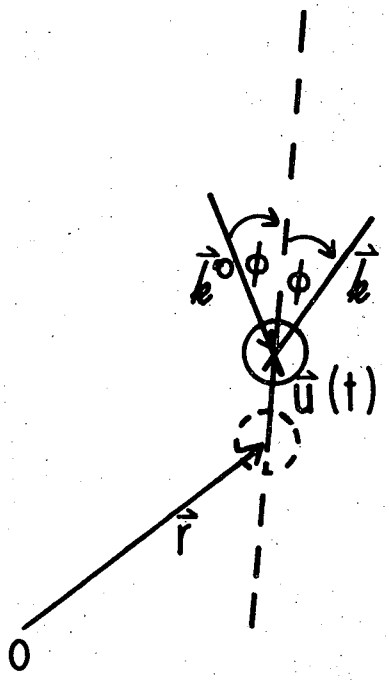

XBL 703-554

Figure 13

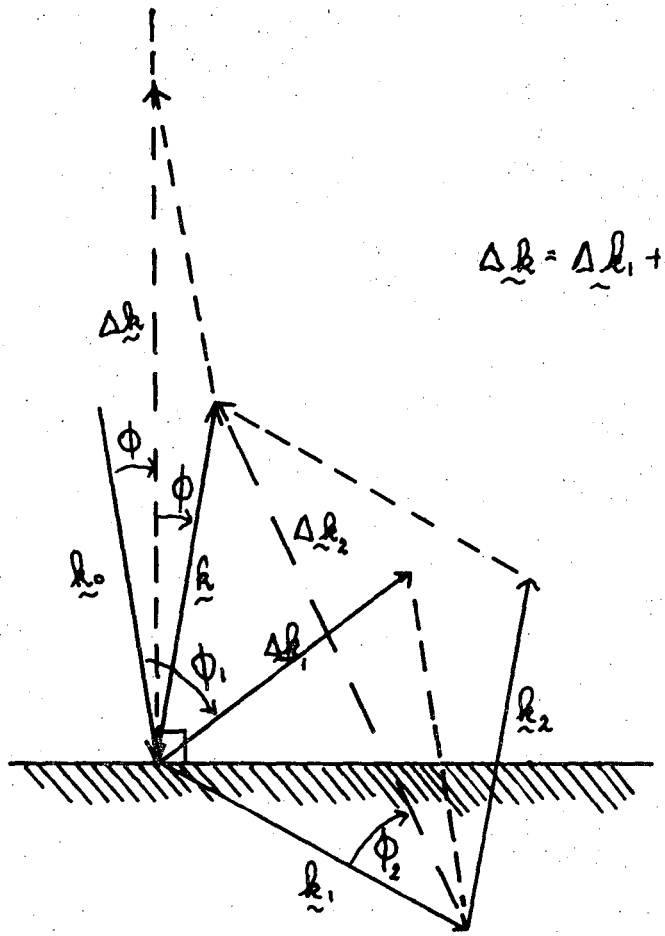

XBL 696-707

Figure 14

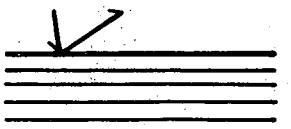

single scattering from the surface

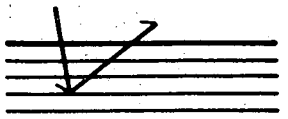

single scattering from the bulk

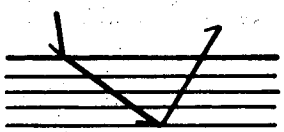

double scattering involving both surface and the bulk

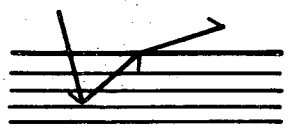

double scattering involving both the surface and the bulk

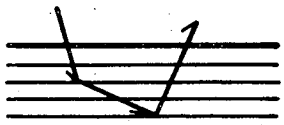

double scattering from the bulk

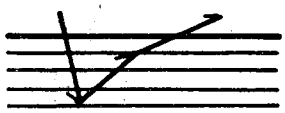

double scattering from the bulk

XBL 703-555

Figure 15

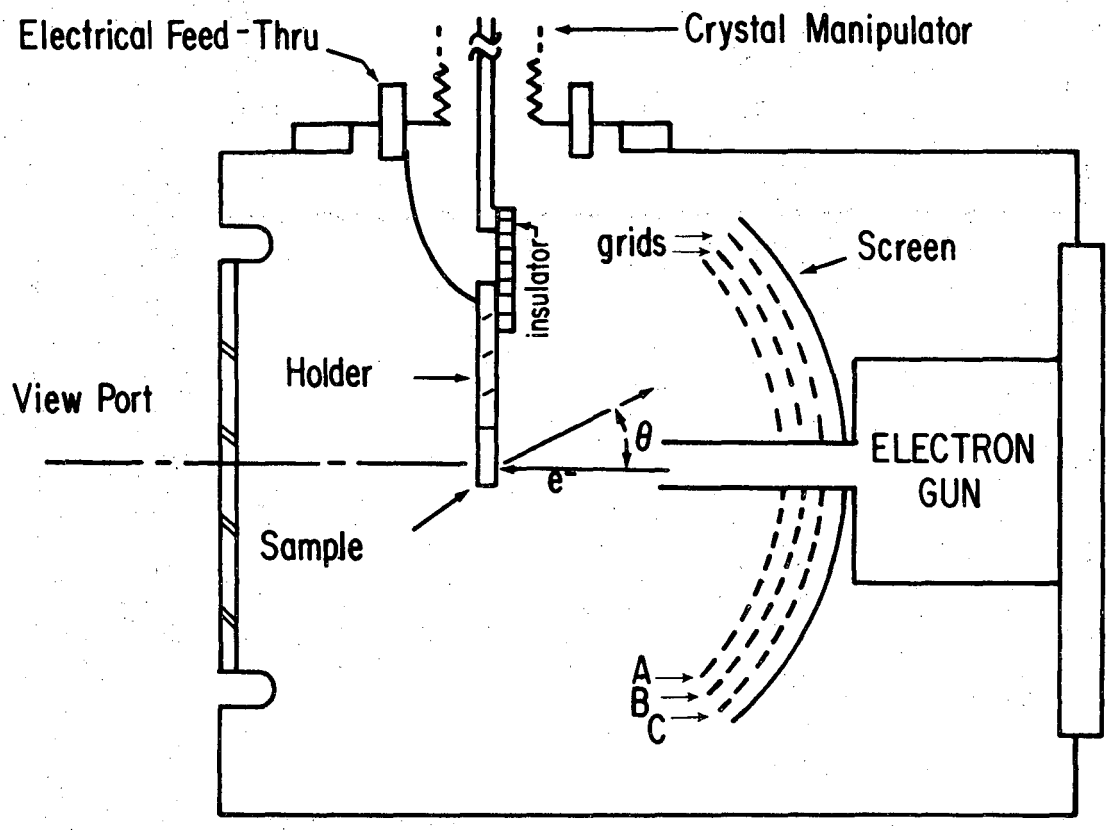

XBL 703-556

Figure 16

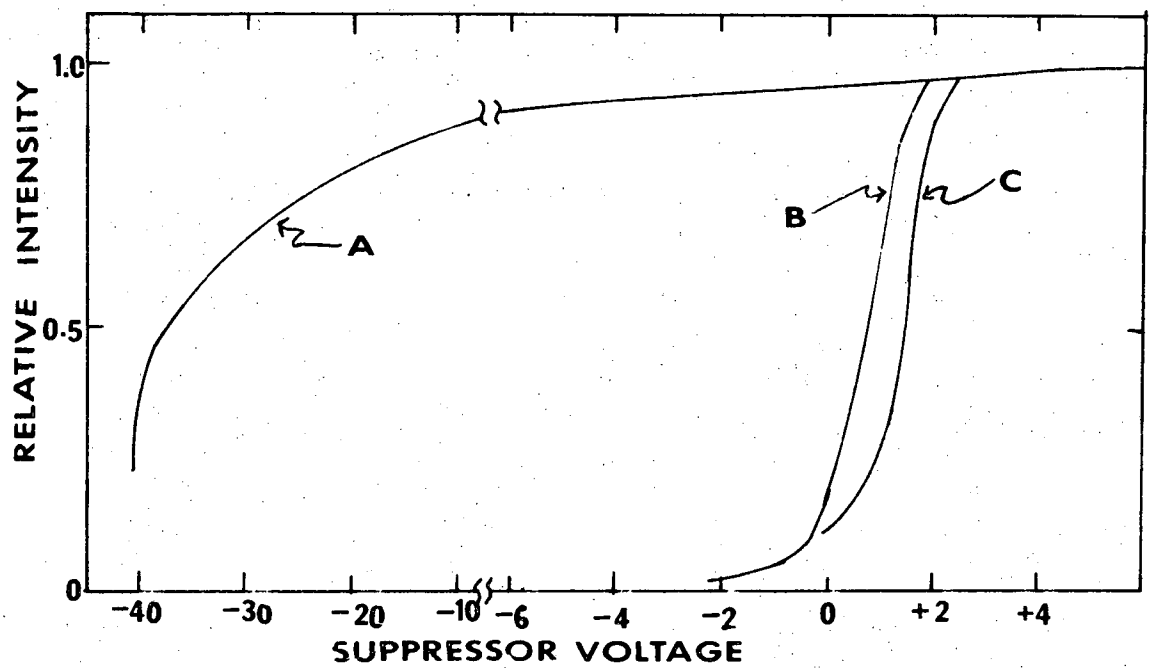

XBL 696-630

Figure 17

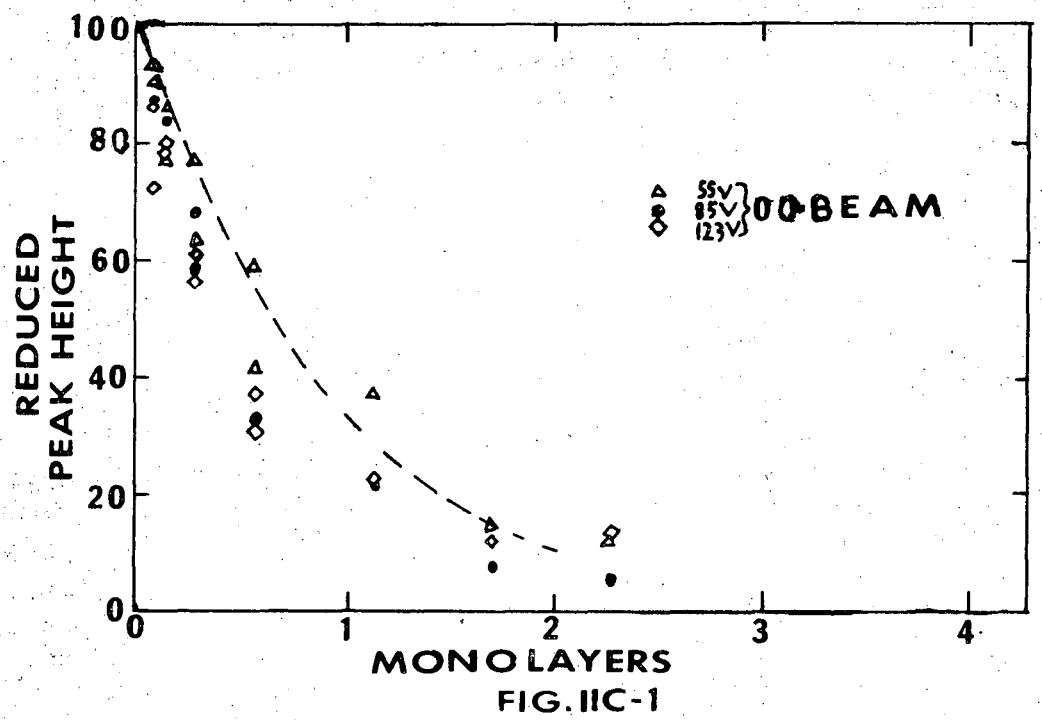

FIG. IIC-1

XBL 696-702

Figure 18

ZN-6026

Figure 19a

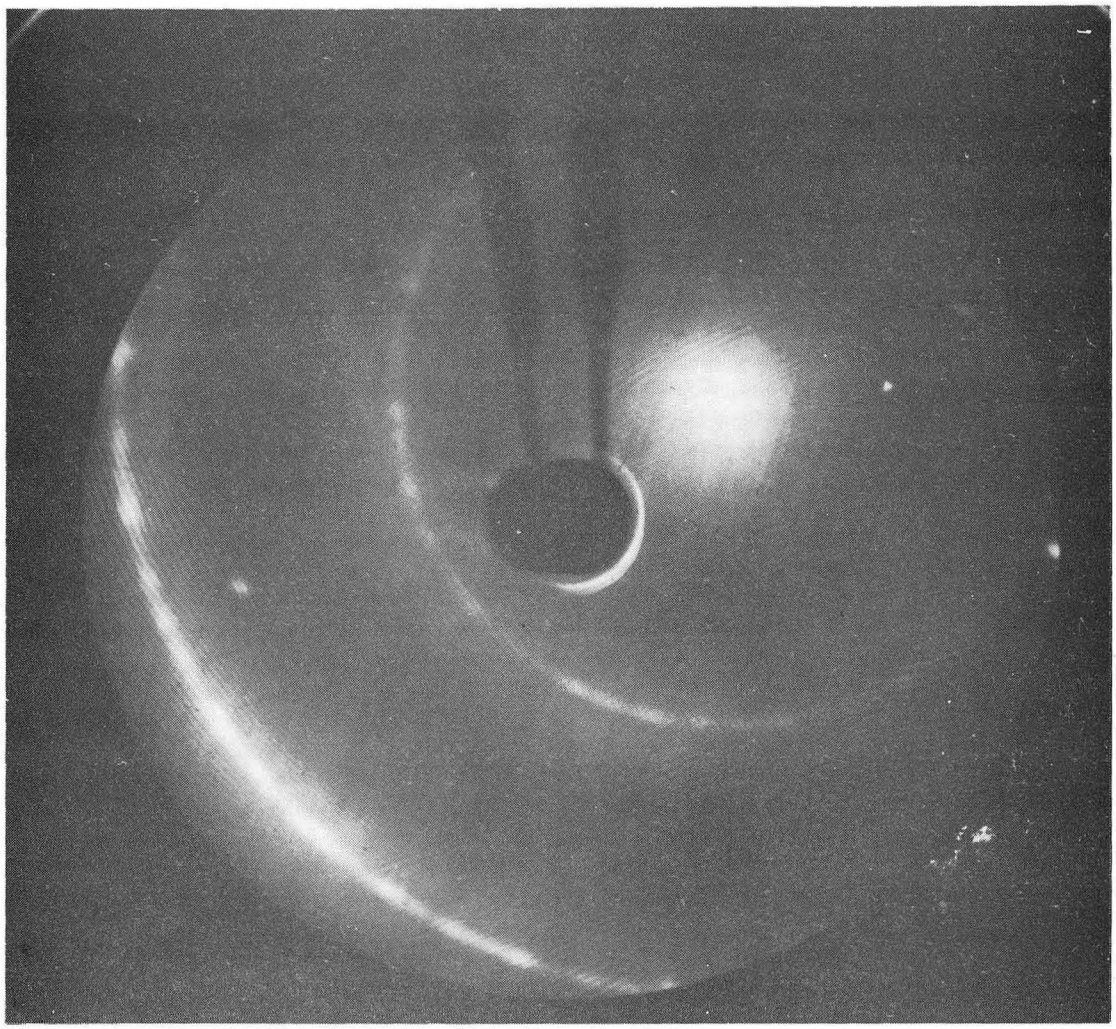

ZN-6028

Figure 19b

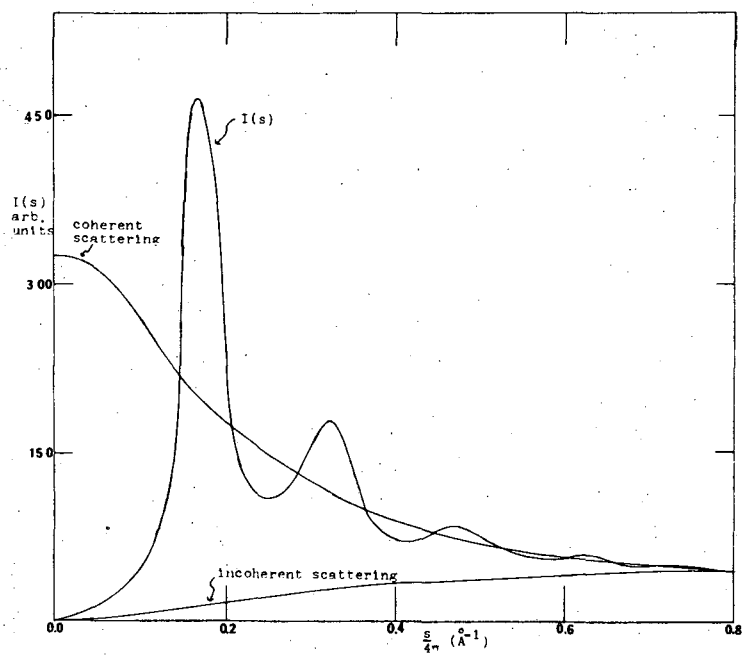

Figure 21

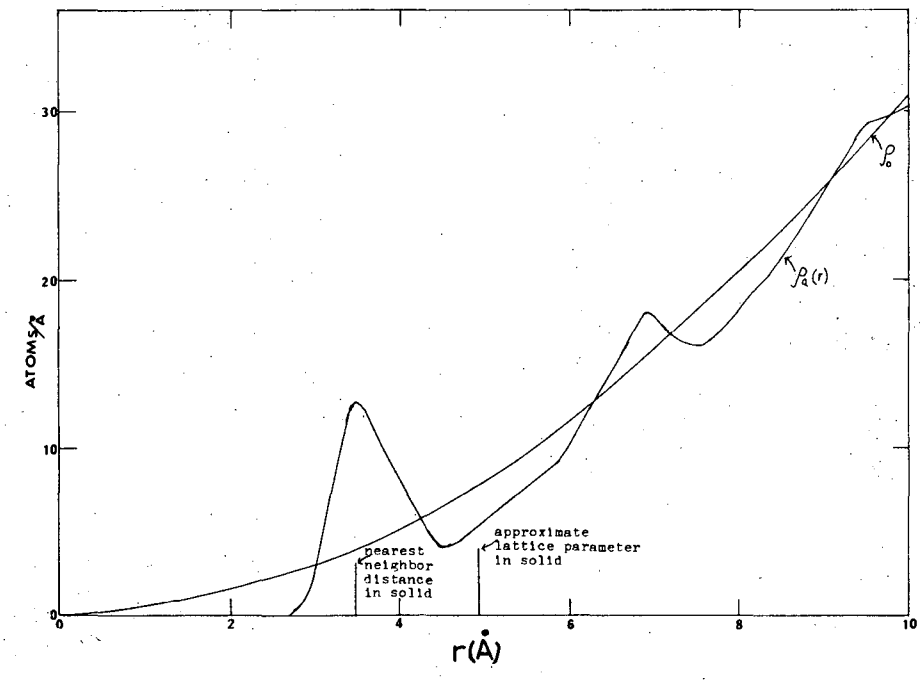

XBL 696-646

Figure 20

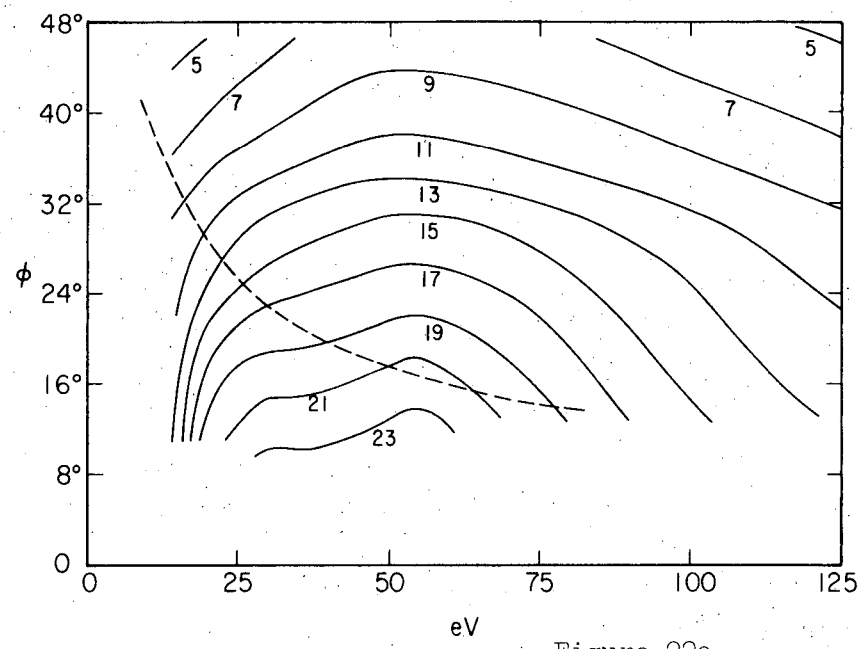

Figure 22a

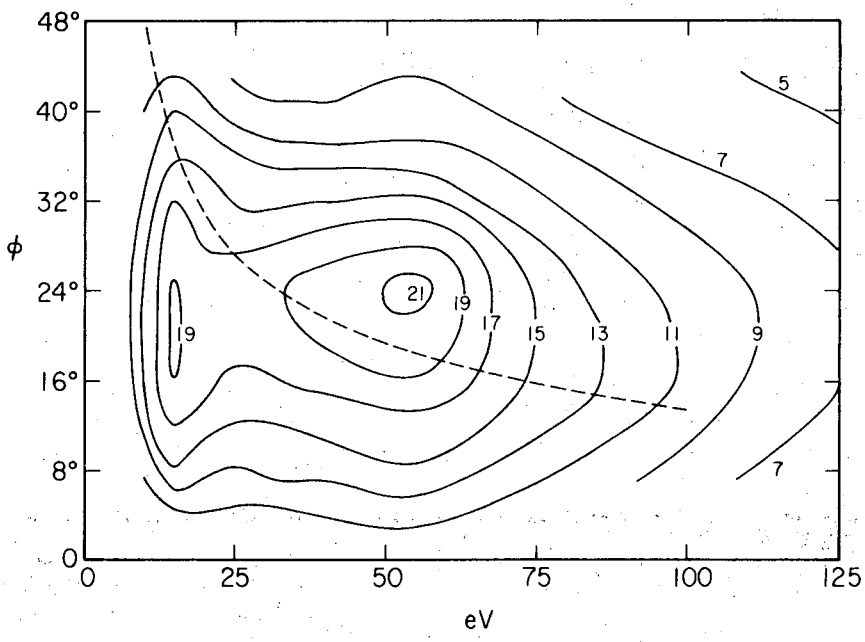

XBL 696-637

Figure 22b

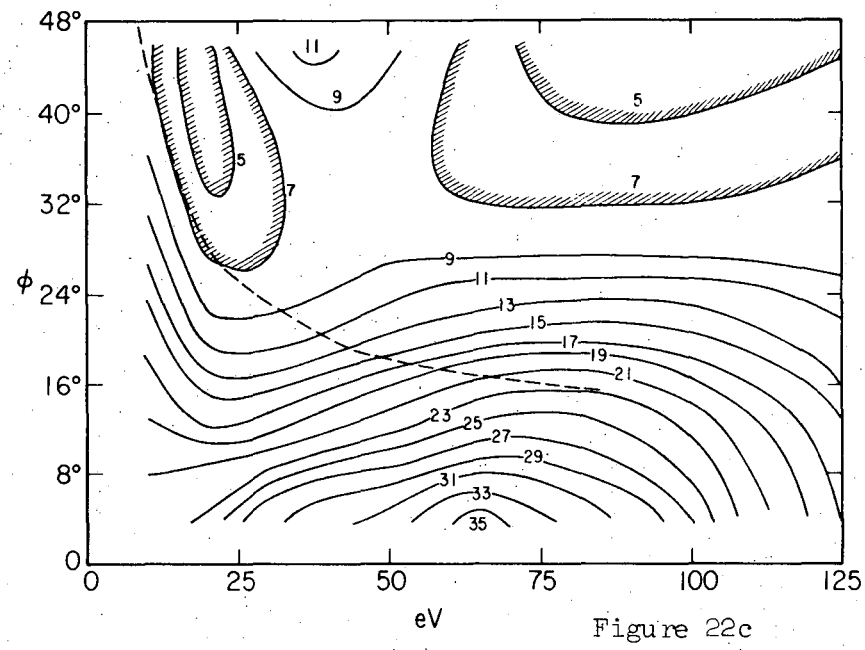

Figure 22c

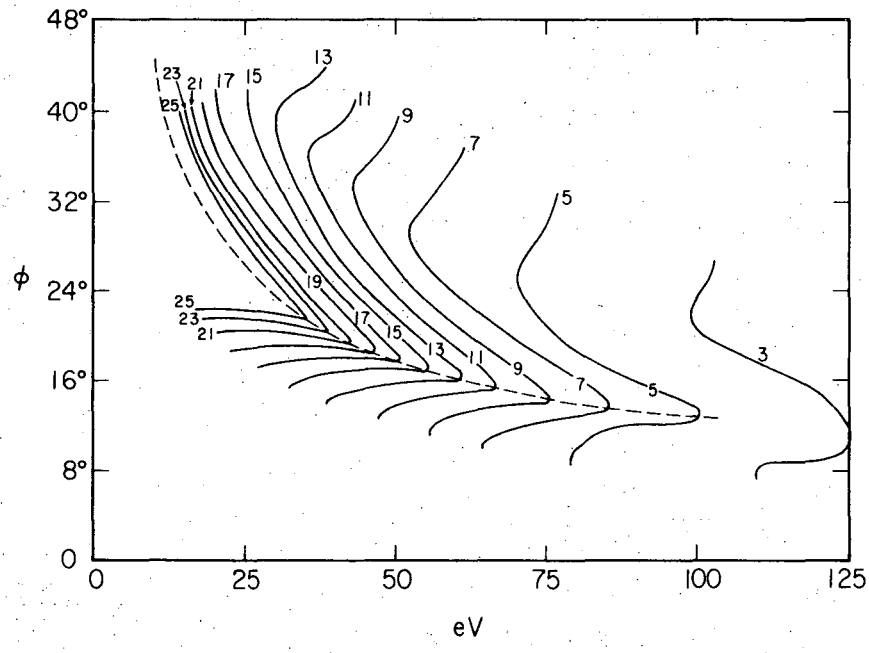

XBL 696-640

Figure 23

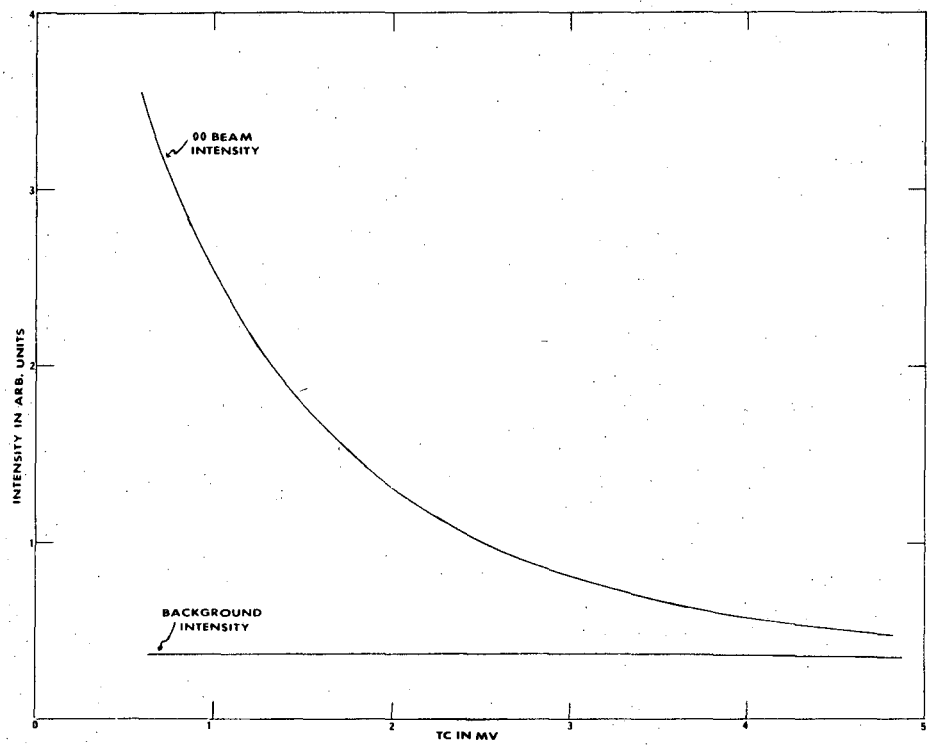

Figure 24

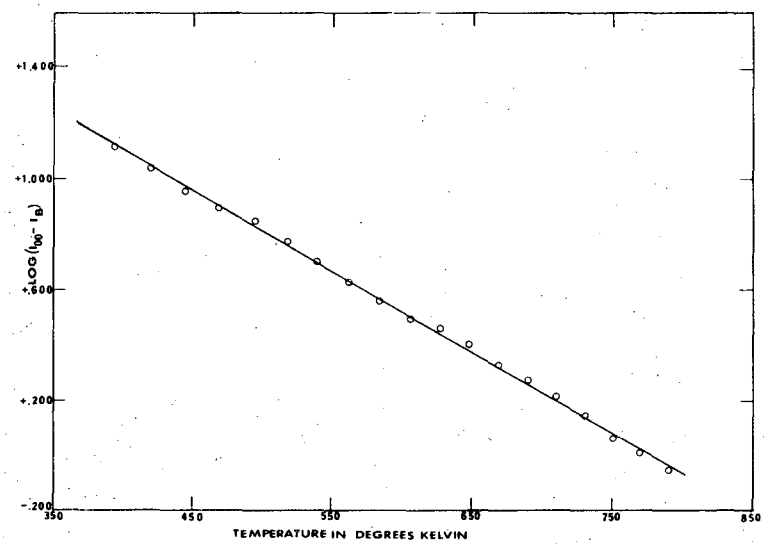

XBL 696-642

Figure 25

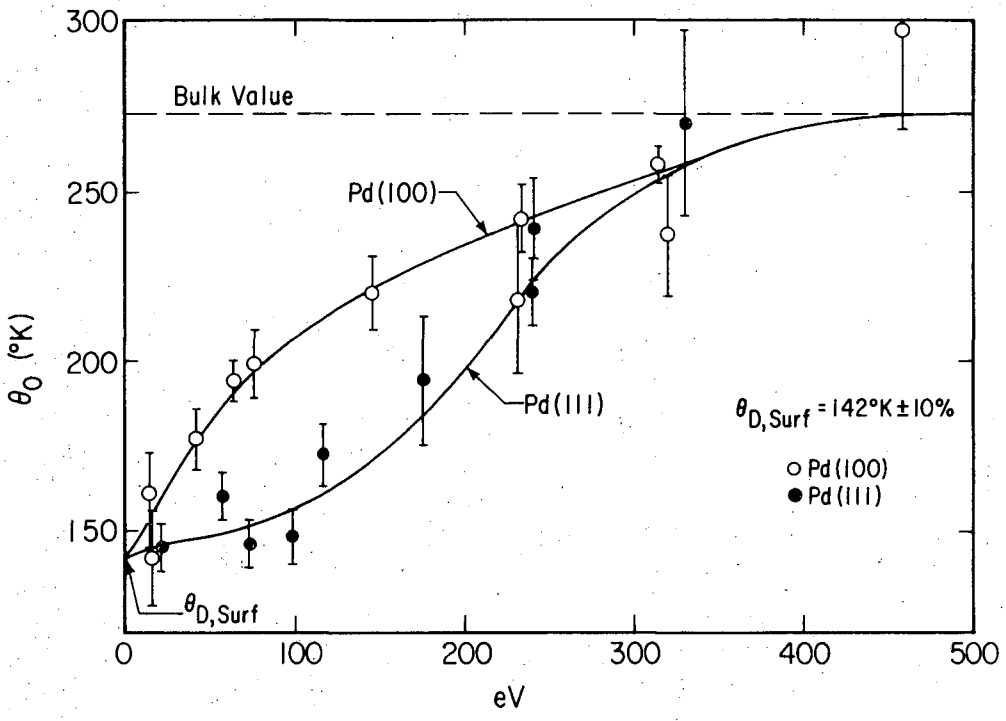

Figure 26a

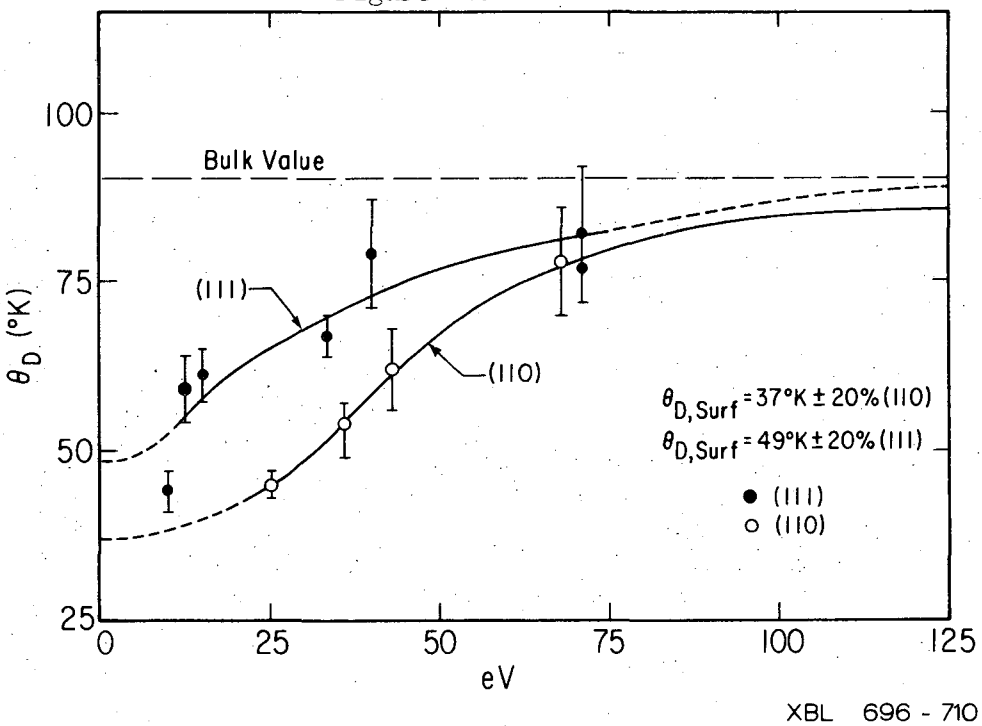

Figure 26b

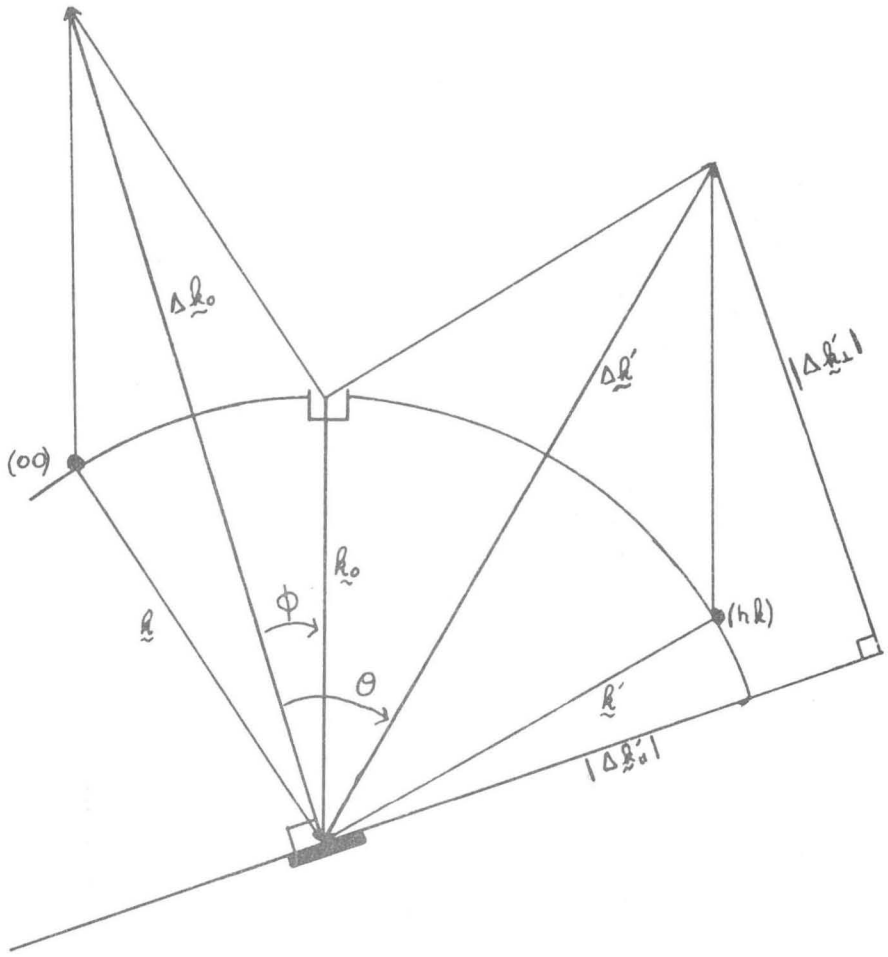

$$|\Delta k'|^2 = |k_o|^2 + |k_o|^2 - 2\, k_o \cdot k_o = 2|k_o|^2 - 2|k_o|^2 \cos[\pi - 2(\theta-\phi)]$$

$$|\Delta k'|^2 = 2|k_o|^2 \left[1 - \cos\{\pi - 2(\theta-\phi)\}\right]$$

$$|\Delta k'|^2 = 2|k_o|^2 \left[1 + \cos 2(\theta-\phi)\right] = 2|k_o|^2 \left[1 + 2\cos^2(\theta-\phi) - 1\right]$$

$$|\Delta k'|^2 = 4|k_o|^2 \cos^2(\theta-\phi)$$

XBL 696-701

Figure 27

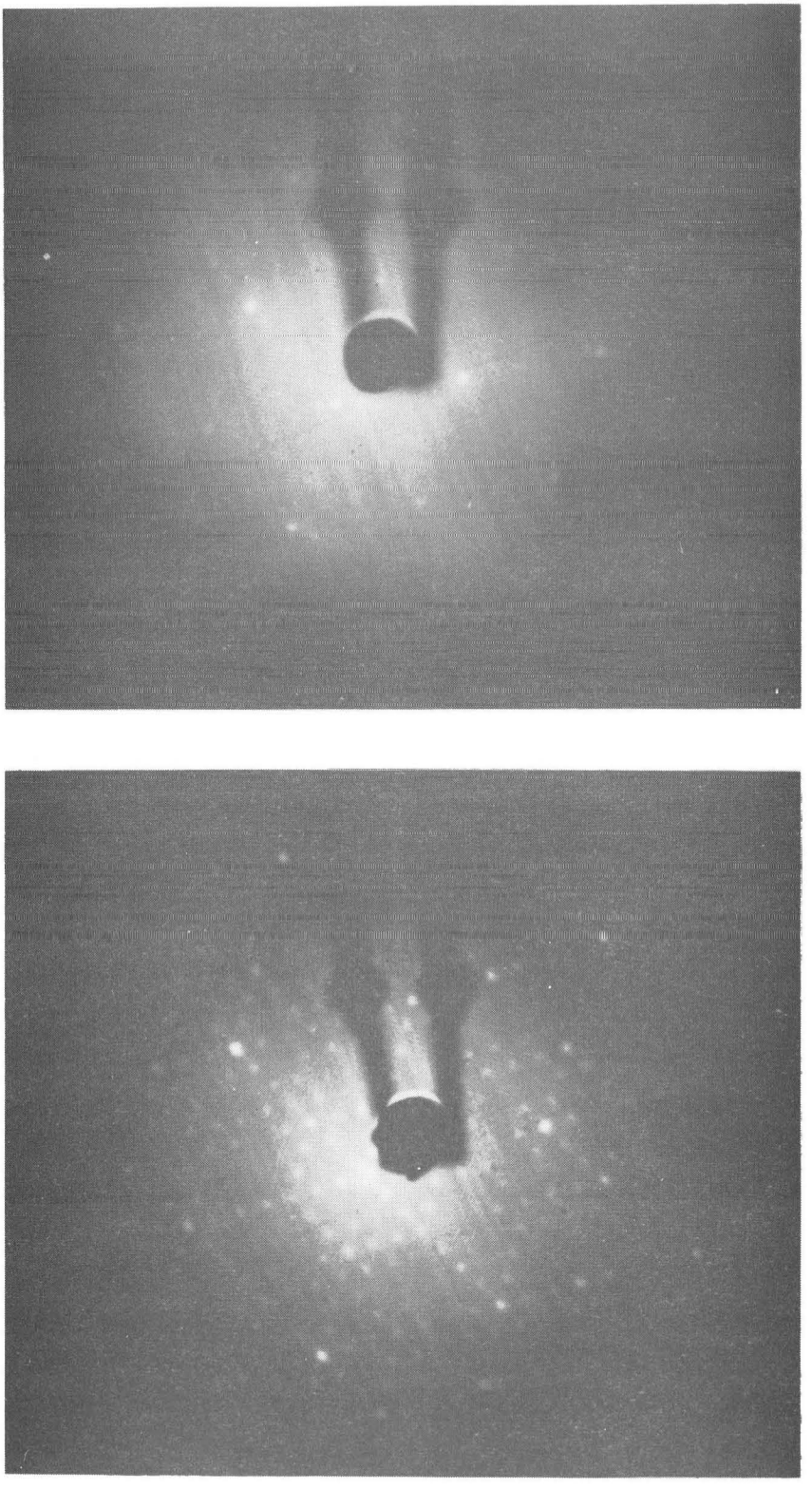

XBB 6911-7077

Figure 28a-b

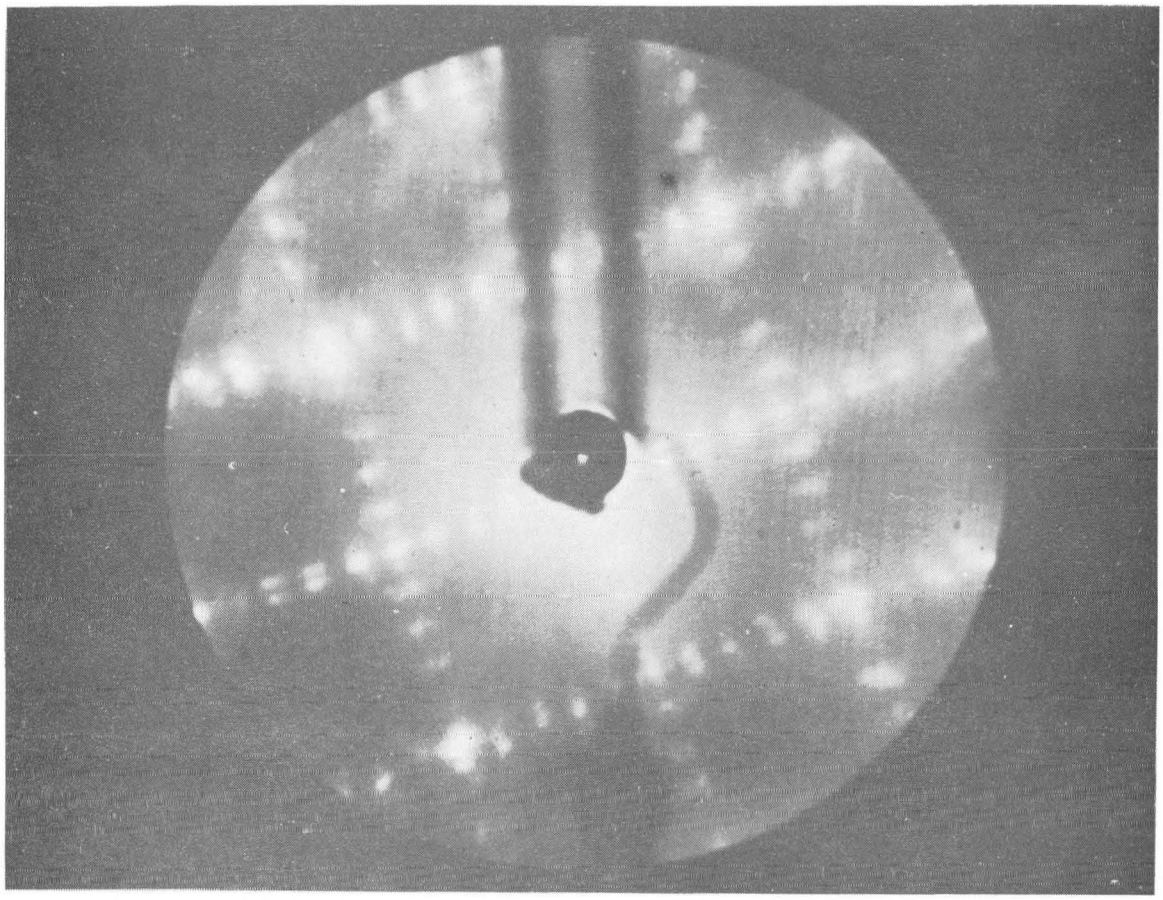

XBB 703-1446

Figure 29

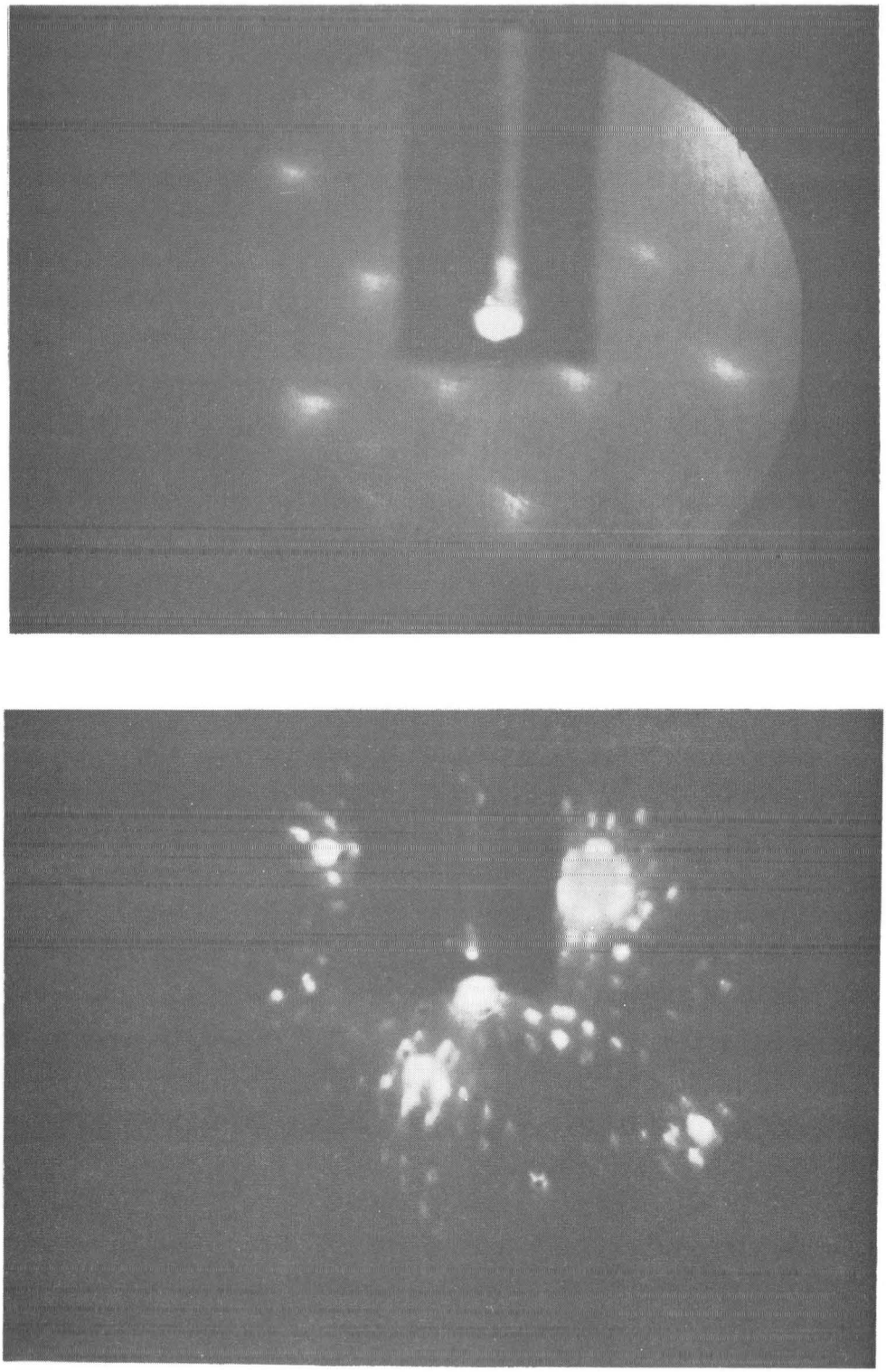

XBB 6910-7008

Figure 30a-b

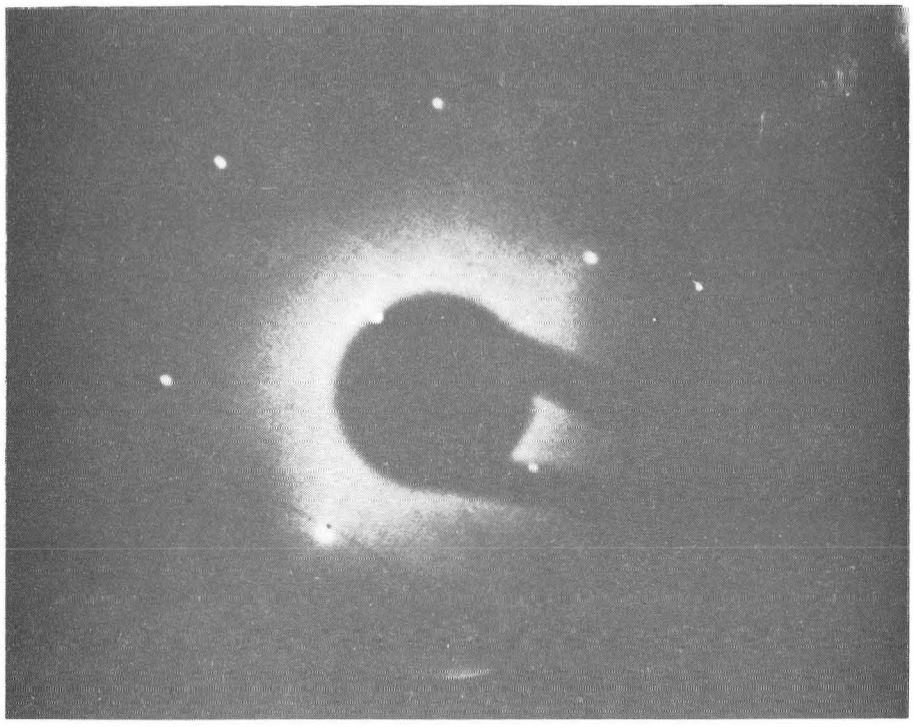

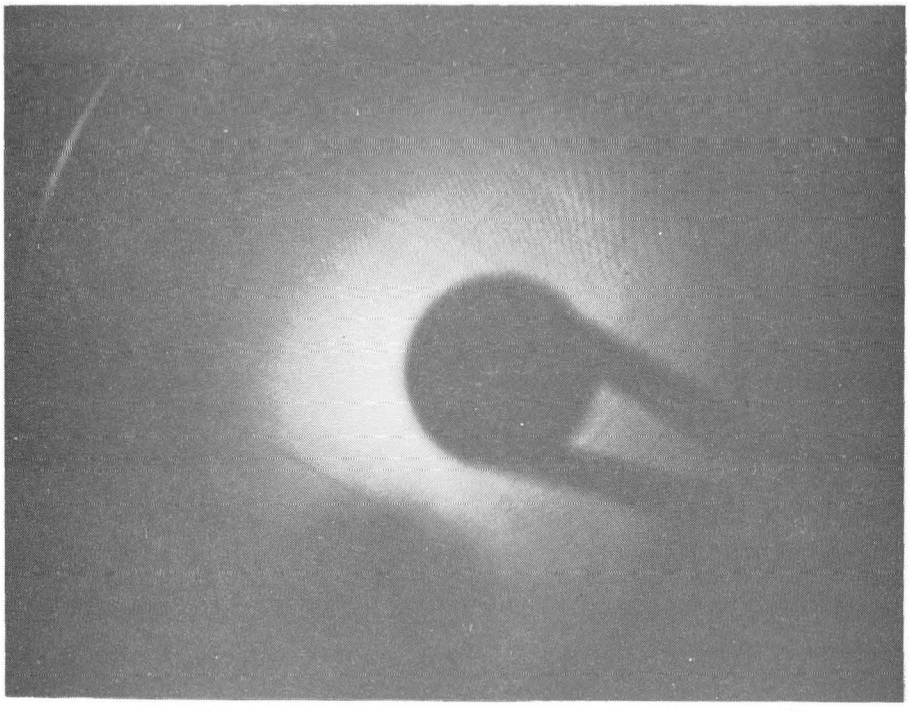

XBB 6911-7608

Figure 31a-b

LEGAL NOTICE

TECHNICAL INFORMATION DIVISION
LAWRENCE RADIATION LABORATORY
UNIVERSITY OF CALIFORNIA
BERKELEY, CALIFORNIA 94720